UNIVERSITA' VITA-SALUTE SAN RAFFAELE

CORSO DI DOTTORATO DI RICERCA
IN MEDICINA MOLECOLARE

Curriculum in Immunologia e Oncologia di Base e Applicate

3D MODELLING OF NON-FUNCTIONING PANCREATIC NEUROENDOCRINE TUMORS FOR FUNCTIONAL STUDIES AND PERSONALIZED MEDICINE

Supervisore: Dott.ssa Cristina Scielzo
Co-supervisore: Prof. Michele De Palma

Tesi di DOTTORATO di RICERCA di Anna Battistella
matr. 022111
Ciclo di dottorato XXXVIII
SSD MED/18

Anno Accademico 2024/2025

CONSULTAZIONE TESI DI DOTTORATO DI RICERCA

Il/la sottoscritto Anna Battistella

Matricola 022111

nata a Biella

il 10/11/1996

Autore della tesi di Dottorato dal titolo

“3D modelling of non-functioning pancreatic neuroendocrine tumors for functional studies and personalized medicine¨

☒ **AUTORIZZA** la Consultazione della tesi

☐ **NON AUTORIZZA** la Consultazione della tesi per 6 mesi

Data 30/11/2025 *Firma* 

DECLARATION

This thesis has been:

- composed by myself and has not been used in any previous application for a degree. Throughout the text I use both 'I' and 'We' interchangeably.
- has been written according to the editing guidelines approved by the University.

Permission to use images and other material covered by copyright has been sought and obtained.

All the results presented here were obtained by myself, except for:

1) *Cell isolation and culture for patient-derived islet-like tumoroids of samples collected from 2018 and 2020 (Aim 3, PDTs section) were performed by Dr. Simon-Leonhard April-Monn (Institute of Pathology, Bern, Switzerland).*

Some of the contents of the present Thesis have been already published, in collaboration with the co-authors included in the publications listed below:

Battistella, A., Tacelli, M., Mapelli, P., Schiavo Lena, M., Andreasi, V., Genova, L., Muffatti, F., De Cobelli, F., Partelli, S., & Falconi, M. (2024). Recent developments in the diagnosis of pancreatic neuroendocrine neoplasms. Expert review of gastroenterology & hepatology, 2024.

Battistella A, Partelli S, Andreasi V, Marinoni I, Palumbo D, Tacelli M, Lena MS, Muffatti F, Mushtaq J, Capurso G, Arcidiacono PG, De Cobelli F, Doglioni C, Perren A, Falconi M. Preoperative assessment of microvessel density in nonfunctioning pancreatic neuroendocrine tumors (NF-PanNETs). Surgery. 2022.

Partelli S*, **Battistella A*,** Andreasi V, Muffatti F, Tamburrino D, Pecorelli N, Crippa S, Balzano G, Falconi M. Critical appraisal of the adequacy of surgical indications for non-functioning pancreatic neuroendocrine tumours. BJS Open. 2024. **Co-first authors* (Aim 1)

Battistella A, Prato F, Andreasi V, Rella R, Guccinelli E, Crippa S, Pecorelli N, Palumbo D, Falconi M, Partelli S. Preoperative predictors of new-onset diabetes mellitus following distal pancreatectomy for nonfunctioning pancreatic neuroendocrine tumors. Surgery. 2025. (Aim 2)

Partelli S, Andreasi V, **Battistella A**, Tamburrino D, Pecorelli N, Crippa S, Falconi M. Gender and Age as Preoperative Predictors of Early Disease Progression in Patients Undergoing Surgery for Pancreatic Neuroendocrine Tumors with Liver Metastases. Ann Surg Oncol. 2025.

All sources of information are acknowledged by means of reference.

ACKNOWLEDGEMENTS

This PhD project was supported by a 2024 Short-Term Fellowship from the Fondazione AIRC, which enabled a three-month research visit to the Institute of Tissue Medicine and Pathology, Bern, Switzerland.

Abstract

Introduction: Pancreatic neuroendocrine tumours (PanNETs) pose persistent therapeutic challenges due to their marked biological heterogeneity and the limited availability of predictive tools to guide treatment selection. A central barrier is the absence of preclinical models that reliably recapitulate both tumour-intrinsic features and the tumour microenvironment (TME), the latter being a critical determinant of disease progression and therapeutic response. This project examined the clinical implications of these gaps and sought to develop complementary patient-derived and 3D bioprinted models that integrate tumour and microenvironmental components, providing a more comprehensive preclinical framework for the study of PanNET biology.

Methods: *Clinical studies*: Retrospective studies were conducted on patients who underwent curative surgery for nonfunctioning (NF)-PanNETs at San Raffaele Hospital (HSR). *1)* The appropriateness of surgical treatment was categorized as appropriate, overtreatment, and undertreatment based on histopathological features and disease relapse. *2)* Postoperative diabetes development was evaluated in patients submitted to distal pancreatectomy. Preoperative clinical, laboratory and radiological data were assessed. *Preclinical studies*: *3)* Patient-derived tumoroids (PDTs) and slices (PCTS) were generated from cryopreserved NF-PanNET specimens from surgically resected patients (HSR and University of Bern); drug sensitivity (sunitinib, everolimus, temozolomide) was quantified and categorized. *4)* 3D bioprinted models were generated using PanNET cell lines and endothelial and stromal cells, embedded in a hydrogel-based bioink. Both simple (mono-culture) and complex (co-culture) models were generated and cultured under static or dynamic conditions using a bioreactor printed in house.

Results: *Clinical studies: 1)* Inadequate treatment was observed in 40% of patients (34% overtreatment, 6% undertreatment), with tumour diameter emerging as the only currently available predictor. *2)* Nearly half of the patients undergoing surgery for localized disease developed postoperative diabetes. A nomogram and online risk calculator were developed to estimate individual risk. *Preclinical studies: 3)* PDTs demonstrated robust concordance with clinical outcomes for cytotoxic chemotherapy across G1–G3 PanNETs, but limited predictive value for targeted agents. In contrast, PCTSs preserved tissue architecture, endocrine cytomorphology, vascular structures, and stromal/immune elements, maintaining viability for at least 10 days *ex vivo*. Drug testing in PCTSs revealed response profiles that diverged from those of PDTs, underscoring the contribution of microenvironmental cues to therapeutic sensitivity. *4)* 3D bioprinted constructs were successfully generated, supporting viability and homo-/hetero-typic cellular interactions. Vessel-like structures enclosed by tumour compartment were generated and perfusion was maintained into a bioreactor. Tumour cell behaviour within these constructs recapitulated intrinsic phenotypic differences observed across PanNET cell lines.

Conclusions: The clinical findings underscore the need for biologically informed criteria to guide treatment decisions and avoid unnecessary long-term sequelae in this often indolent disease. To address this gap, this work present a set of complementary preclinical models, PDTs, PCTSs, and 3D bioprinted constructs, that together capture tumour-intrinsic and microenvironmental dimensions of PanNET biology, providing promising platforms for personalised drug testing and mechanistic studies on PanNET biology.

Introduzione: I tumori neuroendocrini pancreatici (PanNET) non funzionanti (NF) continuano a rappresentare una rilevante sfida clinica in ragione della loro marcata eterogeneità biologica e della scarsità di strumenti predittivi affidabili per orientare la scelta terapeutica. Un limite centrale risiede nella mancanza di modelli preclinici in grado di riprodurre fedelmente sia le caratteristiche intrinseche del tumore sia il microambiente tumorale (TME), elemento cruciale nel modulare la progressione di malattia e la risposta ai trattamenti. Scopo di questo progetto è quello di esaminare le conseguenze cliniche di tali lacune, e di sviluppare modelli derivati da paziente, insieme a modelli biostampati, in grado di integrare componenti tumorali e TME al fine di fornire una piattaforma preclinica più completa per lo studio della biologia dei PanNET.

Metodi: *Studi clinici:* analisi retrospettive su pazienti sottoposti a chirurgia curativa per PanNET non funzionanti presso l'Ospedale San Raffaele (HSR). 1) L'appropriatezza del trattamento chirurgico è stata classificata come appropriata, overtreatment o undertreatment, sulla base di caratteristiche istopatologiche e dell'eventuale recidiva di malattia. 2) L'insorgenza di diabete postoperatorio è stata valutata in pazienti sottoposti a pancreasectomia distale, analizzando dati clinici, laboratoristici e radiologici preoperatori. *Studi preclinici:* 3) generazione di tumoroidi (PDT) e sezioni tissutali (PCTS) da campioni crioconservati di NF-PanNET (HSR e Università di Berna). La sensibilità farmacologica a sunitinib, everolimus, temozolomide è stata quantificata e classificata. 4) sviluppo di modelli biostampati 3D utilizzando linee cellulari di PanNET, cellule endoteliali e stromali, incorporate in un biomateriale. Sono stati generati modelli semplici (mono-coltura) e complessi (co-coltura), mantenuti in condizioni statiche o dinamiche mediante un bioreattore home-made.

Risultati: *Studi clinici:* 1) Un trattamento inadeguato è stato riscontrato nel 40% dei pazienti (34% overtreatment; 6% undertreatment), con il diametro tumorale quale unico predittore attualmente disponibile. 2) Quasi la metà dei pazienti sottoposti a chirurgia per malattia localizzata ha sviluppato diabete postoperatorio. È stato elaborato un nomogramma ed un calcolatore di rischio online, per stimare il rischio individuale. *Studi preclinici:* 3) I PDT hanno evidenziato una robusta concordanza con gli esiti clinici in risposta alla chemioterapia citotossica nei PanNET G1-G3, mentre hanno mostrato capacità predittiva limitata nei confronti dei farmaci a bersaglio molecolare (TT). Le colture ex vivo PCTS hanno preservato l'architettura tissutale, la citomorfologia endocrina, l'organizzazione vascolare e le componenti stromali e immunitarie, mantenendo la vitalità per almeno 10 giorni. I profili di risposta farmacologica alle TT nei PCTS si sono discostati da quelli dei PDT, evidenziando l'influenza determinante del microambiente nella modulazione della sensibilità terapeutica. 4) Sono stati sviluppati costrutti biostampati in grado di supportatare la vitalità cellulare e le interazioni omo- ed eterotipiche. Sono state generate strutture simil-vascolari circondate dal compartimento tumorale, mantenute in perfusione. i costrutti hanno preservato le differenze fenotipiche intrinseche delle diverse linee cellulari di PanNET.

Conclusioni: I risultati clinici evidenziano la necessità di criteri biologicamente informati per ottimizzare le decisioni terapeutiche nei pazienti affetti da NF-PanNET. Questo lavoro propone un insieme di modelli preclinici complementari, PDT, PCTS e costrutti biostampati, che, nel loro complesso, ricapitolano le dimensioni intrinseche e microambientali della biologia dei PanNET e rappresentano piattaforme promettenti per test farmacologici personalizzati e studi meccanicistici.

Table of Contents

Introduction

1. Pancreatic Neuroendocrine Neoplasms

Pancreatic neuroendocrine neoplasms (PanNENs) are rare, heterogeneous neoplasms that originate from the endocrine cells of the pancreas. PanNENs have been traditionally considered as rare neoplasms, with an annual incidence of less than 1 case per 100,000 individuals, accounting for approximately 1-2% of all pancreatic tumours (Halfdanarson *et al*, 2008).

Over the last three decades, the incidence of PanNENs has been steadily increasing (Dasari *et al*, 2025; Thiis-Evensen & Boyar Cetinkaya, 2023). This rise largely reflects the widespread adoption of high-resolution cross-sectional and functional imaging modalities, as well as greater clinical awareness and the establishment of well-defined diagnostic criteria that enable earlier and more accurate tumour identification (**Figure 1 A-B**).

Concurrently, the prevalence of PanNENs also continues to rise, owing to the often slow-growing nature of the disease and the expanding range of treatment options currently available (Kos-Kudła *et al*, 2023), underscoring their growing clinical relevance within the spectrum of pancreatic malignancies (**Figure 1, C-D**).

Figure 1. Incidence (A-United States; B- Europe) and prevalence (C- United States; D-Europe) of Neuroendocrine Neoplasms in the United States and Europe (Dasari *et al*, 2025; Thiis-Evensen & Boyar Cetinkaya, 2023).

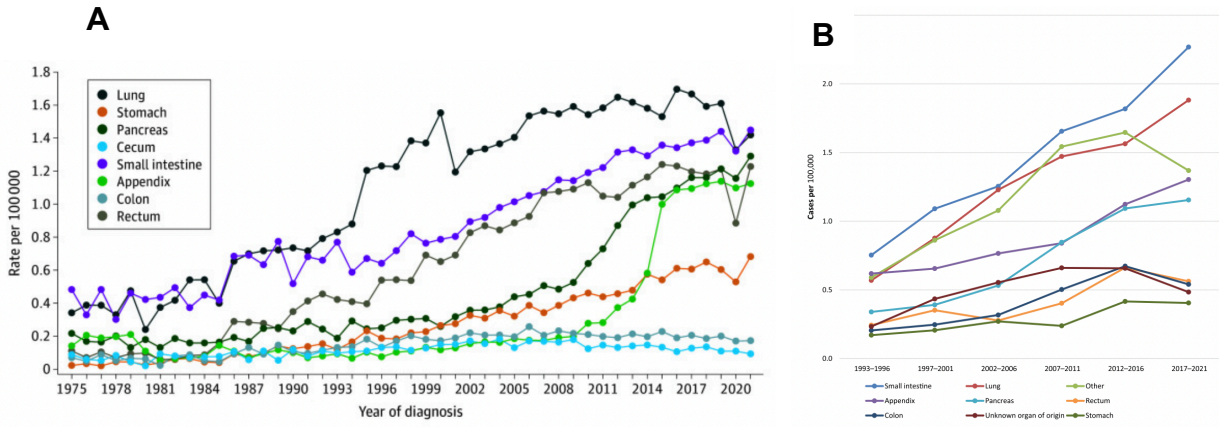

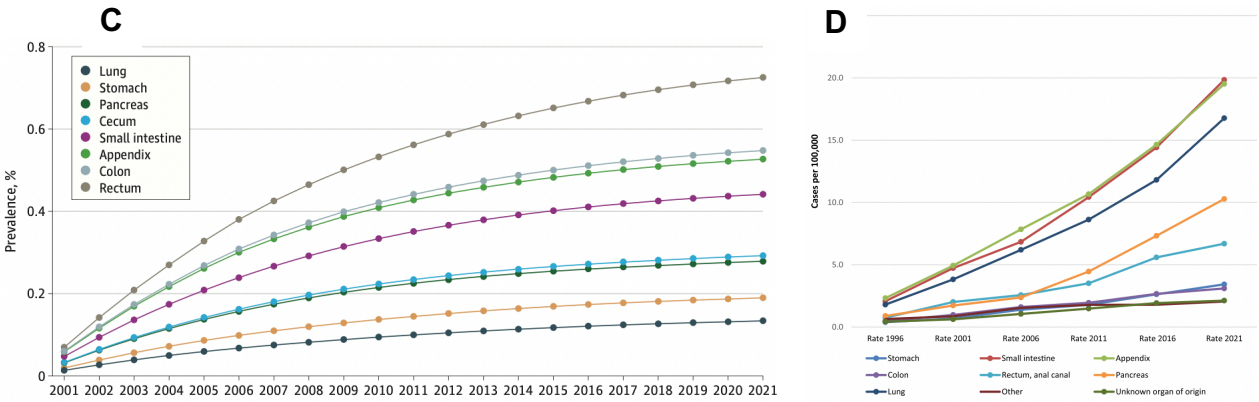

Diagnosis

Histological diagnosis is mandatory in all the patients with suspected PanNENs (e.g. clinical symptoms and/or imaging findings). Based on histo-morphological growth pattern and cytology on hematoxylin eosin (HE)-stained tissue, PanNEN identification can be achieved. The neuroendocrine phenotype of these malignancies is proven by immunohistochemical detection of the neuroendocrine markers synaptophysin (SYN) and/or chromogranin A (CgA) (Rindi *et al*, 2022). Moreover, NEN commonly overexpress somatostatin receptors (SSTR), feature which is exploited both for diagnostic and therapeutic purposes. Indeed, SSTR expression can be assessed both immunohistochemically and non-invasively through ^{68}Gallium-labelled somatostatin analogue positron emission tomography/computed tomography (^{68}Ga-SSA PET/CT), which enables highly sensitive detection of receptor-positive lesions (Khanna *et al*, 2020). In addition, SSTR expression carries direct therapeutic implications: synthetic somatostatin analogues (SSAs) and radiolabelled SSAs, constitute approved treatments for patients with advanced, well-differentiated PanNENs (Strosberg, 2018; Kos-Kudła *et al*, 2023).

Clinical classification

PanNENs are broadly classified into functioning and non-functioning tumours, based in the presence or absence of clinical syndromes caused by hormonal hypersecretion. Functioning PanNENs (F-PanNENs) account for 30% of all cases, and are named

according to the predominant hormone secreted (i.e., insulinoma, gastrinoma, somatostatinoma). The resulting hormone-related clinical syndromes often lead to earlier detection. On the other hand, nonfunctioning neoplasms (NF-PanNENs), accounting for the majority of PanNEN, do not secrete biologically active substances or do so at levels insufficient to produce clinical symptoms, and are therefore often detected incidentally or at an advanced stages, when symptoms due to mass effect, local invasion or distant metastases arise (Guilmette & Nosé, 2019; Fang & Shi, 2019; Halfdanarson *et al*, 2008; Patel *et al*, 2019; Singh *et al*, 2015).

Established Prognostic factors

Histologically, PanNENs are classified according to their cell morphology into well-differentiated pancreatic neuroendocrine tumours (PanNETs, G1-G2-G3), which represents the vast majority of these neoplasms, and poorly differentiated pancreatic neuroendocrine carcinomas (PanNECs, G3). The latter are further distinguished in large-cell NECs and small-cell NECs and represent only a minority of all NENs. Besides PanNETs and PanNECs, a third class, is represented by mixed Neuroendocrine–Non-neuroendocrine Neoplasms (MiNENs), characterized by the association between NENs and other non-neuroendocrine neoplasms. Tumour grading is based on the proliferative activity measured by the Ki-67 proliferative index and mitotic count. The World Health Organization classification distinguishes three grades: G1, mitotic count <2 per 10 high-power field (HPF) and/or Ki67 < 3%; G2, mitotic count 2-20 and/or Ki67 3-20%; G3, mitotic count >20 per 10 HPF and/or Ki67 index >20% (Rindi *et al*, 2022) (**Table 1**). When Ki67 and mitotic count are discordant, the parameter classifying the tumour in the higher grade category is considered. PanNETs G3 tumours are generally associated with poor prognosis, whereas G1-G2 lesions display an unpredictable disease course, varying from indolent to highly malignant lesions.

Table I. WHO 2022 classification for gastroenteropancreatic neuroendocrine neoplasms (Rindi *et al*, 2022)

Morphology	Grade	Mitotic count (mm2)	Ki67 index (%)
Well-differentiated NETs	G1	<2	<3
Well-differentiated NETs	G2	2-20	3-20
Well-differentiated NETs	G3	>20	>20
Poorly-differentiated NECs - small cell - large cell	G3	>20	>20
MiNEN **Tumour-like lesions**			

Tumor stage also influences outcome. Localised PanNETs confined to the pancreas have a five-year relative survival of approximately 91 %, whereas regionally advanced tumours have survival rates around 64 %, and metastatic disease carries a five-year survival near 19 % (American Cancer Society, 2025).

Table II. European Neuroendocrine Tumour Society (ENETS) TNM staging system (Rindi *et al*, 2006)

T-primary tumour	ENETS
Tx	Primary tumour cannot be assessed
T0	No evidence of Primary Tumour
T1	Tumour limited to the pancreas and <2cm
T2	Tumour limited to the pancreas and diameter 2-4 cm
T3	Tumour limited to the pancreas and size >4cm or invading duodenum or bile-duct
T4	Tumour invading nearby organs (stomach, spleen, colon adrenal gland) or the wall or large vessels (celiac axis or superior mesenteric artery)

N-regional lymph node	ENETS
Nx	Regional lymph node cannot be assessed
N0	No regional lymph node metastases
N1	Regional lymph node metastases

M-distant metastasis	ENETS
Mx	Distant metastases cannot be assessed
M0	No distant metastases
M1	Distant metastases

STAGE	ENETS
I	T1 N0 M0
II	IIA T2 N0 M0 IIB T3 N0 M0
III	IIIA T4 N0 M0 IIIB anyT N1 M0
IV	anyT anyN M1

Other than tumour stage and grade, which remain the principal determinants of aggressiveness, prognosis, and therapeutic strategy, only a limited number of additional prognostic markers have been identified. These include specific molecular and genetic alterations, as well as features of tumour vasculature, although they have not yet been fully integrated into routine clinical decision-making (Kos-Kudła *et al*, 2023). Consequently, the appropriate management of pancreatic neuroendocrine tumours remains particularly challenging, as the mechanisms underlying tumour progression and therapeutic response remain to be fully elucidated.

Molecular Alterations

PanNENs encompass a heterogeneous group of tumours that differ not only in cell morphology and proliferative activity but also in their underlying molecular alterations. High grade PanNECs harbour alterations typical of aggressive carcinomas, including TP53 and RB1 inactivation (Scarpa *et al*, 2017), which correlates with aggressive clinical behaviour and poor prognosis.

Conversely, for well-differentiated PanNETs high-throughput sequencing has revealed recurrent alterations in a restricted number of genes implicated in chromatin

remodelling, DNA-damage repair, and the mTOR signalling pathway. Loss-of-function mutations in MEN1 (menin), DAXX (death-domain– associated protein), and ATRX (thalassemia/mental retardation syndrome X-linked) collectively occur in more than 50% of well-differentiated PanNETs, constituting the most prevalent molecular hallmark of these neoplasms (Scarpa *et al*, 2017).

MEN1, encoding the tumour suppressor menin, regulates histone methylation and transcriptional control at promoters involved in growth and DNA repair. DAXX and ATRX encode chromatin remodelling proteins responsible for histone H3.3 deposition at telomeric and pericentromeric regions. Their inactivation results in alternative lengthening of telomeres (ALT), a phenotype associated with chromosomal instability and increased metastatic potential (Marinoni et al, 2014).

Mutations in mTOR-pathway components such as PTEN, TSC1, TSC2, and DEPDC5 occur in almost 10 % of tumours (Scarpa *et al*, 2017). These alterations lead to constitutive activation of the PI3K–AKT–mTOR axis, driving anabolic metabolism and proliferation (Maharjan *et al*, 2021; Briest & Grabowski, 2014). Functionally, mTOR-pathway mutations are enriched in intermediate- to high-grade tumours and are associated with more aggressive biological behaviour (Scarpa *et al*, 2017) .

Moreover, structural gene fusions have recently been identified as independent negative prognostic markers in NF-PanNETs. In particular, rearrangements involving BEND2, most notably CHD7::BEND2 and EWSR1::BEND2, have been described as new oncogenic mechanism in aggressive NF-PanNETs (Wood-Trageser *et al*, 2025). These fusions drive aberrant transcriptional activation and chromatin deregulation, correlating with higher metastatic potential, and poorer overall prognosis.

Epigenomic profiling has revealed distinct DNA-methylation and histone-modification signatures that differentiate indolent from aggressive pancreatic neuroendocrine tumours (Moser *et al*, 2024; Di Domenico *et al*, 2020; Lakis *et al*, 2021), providing a superior prognostic stratification compared with genetic alterations alone. Across all the analyses, two principal epigenetic NF-PanNETs subtypes have been consistently delineated: α-cell–like tumours, associated with MEN1 mutations, ARX expression, and hypomethylation of α-cell–specific enhancers (*α-like* group (Di

Domenico *et al*, 2020), groups *A1-A2* (Moser *et al*, 2024) , group *T3* (Lakis *et al*, 2021)), and intermediate tumours, frequently harbouring DAXX or ATRX loss and exhibiting high chromatin remodelling activity, ALT phenotype, and worse prognosis (*intermediate* group (Di Domenico *et al*, 2020) , group *D* (Moser *et al*, 2024), group *T2* (Lakis *et al*, 2021)).

A proteogenomic profiling has recently been proposed to further refined PanNET classification. In an integrated multi-omics study, Ji *et al.* (Ji *et al*, 2025) integrated genomic, transcriptomic, and proteomic data, and identified a three-protein signature that independently stratifies patient prognosis. Comprehensive proteomic and phosphoproteomic analyses delineated four molecular subtypes, each characterised by distinct signalling pathways, immune compositions, and clinicopathological features, with implications on precision treatment.

2. The Tumour Microenvironment

PanNETs possess a distinctive tumour microenvironment (TME) that plays a pivotal role in their biology, progression, and response to therapy. The PanNET microenvironment comprises a complex interplay between tumour cells, endothelial and stromal compartments, immune elements, and the extracellular matrix. This ecosystem sustains tumour growth through the promotion of angiogenesis, metabolic crosstalk, and immune evasion, and is increasingly recognised as a key therapeutic target in the oncologic management (De Palma *et al*, 2017; Cives *et al*, 2019).

Vascular compartment

A defining feature of PanNETs is their remarkable vascularity, which reflects their endocrine origin. Normal endocrine organs display a dense capillary network that facilitates the rapid exchange of hormones and metabolites and allows tight feedback regulation. This specialised architecture depends on the constitutive expression of potent angiogenic mediators, chiefly vascular endothelial growth factor A (VEGF-A), by normal endocrine cells (Dumortier *et al*, 1999). PanNETs retain this property, exhibiting hypervascularisation that is both a hallmark of their biology and a diagnostic signature readily visualised on contrast-enhanced imaging (Öberg, 1994; Kim et al, 2015). Up-regulation of VEGF-A, its receptors VEGFR1 and VEGFR2, and other pro-angiogenic

factors such as platelet-derived growth factor (PDGF) and fibroblast growth factors (FGFs) sustains continuous endothelial activation within both tumour and stromal compartments (Capdevila *et al*, 2017), promoting nutrient delivery and interstitial remodelling. However, paradoxically, vascular density (microvascular density, MVD) does not correlate with aggressiveness in the conventional sense. Multiple studies have demonstrated the so-called "neuroendocrine paradox", whereby highly vascularised PanNETs are the most differentiated and least aggressive lesions, whereas poorly differentiated high-grade neoplasms are hypovascular but more malignant (Couvelard *et al*, 2005; Marion–Audibert *et al*, 2003; Takahashi *et al*, 2007; Scoazec, 2013). In physiological terms, the maintenance of a dense vascular network appears to represent a marker of endocrine differentiation, rather than a predictor of proliferation or metastatic potential. Indeed, VEGF expression tends to decrease with increasing tumour grade, and well-differentiated G1-G2 tumours preserve VEGF levels similar to normal islets, showing minimal hypoxia (Couvelard *et al*, 2008, 2005). By contrast, aggressive PanNETs lose the capacity to sustain microvascular development and instead exhibit reduced MVD, irregular capillaries, and activation of a compensatory angiogenic switch in response to hypoxia (Terris B *et al*, 1998; Takahashi *et al*, 2007; Turner *et al*, 2003). The resulting vessels are tortuous and permeable, with irregular endothelial morphology and incomplete pericyte coverage, features typical of functionally abnormal tumour vasculature (Carrasco *et al*, 2017; Baluk *et al*, 2005).

Figure 2. The neuroendocrine paradox in pancreatic neuroendocrine neoplasms. *(Created with BioRender). Schematic representation of the relationship between vascular architecture, differentiation, and tumour aggressiveness* (Couvelard *et al*, 2005; Carrasco *et al*, 2017). *Well-differentiated PanNETs exhibit high MVD and maintain VEGF expression levels comparable to normal endocrine tissue. These tumours display a stable and organised capillary network with tight endothelial junctions, minimal hypoxia, and limited angiogenic activity. In contrast, aggressive PaNENs lose the capacity to sustain dense microvasculature, resulting in reduced MVD, hypoxia, and activation of the angiogenic switch. Their vasculature is characterised by irregular, fenestrated, and highly permeable vessels, reflecting structural and functional instability.*

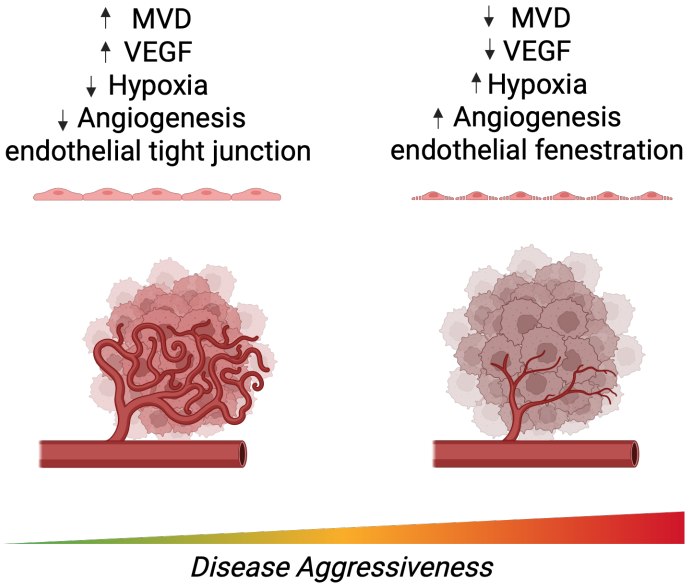

MVD, microvascular density; *VEGF*, vascular endothelial growth factor

Clinically, this inverse correlation between vascular density and tumour grade carries prognostic significance: lesions with low MVD are associated with greater metastatic potential and poorer survival, while highly vascular tumours correspond to indolent disease courses (Couvelard *et al*, 2005; Marion–Audibert *et al*, 2003). Another feature that has been subject of studies in PanNENs, is the presence of hypoxia within the neoplastic tissue, condition that occurs due to a decrease in MVD, as vessels progressively regress upon the progression of the tumour. Hypoxia is a common characteristic of various cancers, and it is an indicator of aggressiveness and poor survival (Harris, 2002). Hypoxia-inducible factor 1 (HIF-1) is a transcription factor that regulate the adaptive responses to a reduced oxygen availability, and it plays a critical role in the expression of numerous genes involved in angiogenesis, glycolysis, cell proliferation, cell survival and metastasis upon hypoxic conditions (Semenza, 2003; Semenza & Glazer, 2000).

Specifically, hypoxia-inducible factor-1 (HIF-1), carbonic anhydrase IX (CA-9) and glucose transporter 1 (GLUT-1) and lactate transporter monocarboxylate transport 4 (MCT-4) have been identified as prognostic markers in PanNETs, involved in adaptive response to reduced oxygen availability. HIF-1 is a heterodimer formed by a HIF-1β subunit and a HIF-1α subunit. Under normoxia, the HIF-1α subunit is rapidly hydroxylated and degraded through von Hippel-Lindau (VHL)-mediated ubiquitylation; however, in hypoxic conditions, it stabilises and translocates to the nucleus, activating transcription of genes regulating angiogenesis, glycolysis, and cell survival (Semenza, 2003; Semenza & Glazer, 2000), Among these targets, CA-9 (Couvelard *et al*, 2005), GLUT-1(Fujino *et al*, 2016), and MCT- 4 (Ullah *et al*, 2006), are particularly relevant, favouring tumour progression. In PanNENs, it was observed that well-differentiated tumours showed a higher HIF-1α cytoplasmic expression whereas poorly differentiated ones, with high mitotic index and low MVD, have a lower HIF-1α cytoplasmic score (Couvelard *et al*, 2005). CA-9 maintains intracellular pH homeostasis under glycolytic stress and promotes extracellular acidification, matrix degradation, and epithelial-to-mesenchymal transition (Mcdonald *et al*, 2012; Shin *et al*, 2011; Švastová *et al*, 2003). In PanNENs, CA-9 expression correlates positively with WHO grade and stage, as well as with reduced MVD and poorer recurrence-free survival (Kim *et al*, 2018; Couvelard *et al*, 2005). GLUT-1 up-regulation similarly reflects enhanced glucose demand and metabolic reprogramming under hypoxia, and its expression in PanNETs associates with increased Ki-67 index and adverse outcome (Fujino *et al*, 2016; Macheda *et al*, 2005; Sampedro-Núñez *et al*, 2020). Moreover, glycolytic cells are characterized by the expression of the lactate transporter MCT-4, which is involved in the efflux of lactic acid. MCT-4 expression was observed to be associated with hypoxic conditions, and its upregulation dependent on HIF-1α. Indeed, its overexpression is a cellular adaptive response that enables the export of the increased lactic acid quantities produced during hypoxia (Ullah *et al*, 2006). MCT-4 has been demonstrated to be a relevant predictor of PanNENs behavior, as it was observed to be positively correlated with tumour stage, grading and relapse (Straub J et al, 2020; Bräutigam, […], Battistella et al, *submitted*).

Other key angiogenic pathways implicated in PanNET progression and interconnected with VEGF signalling include the FGF/FGFR and PDGF/PDGFR axes, semaphorins and angiopoietins (Lauricella *et al*, 2022). FGF signalling has a dual action: it directly

promotes endothelial cell migration, vessel formation, and maturation, and also acts as a central regulator of pro-angiogenic molecules (Vitale *et al*, 2021; Beenken & Mohammadi, 2009). PDGF primarily mediates pericyte recruitment and vessel coverage, contributing to vascular stabilisation (Cavalcanti *et al*, 2019; Allt & Lawrenson, 2001). Finally, increasing evidence highlights the role of semaphorins (Saxena *et al*, 2018; Zuazo-Gaztelu *et al*, 2019) and angiopoietin-2 (Ang-2) (Detjen *et al*, 2010; Srirajaskanthan *et al*, 2009), in driving neoangiogenesis through the induction of vascular instability and increased permeability. Furthermore, increasing evidence also highlights the tight interplay between angiogenesis and immune regulation in PanNETs, with pro-angiogenic pathways, Ang-2, contributing to the development of an immunosuppressive tumour microenvironment (Cives *et al*, 2019; Lee *et al*, 2023).

From a therapeutic standpoint, the distinctive vascular biology of PanNETs provides a strong rationale for the clinical activity of anti-angiogenic agents, which leverage the dependence of well-differentiated tumours on pro-angiogenic signalling (Lauricella *et al*, 2022).

In summary, the vascular compartment represents a paradoxical yet biologically consistent phenomenon, wherein hypervascularisation reflects cellular differentiation rather than aggressiveness (Scoazec, 2013). In contrast, poorly differentiated lesions exhibit diminished vascular density yet heightened angiogenic signalling activity. Understanding this complex interplay, linking angiogenic maintenance, hypoxic adaptation, and immune modulation, is therefore fundamental to elucidating PanNET pathophysiology and optimising therapeutic strategies for these neoplasms.

Stromal Compartment

Cancer-associated fibroblasts (CAFs) are a major component of the tumour microenvironment. Although their role in PanNETs has been less extensively characterised than in ductal counterpart (Zhang *et al*, 2022), accumulating evidence underscores their relevance in the neuroendocrine setting. Both in vitro and in vivo studies have demonstrated that CAFs can promote NET cell proliferation through the secretion of pro-mitogenic cytokines (Dumortier *et al*, 2000; Cives *et al*, 2019). Clinically, more aggressive PanNETs display reduced microvascular density and increased stromal

fibrosis (Battistella *et al*, 2022), features associated with advanced disease and higher proliferative index, suggesting a role for stromal remodelling in tumour progression. Supporting this concept, a recent study (Lou *et al*, 2025) identified tumour-derived apolipoprotein E (ApoE) as a central mediator of tumour-stroma crosstalk: ApoE drives endothelial cells toward a tip-like angiogenic phenotype and activates ATF6-PDGF signalling, promoting fibroblast recruitment and activation. This cascade enhances fibrosis, angiogenesis, and hypoxia, collectively fostering a pro-tumoural microenvironment and correlating with adverse clinical outcomes.

Immune Compartment

Despite their pronounced vascularisation, well-differentiated PanNETs are widely regarded as immunologically "cold" tumours, characterised by low effector T-cell infiltration and limited antitumour immune activation. To date, relatively few studies have focused on the immune compartment in PanNETs and, although further characterisation is warranted, the following immune features have been described:

T-cell infiltration has been detected in the majority of metastatic PanNETs; nonetheless, those with low intratumoral $CD3^+$ T-cell density exhibited significantly poorer disease-free survival after surgical resection (Katz *et al*, 2010). Regulatory T cells are enrinched in higher-grade PanNETs and are associated with adverse prognosis (Katz *et al*, 2010; de Reuver *et al*, 2016), underscoring the progressive establishment of an immunosuppressive microenvironment.

Mast cells also appear to contribute to PanNET progression, through the regulation of inflammatory and neoangiogenic pathways (Soucek *et al*, 2007). In addition, tumour-associated macrophages are also involved in the angiogenic switch, tumour growth, and metastatic spread (Pyonteck *et al*, 2012), and their intratumoral density intratumoral density has been identified as an independent prognostic factor for postoperative recurrence (Wei *et al*, 2014).

Finally, in recent years several investigations have explored the role of immune checkpoint signalling in NET and NEC (Al-Toubah *et al*, 2020). PD-L1 expression and PD-1^+ lymphocytic infiltration appears to be low in well-differentiated PanNETs and to

become more pronounced only in higher-grade or poorly differentiated neuroendocrine carcinomas.

Multiple mechanisms contribute to the establishment of this tolerogenic niche. Among them, VEGF-A-induced endothelial dysfunction is a key determinant. Indeed, sustained VEGF-A signalling remodels the tumour vasculature and downregulates endothelial ICAM-1 and VCAM-1, two adhesion molecules essential for lymphocyte tethering and trans-endothelial migration, thereby restricting T-cell entry into the tumour bed (Motz & Coukos, 2013, 2011).

Moreover, a study by De Palma et al. (De Palma *et al*, 2005) identified a population of pro-angiogenic myeloid cells, TIE2-expressing monocytes (TEMs), that are actively recruited into the tumour tissue. TEMs mobilization is drive by tumour-derived Ang-2, and within the TME, TEMs promote inflammation and angiogenesis, cooperating in tumour growth and metastases formation (Figueroa-Vega *et al*, 2010).

This tight coupling between aberrant angiogenesis and immune suppression highlights the urgent need for translational preclinical models that faithfully recapitulate the PanNET microenvironment, enabling the investigation of mechanisms underlying tumour progression and the evaluation of emerging therapeutic strategies targeting both tumour-intrinsic and microenvironmental vulnerabilities.

3. Therapeutic Options for Pancreatic Neuroendocrine Tumours

The therapeutic management of PanNETs is primarily determined by tumour stage, which stratifies lesions as resectable or unresectable, in association with tumour grade, SSTR expression, and clinical behaviour (Kos-Kudła *et al*, 2023). According to these parameters, three main therapeutic options may be followed: active surveillance, surgery, and medical treatment (**Figure 3**) (Pavel *et al*, 2020).

Figure 3. Therapeutic management of Pancreatic Neuroendocrine Tumours (adapted from Pavel et al, 2020**).** *PanNET*, pancreatic neuroendocrine tumour, *F*-, functioning; *NF*-, nonfunctioning

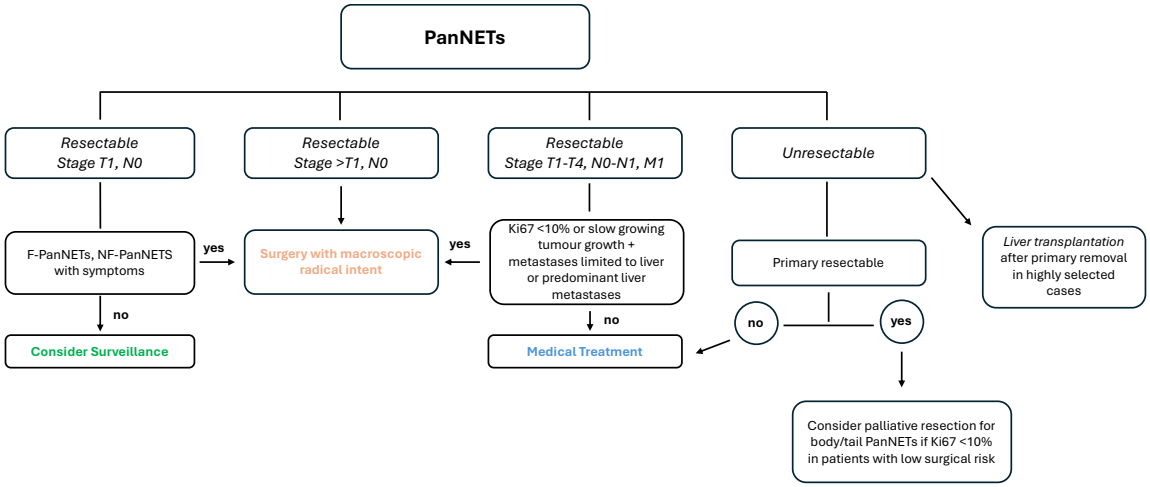

Local disease

Active surveillance Strategy

For small (<2 cm), asymptomatic, low-grade NF-PanNETs with no signs of radiological progression, a policy of active surveillance is recommended (Kos-Kudła *et al*, 2023). Several retrospective series confirm that well-differentiated G1 lesions can remain stable for years, and surgical intervention does not improve outcomes (Partelli et al, 2016; Gaujoux et al, 2013; Ricci et al, 2022; Partelli et al. 2025, ASPEN trial). Small umours showing sign of aggressiveness, as tumour growth, ductal dilation, vascular invasion, or nodal disease, however, should prompt therapeutic intervention (Kos-Kudła *et al*, 2023).

Surgical Resection

Surgery remains the only curative option for localised PanNETs. Surgery is indicated for resectable, non-metastatic tumours. In this context, formal pancreatic resections (i.e., pancreatoduodenectomy, distal pancreatectomy, total pancreatectomy) are generally recommended. Of note, lymphadenectomy is recommended for tumours > 3 cm or with radiological suspicion of nodal involvement (Kos-Kudła *et al*, 2023; Partelli *et al*, 2025).

Despite the high curative rates associated with surgical resection, approximately 15-30% of patients experience disease recurrence within five years from surgery (Pulvirenti *et al*, 2023; Genç *et al*, 2018; Dong *et al*, 2020; Andreasi *et al*, 2022). These observations underscore the need for a careful and biologically informed evaluation of the risks associated with surgical decision-making. In selected cases, surgery may ultimately represent a futile intervention, and the use of multimodal treatment strategies might better mitigate the risk of early postoperative recurrence. Conversely, in other instances, nonoperative management may constitute a more appropriate therapeutic choice, particularly for patients with lesions that exhibit features of low-risk aggressive potential. Importantly, pancreatic surgery carries a substantial burden of perioperative morbidity, including major complications (Souche *et al*, 2020; van Hilst *et al*, 2019), as well as long-term metabolic sequalae (De Mestier *et al*, 2020; Slezak & Andersen, 2001; Yu *et al*, 2020). Thus, in specific cases, surgical resection may constitute an overtreatment, exposing patients to unnecessary and potentially harmful interventions without proportional oncologic benefit.

Advanced disease

Surgery

Surgery, both curative and palliative, can play a role in metastatic disease in selected patients with for well-differentiated, indolent PanNETs with hepatic involvement. Spe-Specifically, radical surgery is associated with improved overall survival (OS) and prognosis; however, even less radical procedures, such as debulking or resection of the primary tumour alone, have been shown to provide prognostic benefits (Scott & Howe, 2019; Morgan *et al*, 2018). In terms of LM burden classification, type I is defined by the presence of a single LM, type II includes an isolated metastatic bulk accompanied by smaller deposits, and type III is characterized by diffuse, widespread liver involvement (Frilling *et al*, 2009). According to current guidelines (Partelli *et al*, 2017; Pavel *et al*, 2020) patients with type I and type II LMs are considered suitable candidates for radical surgery, while those with type III LMs are generally recommended for systemic treatment or, in highly specific cases, liver transplantation.

Somatostatin Analogues

Somatostatin analogues (SSAs) constitute the first-line therapy for well-differentiated, SSTR-positive PanNETs with low proliferative activity (Ki-67 < 10%), in accordance with ENETS 2023 guidelines (Kos-Kudła *et al*, 2023). Somatostatin inhibits hormone secretion, angiogenesis, and tumour proliferation via five receptor subtypes (SSTR1-5) belonging to the G-protein-coupled receptor family (Öberg, 1994). The clinically approved SSAs, octreotide and lanreotide, share high affinity for SSTR2 and moderate affinity for SSTR5, aligning with the receptor profile typically expressed in PanNETs (Khanna *et al*, 2020). Initially introduced for symptom control, both agents have demonstrated antiproliferative efficacy, significantly prolonging progression-free survival (Caplin *et al*, 2014; Rinke *et al*, 2017). Their mechanisms involve receptor-mediated inhibition of growth and induction of apoptosis, as well as indirect modulation of angiogenesis and immune activity (Rinke & Krug, 2016).

Targeted Therapies

The introduction of molecularly targeted agents has transformed the systemic landscape for advanced PanNETs. Two agents, everolimus and sunitinib, are established second-line therapies:

- Everolimus, an mTOR inhibitor, acts downstream of PI3K–AKT signalling(Wullschleger *et al*, 2006). In the RADIANT-4 trial, everolimus prolonged progression-free survival (PFS) compared with placebo in well-differentiated PanNETs (Yao *et al*, 2016).
- Sunitinib, a multitargeted tyrosine-kinase inhibitor (TKI) acting on VEGFR, PDGFR, KIT, and FLT3 (Raymond *et al*, 2011b), demonstrated significant improvement in PFS and overall survival (Raymond *et al*, 2011b, 2018). The dual inhibition of angiogenic and growth-factor pathways aligns with the highly vascular phenotype of PanNETs.

However, the clinical efficacy of everolimus and sunitinib is limited by the development of resistance and by treatment-related toxicities (Beyens *et al*, 2019), underscoring the need for new, more effective molecularly targeted strategies.

More recently, the CABINET phase III trial (Chan *et al*, 2025) evaluated cabozantinib, a TKI targeting VEGFR2, MET, AXL, and RET (You *et al*, 2011). In PanNETs, cabozantinib reduced the risk of progression or death by nearly 40 % compared with placebo, confirming potent anti-angiogenic and stromal-modulating activity. The drug has recently received approval from the *European Medicines Agency* (17.09.2025) and is expected to be incorporated soon into recommended therapeutic options.

Cytotoxic Chemotherapy

Chemotherapy remains relevant for tumours of intermediate or high grade (Ki-67 > 10 %), for rapidly progressive disease, or when targeted agents fail. The CAP-TEM regimen (capecitabine with temozolomide) represents the preferred cytotoxic backbone (Pavel *et al*, 2020; Kunz *et al*, 2023). Temozolomide activity has proven to correlate with O6 methylguanine-DNA-methyltransferase (MGMT) promoter methylation status (Liu & Gerson, 2006) in retrospective and prospective studies (Walter *et al*, 2015; Brighi *et al*, 2023), supporting its potential role as predictive biomarkers.

Streptozocin-based combinations, once standard, remain an alternative where temozolomide is contraindicated or as rescue therapy (Capdevila *et al.* ESMO abstract 2024). Platinum/etoposide, or irinotecan- , oxaliplatin-based protocols can be considered for high-grade poorly-differentiated NECs (Garcia-Carbonero *et al*, 2016).

Radioligand Therapy

Peptide receptor radionuclide therapy (PRRT) represents a major therapeutic advance in the management of SSTR-positive PanNETs. This treatment modality delivers targeted internal radiation through radiolabelled somatostatin analogues that bind SSTR-expressing tumour cells, enabling the selective deposition of cytotoxic β-particles. The β-emitter ^{177}Lu-DOTATATE is currently the most widely used agent: it induces double-stranded DNA breaks and apoptosis while sparing surrounding healthy tissue (van der Zwan *et al*, 2015). The pivotal *NETTER-1* trial first demonstrated the efficacy of ^{177}Lu-DOTATATE in well-differentiated, progressive neuroendocrine tumours, significantly prolonging progression-free survival in advanced, progressive midgut neuroendocrine

tumours (Strosberg *et al*, 2017). More recently, the *NETTER-2* study (Singh *et al*, 2024) extended these findings by showing that first-line ^{177}Lu-DOTATATE plus octeotride confers a marked improvement in disease control in advanced grade 2-3 gastroenteropancreatic NETs, including PanNETs.

Moreover, the potential role of PRRT as a neoadjuvant therapy in locally advanced disease has recently been investigated in the *NEOLUPANET* study (Partelli *et al*, 2024b), yielding promising results.

Therapeutic Sequencing

Treatment selection depends on multiple variables, including clinical presentation, tumour differentiation, proliferation index, SSTR expression, disease dissemination, and patient comorbidities (Panzuto *et al*, 2024).

For indolent, SSTR-positive NF-PanNETs, the sequence SSA, followed by second line treatment target therapies/ PRRT remains reasonable. In higher-grade or receptor-poor tumours, earlier introduction of chemotherapy is appropriate (Kos-Kudła *et al*, 2023). Clinical decisions should also consider toxicity profiles and patient preference, as PanNETs often follow a chronic course requiring long-term management. Despite substantial advances with targeted and radionuclide therapies, the treatment of advanced PanNETs remains challenging, and only a fraction of patients treated profits, as most patients eventually experience disease progression (Coelho *et al*, 2022).

The recent focus of translational research has shifted towards therapies that exploit angiogenic dependence, stromal biology, tumour immunogenicity, and drugs combinations (Cives *et al*, 2019; Lauricella *et al*, 2022; Rinke *et al*, 2021; Gulde *et al*, 2022; Al-Toubah *et al*, 2020; Mandriani *et al*, 2022; Cives *et al*, 2020). These emerging therapeutic strategies underscore the need for physiologically relevant models that recapitulate the PanNET microenvironment, enabling the study of treatment responses as well as the mechanisms underpinning tumour evolution and therapeutic resistance or sensitivity.

Figure 4. Algorithm of G1-2 nonfunctioning pancreatic neuroendocrine tumours treatment *(adapted from* Kos-Kudła *et al*, 2023) *[a]Preferably for Ki 67 < 10%. [b]PRRT or chemotherapy or TAE/other liver directed therapy if cytoreductive intent. SRI, somatostatin receptor imaging; PRRT, peptide receptor radionuclide therapy*

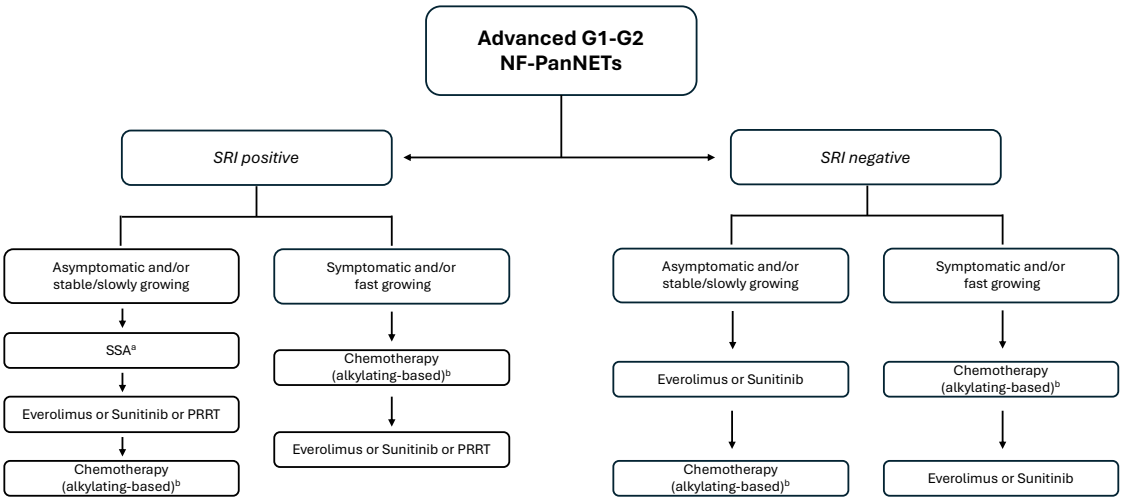

4. Tumours Preclinical Models

Different preclinical Models in Oncology

Preclinical models are indispensable tools in experimental oncology for understanding tumour biology, elucidating therapeutic mechanisms, and developing personalised-medicine strategies. Models range from conventional two-dimensional (2D) cell cultures to advanced three-dimensional (3D) and *in vivo* systems, each offering distinct advantages and limitations (Ear et al., 2024; Cros et al., 2025) (**Table III**).

Table III. Advantages and disadvantages of 2D and 3D in vitro cultures *(Adapted from* Barozzi & Scielzo, 2023)

2D cultures	3D cultures
Non-physiological adhesion to plastic surface	Surrounded by ECM
Adhesion restricted to 1 plane	Adhesion distributed to all 3 dimensions, preserving natural cell shape
Lower number of cell junctions	Higher number of cell junctions that allow for cell-cell communication
High stiffness (GPa range) of both coated and non-coated glass or plastic surfaces	More physiological stiffness (KPa range) of 3D matrices in scaffold-based models
X-Y plane migration	X-Y-Z multidimensional migration
Absence of soluble gradients	Presence of soluble gradients created in the complexity of a tissue-like environment
Often high sensitivity to drugs	More accurate metabolism of drugs and their effects
Unnatural proliferation rate and poor differentiation	Realistic proliferation rate and higher predisposition to differentiation
Cheaper	More expensive and time-consuming
Easily standardizable and optimal for large-scale studies	More difficult to standardize for large-scale studies
Easily interpretable analysis	More difficult to interpret data, and often necessary to optimize protocols used for 2D cultures
Necessarily used with animal models	Help reduce the need for animal models

In green are highlighted the advantages of cell culture methods.
2D, two-dimensional; 3D, three-dimensional; ECM, extracellular matrix

Traditional 2D monolayer cultures enable rapid, cost-effective assessment of tumour-cell proliferation, signalling, and drug sensitivity. However, they fail to recapitulate key features of tumour organisation, extracellular matrix (ECM) interactions, and microenvironmental gradients that define *in vivo* behaviour (Jensen & Teng, 2020). As a result, many drugs demonstrating potency in 2D assays underperform in clinical trials.

The advent of 3D culture systems, including spheroids, patient-derived tumour organoids, and patient-derived tumoroids, has markedly advanced the study of tumour biology in oncological field. These "scaffold-free" models provide a closer approximation of *in vivo* architecture and inter-cellular interactions than traditional 2D

cultures. Moreover, they reproduce gradients of oxygen, nutrients, and waste similar to those in solid tumours. In particular, spheroids are generated from established cell lines whereas organoids and tumoroids are derived directly from patient tissue. Specifically, organoids represent long-term, self-organising aggregates of patient-derived cells (either tumour cells or pluripotent, stem, progenitor or differentiated cells) that can be expanded *in vitro* indefinitely. Tumoroids derive only from tumour cells and are suitable for short-term analysis as can be expanded only for few passages (Zhao *et al*, 2022; Durymanov, 2025).

More recently, cell seeding on scaffolds (Barozzi *et al*, 2025; Peloso *et al*, 2018), bioprinted constructs (Ribezzi *et al*, 2025; Sbrana *et al*, 2021; Neufeld *et al*, 2022), precision-cut tumour slices (Collins *et al*, 2025), and "tumour-on-chip" devices (Chen *et al*, 2017)**,** have revolutionised translational research by allowing the reconstruction of tissue architecture and cellular heterogeneity. These models enable co-culture with endothelial, stromal or immune cells in a 3D environment, to simulate the tumour microenvironment and vasculature.

Cell seeding on scaffolds involves the deposition ("seeding") of tumour or stromal cells onto pre-formed three-dimensional matrices composed of natural polymers (e.g., collagen, fibrin, silk) or synthetic materials (e.g., PLLA, PEG-based hydrogels), allowing cells to freely organize within the matrix (Caliari & Burdick, 2016). This method provides mechanical support and topographical cues that guide proliferation and differentiation, while preserving physiological stiffness and porosity (Saydé *et al*, 2021). Scaffold composition can be tuned to replicate specific tissue mechanics, and decellularized extracellular matrices offer organ-specific biochemical signals (Rosellini & Cascone, 2025; Guruswamy Damodaran & Vermette, 2018). Such systems are particularly useful for modelling interactions between neoplastic and stromal compartments and for evaluating drug penetration across complex matrices (Nyga *et al*, 2011). However, this technique presents two major limitations: substantial technical variability introduced by repeated manual seeding, and the difficulty of achieving defined, customised, and spatially precise architectures or compartments.

Bioprinted constructs (Neufeld *et al*, 2022) employ additive manufacturing to reproduce spatially organised tumour tissue by embedding living cells in biocompatible "bioinks." Bioinks are hydrogel which are mixed in their liquid form with cells extruded into predefined architectures generated through computer-aided design (CAD) (Murphy & Atala, 2014; Hull *et al*, 2022; Jung *et al*, 2022a). Following printing, the hydrogel matrices are crosslinked to provide mechanical stability while maintaining high cell viability. Composed of natural polymers (e.g., collagen, gelatin, fibrin, alginate, decellularized matrix), as well as synthetic materials (e.g., PEG or PLLA), these hydrogels function as extracellular matrix analogues that support cell proliferation, differentiation, and migration. Careful selection of the most appropriate bioink formulation is therefore essential to ensure compatibility with the biological requirements of the incorporated cell types (Murphy & Atala, 2014; de Barros *et al*, 2023; Jung *et al*, 2022b). Bioprinted constructs can accommodate diverse cellular populations to emulate tissue organisation or the tumour microenvironment. Importantly, this technology allows the precise compartmentalisation of distinct cell types within defined three-dimensional arrangements, thereby recapitulating the spatial complexity of native tissues, an advantage over conventional cell-seeding approaches, which cannot ensure homogeneous or spatially controlled distribution. Recent advances in multi-material bioprinting further enable the integration of multiple bioinks with varied mechanical and biochemical properties within a single construct, enhancing control over microenvironmental cues and facilitating the study of intercellular communication and gradient-mediated signalling (Ribezzi *et al*, 2023; Shukla *et al*, 2024; Sharma *et al*, 2023).

Precision-cut tumour slices (PCTS) constitute an *ex vivo* platform preserving the native tissue architecture, vasculature, and immune microenvironment. Thin slices obtained from surgical or experimental tumours can be cultured under controlled oxygenation and perfusion, maintaining cellular heterogeneity and metabolic activity for several days. PCTS retain the histological and transcriptional complexity of the parent tumour and are amenable to high-throughput pharmacological screening, providing a clinically relevant bridge between *in vitro* systems and *in vivo* responses (Collins *et al*, 2025).

Finally, tumour-on-chip devices integrate microfluidics and 3D culture to reproduce dynamic aspects of tumour physiology such as nutrient gradients, shear stress, and

immune–vascular interactions. These microscale bioreactors allow precise control of flow and enable real-time imaging of processes including intravasation and endothelial barrier modulation (Chen *et al*, 2024; Quintard *et al*, 2024). By co-culturing tumour, stromal, and immune cells within interconnected microchannels, tumour-on-chip models provide an advanced platform for investigating therapy response under near-physiological conditions.

Indeed, dynamic perfused systems, such as micro- and milli-fluidic platforms, further emulate vascular perfusion and interstitial shear stress, thereby reproducing the biomechanical forces of the native tumour milieu. These systems provide a controllable environment in which to study mechanisms of tumour invasion and metastatisation. Moreover, these systems offer a physiologically relevant pharmacokinetic conditions for drug-response assessment.

Complementary *in vivo* models, primarily murine xenografts and genetically engineered mice (GEMMs) (Ireson *et al*, 2019), as well as zebrafish (Phillips & Westerfield, 2014) remain essential for studying systemic interactions, angiogenesis, metastasis, and immune responses, that cannot be captured *ex vivo*. Yet these models carry limitations: cost, ethical considerations, and interspecies differences in tumour biology and pharmacodynamics. Hence, a rational integration of *in vitro*, *ex vivo*, and *in vivo* platforms is crucial to developing predictive and clinically translatable models.

Figure 5. Overview of the spectrum of available preclinical models, arranged according to their relative throughput and physiological relevance. *(Created with BioRender)*

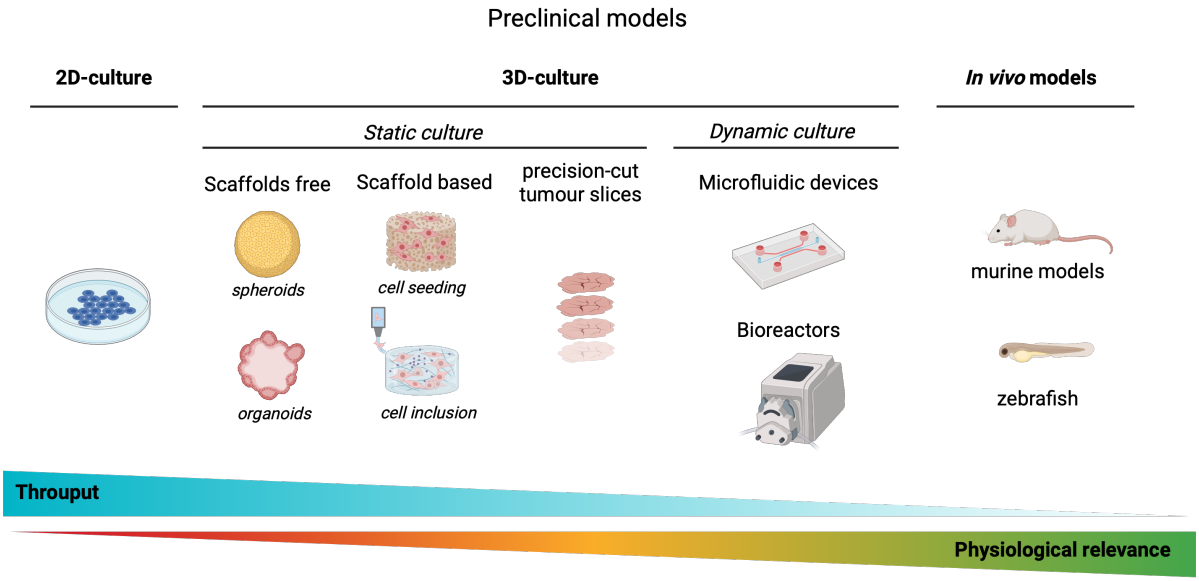

Preclinical Models of Pancreatic Neuroendocrine Tumours

Only a limited number PanNEN-derived cell lines are currently available, mainly due to the rarity of these neoplasms and to the disease biological heterogeneity, making it difficult to generate them.

Two-dimensional (2D) culture Models

Owing to the typically low proliferative rate of the majority of PanNENs, the establishment of cell lines results particularly challenging. PanNENs cell lines include: poorly differentiated lines BON-1 and QGP-1, and, more recently, four well-differentiated PanNET cell lines, NT-3, NT-36, and the isogenic pair NT-18P and NT-18LM, which better recapitulate the molecular and phenotypic features of human disease.

- **BON-1**, derived from a lymph-node metastasis of a serotonin-producing pancreatic carcinoid, is a poorly-differentiated line (PanNEC) with mutations in *PIK3CA* and *TP53* (Vandamme *et al*, 2015). It exhibits robust proliferation with a Ki-67 of 80.6% ± 3.3%, expresses chromogranin A and synaptophysin and low SSTR expression.
- **QGP-1**, established from a poorly differentiated somatostatin-producing pancreatic tumour (PanNEC), TP53 mutant, and exhibits low SSTR expression level. QGP-1 cells display high proliferation rates with a Ki-67 of 82.6% ± 1.0% (Kaku et al, 1980).
- **NT-3**, isolated from a lymph-node metastasis of an insulinoma**,** that has lost insulin secretion and retains well-differentiated morphology and neuroendocrine markers expression. It shows wild-type *TP53* and *KRAS* status, MEN1 mutant, and a Ki67 of 14.6% ± 1.0% (Benten *et al*, 2018).
- **NT-36**, isolated from a local recurrence 12 months after initial surgery and chemotherapy treatment (Viol *et al*, 2022). NT-36 retain well-differentiate morphology and neuroendocrine markers. The cell line exhibits low SSTR expression, a Ki-67 index of approximately 27.71% ± 2.34%, and harbours MEN1 and DAXX mutation. NT-36 retain well-differentiate morphology and neuroendocrine markers.

- **NT-18P** and **NT-18LM**, derived respectively from primary and liver-metastatic lesions of the same non-functioning PanNET G3, provide a unique isogenic pair for analysing metastatic evolution (Viol *et al*, 2022). Both cell lines are MEN1, DAXX mutant. Proliferative index of NT-18P and -18LM are Ki67: 25.18% ± 2.35% and Ki67: 25.57% ± 1.59%, respectively.

These 2D culture models collectively capture key features of PanNET biology, chromatin dysregulation, mTOR signalling, and vascular gene expression, but remain limited in their ability to model stromal and immune components. Moreover, another constrains related to these models, is the lack of cell lines derived from low-grade (G1-G2), NF- PanNETs, which constitute the predominant clinical subtype. These limitations represent a major gap in the PanNET field.

Three-dimensional (3D) culture Models

In Vitro and Ex Vivo Models

3D systems represent a major step toward recapitulating *ex vivo* PanNETs. Cell lines spheroids (Bresciani *et al*, 2019), as well as patient-derived tumoroids (April-Monn *et al*, 2021) and organoids (Dayton *et al*, 2023) have been successfully generated from surgical specimens, maintaining neuroendocrine markers and somatostatin-receptor expression. Nevertheless, the TME is not represented in these models, therefore decreasing their power of representation of the tumour.

To overcome these limitations, Herring et al (Herring *et al*, 2021) developed dynamic culture systems for patient-derived PanNET surrogates, in which dissociated primary tumour tissue was re-embedded in Matrigel. This approach successfully preserved tumour cellularity and partial representation of endothelial and immune components although in minimal side. However, it failed to maintain the native tissue architecture and spatial organisation of the tumour compartments.

More recently, with a specific focus on the tumoral immune compartment, Doornebal et al. (Doornebal *et al*, 2022) introduced immunocompetent PCTS models derived from neuroendocrine liver metastases. While these models maintain tumour architecture and

inter-cellular interactions *ex vivo*, their use of metastatic tissue alone limits their applicability for guiding therapeutic decisions at the time of primary disease progression.

In Vivo Models

Murine models have long served as the foundation of in vivo PanNET research. The RIP1-Tag2 transgenic mouse, expressing the SV40 T-antigen under the rat insulin promoter, remains the most widely used model in the field (Hanahan, 1985). RIP1-Tag2 mice develop aggressive, fast-growing and insulin-secreting PanNECs. Although the biology of these tumours does not recapitulate the slow-growing nature of G1 or G2 human PanNETs, this model has been instrumental in studying angiogenesis, mTOR signalling, and immune evasion, as well as in testing therapeutic effects.

More recently, patient-derived xenografts (PDXs) and cell-line-derived xenografts (CDXs) have expanded the *in vivo* repertoire. However, NET xenografts have a very low successful rate and require a considerable time period (years) (Ear *et al*, 2024; Kaemmer *et al*, 2021). In this context, an emerging alternative is the zebrafish xenograft model (Vitale *et al*, 2014; Gaudenzi *et al*, 2020), which allows live, high-resolution imaging of tumour–stroma–immune interactions in transparent larvae. Human PanNET cell xenografts in zebrafish have been successfully used to study angiogenesis, cell migration, and metastatic dissemination. The model's optical accessibility, rapid assay turnaround, and low cost make it an attractive bridge between *in vitro* and murine studies. Nevertheless, differences in immune maturity and drug metabolism warrant cautious interpretation of translational results.

A further biologically relevant model is represented by spontaneous canine insulinomas, which occur at an incidence approximately ten times higher than in humans (Capodanno *et al*, 2022). Canine models offer distinct translational advantages, including an intact immune system, natural tumour heterogeneity, and shared environmental exposures with humans. However, further genomic characterisation is required to determine the extent to which these tumours share the molecular drivers of human disease, a prerequisite for their validation as comparative oncology models. Moreover, NF-PanNETs are not represented in this model, limiting its applicability to the broader spectrum of pancreatic neuroendocrine neoplasms.

Table IV. PanNETs preclinical models available: pros, cons and preferential applications. *(Adapted from Cros et al, 2025a)*

Model	Pros	Cons	Preferential applications
Cell lines	Easy to handle and to manipulate	Mainly high grade	Mechanistic studies
PDTs	High efficiency Recapitulate molecular features of patients	Cannot be genetically modified Lack of TME Short-term use	Drug screening
PDTOs	Recapitulate molecular features of patients Can be genetically manipulated	Mainly high grade Low efficiency and time-consuming Lack of TME	Drug screening Mechanistic studies
Tumour surrogate	Recapitulate molecular features of patients Include part of TME	Lack tissue architecture and spatial organisation	Drug screening
NELM PDTS	Maintain tumour spatial architecture Include immune components	Only from liver metastases	Drug screening Molecular studies
Mouse models (GEMM)	Full TME	Mainly insulinoma Rarely metastases	Studies on angiogenesis interaction with TME Tumour progression
Xenotransplant (Mouse)	Include part of the TME	Low efficiency in mice Lack of immune system	Drug screening Tumour-stroma interactions
Xenotransplant (Zebrafish)	Include part of the TME High efficiency	Short-term use Difference between human-fish biology	Drug screening Cell migration
Canine models	Full TME	Only aggressive insulinoma Difference between human-dog biology	Tumour progression Drug screening

NET, neuroendocrine tumour; *PDTs*, patient-derived tumoroids; *PDTOs*, patient-derived tumour organoids; *TME*, tumour microenvironment; *NELM*, neuroendocrine tumour liver metastases; *PDTS*, patient-derived tumour slices, *GEMM*, genetically engineered mouse models

Project Aims

The clinical management of PanNETs remains challenging due to their biological heterogeneity, paucity of prognostic markers and reliable preclinical models. The mechanisms underpinning tumour progression and therapeutic resistance are still poorly understood, and consequently, treatment selection often lacks a solid biological rationale.

This thesis seeks to address these gaps by evaluating treatment appropriateness and postoperative morbidity in patients with localised PanNETs, and by integrating *ex vivo*, and advanced bioengineering approaches to develop more predictive platforms for understanding PanNET biology and guiding personalised therapy.

Aim 1) In the first part of this project, we focused on the clinical dimension to assess the currently unmet clinical need. Specifically, we examined surgical appropriateness across a cohort of patients with localized NF-PanNETs to identify potential gaps in patient selection.

Aim 2) Furthermore, we evaluated postoperative morbidity associated with these procedures, focusing on patients undergoing distal pancreatectomy. This analysis provides a critical framework for evaluating current standards of care and identifying areas in which biological insights may refine patient selection.

Aim 3) The third component of the project focused on the predictive value of currently available personalised preclinical models for assessing individual therapeutic response. In particular, we evaluated patient-derived tumour slices (PDTs) from PanNETs spanning grades G1–G3, determining their validity as ex vivo platforms for personalised drug testing. In parallel, developed and optimize the protocol for generation PCTS from primary NF-PanNETs specimens, ensuring preservation of native tissue architecture, vasculature, and stromal composition. To support this work, we established a dedicated study protocol (*3DPanNET, PI A. Battistella, CET 26-2023*), which enabled systematic collection of PanNET specimens from surgical patients at San Raffaele Hospital (HSR). Together, these models permitted interrogation of tumour-microenvironment interactions and their influence on therapeutic response in a physiologically relevant context.

Aim 4) The fourth aim was to establish advanced three-dimensional preclinical models capable of recapitulating both PanNET architecture and its microenvironment. We developed custom-engineered 3D bioprinted constructs to reconstruct the tumour–microenvironment interface, with a particular emphasis on the endothelial compartment. These biofabricated systems provide a novel platform for functional studies aimed at dissecting mechanisms governing tumour progression, invasion, and TME-mediated therapeutic resistance, while also enabling the evaluation of innovative therapeutic strategies targeting both tumour cells and their supporting stroma.

Given the pivotal role of the microenvironment in shaping tumour behaviour, drug response, and progression, the development of physiologically relevant *in vitro* and *ex vivo* systems is critical. Together, the approaches described in this thesis seek to bridge the persistent gap between conventional two-dimensional cultures and *in vivo* models, thereby advancing the establishment of more predictive, mechanistically informative, and personalised translational platforms for PanNET research.

1. Critical appraisal of the adequacy of surgical indications for non-functioning pancreatic neuroendocrine tumours (Partelli, Battistella et al, 2024)

Aim: to investigate treatment appropriateness in patients submitted to surgical resection for localized NF-PanNET to identify potential gaps in patient selection.

Materials and Methods

Study Design and Participants

The present retrospective observational study adhered to the Strengthening the Reporting of Observational Studies in Epidemiology (STROBE) guidelines (von Elm *et al*, 2014). All consecutive patients who underwent potentially curative surgery (R0-R1) for NF-PanNETs at San Raffaele Hospital (Milan, Italy) from November 2002 to March 2022 were considered. Exclusion criteria encompassed patients under the age of 18 years, patients with functioning neoplasms, and individuals diagnosed with poorly differentiated pancreatic neuroendocrine carcinomas (PanNECs). Palliative tumour resection (R2) cases were also excluded. Ethical committee approval was not required due to the retrospective nature of the study.

Definition of Surgical Treatment Appropriateness

The appropriateness of surgical treatment was categorized into three groups: potential overtreatment, appropriate treatment, and potential undertreatment, based on final histologic findings and occurrence of disease relapse within 1 year following surgery.

Radical resection (R0/R1 resection) was achieved in all cases across the three categories, including in presence of distant metastases.

Potential overtreatment group included patients who underwent radical surgical resection but had no histologic evidence of tumour aggressiveness (i.e., G1, T1-T2, N0, M0, no microvascular and/or perineural invasion) and did not experience disease recurrence. Appropriate surgical treatment group included patients who underwent radical surgical resection and had histologic evidence of at least one feature of aggressiveness (i.e., G2-G3, T3-T4, N1, M1, microvascular or perineural invasion) but did not experience disease recurrence within one year following surgery. Potential

undertreatment group comprised patients who underwent radical surgical resection and experienced disease recurrence within one year from surgery.

Data Collection

A comprehensive collection of preoperative, intraoperative and postoperative data was conducted by retrospectively retrieving information from a prospectively maintained institutional database. Preoperative variables, including demographic characteristics (age and gender), body mass index (BMI), and presenting symptoms were reviewed. Performed diagnostic procedures, including computed tomography (CT), magnetic resonance imaging (MRI), endoscopic ultrasound (EUS), and ^{68}Gallium positron emission tomography (^{68}Ga-PET), were documented, along with the radiological tumour site (head/uncinate process vs body/tail) and size (maximum diameter assessed by imaging techniques). The date of surgery was categorized into four surgical time periods (2002-2007, 2008-2012, 2013-2017, 2018-2022) for analysis. Intraoperative parameters included the type of surgery (pancreatoduodenectomy, distal pancreatectomy, total pancreatectomy, enucleation, middle pancreatectomy), surgical approach (laparoscopic *vs* open), and vascular resection. The length of hospital stay (LOS) was calculated from the date of surgery to the date of discharge. Postoperative complications were classified according to the Dindo-Clavien classification of surgical complications (Dindo *et al*, 2004). Postoperative pancreatic fistula (POPF) was graded according to the 2016 definition proposed by the International Study Group on Pancreatic Surgery (ISGPS) (Bassi *et al*, 2017). Long-term pancreatic impairment (endocrine and/or exocrine insufficiency) occurring after surgery was also recorded. Tumour grade was determined based on the 2017 World Health Organization (WHO) classification into G1 (Ki67 <3%), G2 (Ki67 3-20%) and G3 (Ki67 >20%) (Lloyd *et al*, 2017). The Ki67 proliferative index was assessed by MIB1 antibody staining and expressed as the percentage of cells with nuclear staining in 2000 cells, counted in the area of highest nuclear labelling (Klimstra *et al*, 2010). Tumour stage was categorized following the current European Neuroendocrine Tumour Society (ENETS) TNM staging system (Rindi *et al*, 2006). The status of the surgical margins was evaluated and classified as R0 (no residual tumour) and R1 (microscopic residual tumour). R1 resection was defined as the presence of microscopic residual tumour at the resection margins, or in presence of a minimum margin length ≤1 mm. Additionally, the presence of microvascular invasion, perineural

invasion and necrosis was reviewed. Disease-free survival was defined as the time from surgery to any kind of disease recurrence. Overall survival was calculated as the time from surgery to the date of death for any cause, and censored. Disease-specific survival (DSS) was defined as the time from surgery to disease-related death. DFS, OS, and DSS were censored at the last follow-up.

Statistical Analysis

Categorical variables were presented as absolute numbers with corresponding percentages (%), and compared using the the χ^2 or Fisher exact test, as appropriate. Continuous variables were reported as median with interquartile ranges (i.q.r.) for skewed distribution, or as mean (± SD) for normal distributions. The normality of continuous variables was assessed using the Kolmogorov-Smirnov test. Continuous variables were compared between two groups by using Student's t test or Mann-Whitney U test, as appropriate based on the variables' distribution. Kruskal-Wallis test was performed to compare continuous variables between multiple groups. Bonferroni correction was applied to account for multiple comparisons, both for categorical and continuous variables. Receiver operating characteristic (ROC) curve analysis was performed to evaluate radiological tumour size as predictor of treatment appropriateness and to find the best cut-off to preoperatively identify patients at higher risk of overtreatment. The global performance was expressed as area under the curve (AUC). Multivariable logistic regression analysis was performed to identify preoperative predictors of potential surgical overtreatment and undertreatment. Only variables that exhibited significant associations with treatment appropriateness in the univariate analysis were included in the initial multivariable model. A backward stepwise selection procedure was employed to derive the final multivariable model. When necessary, continuous variables were categorized based on their median value.

Survival probability was estimated using the Kaplan-Meier method. The log-rank test was employed to compare DFS, OS, and DSS among the potential overtreatment, potential undertreatment, and appropriate treatment groups. Statistical significance was set at a p-value less than 0.05. All statistical analyses were performed using SPSS version 26.0 for Mac software (SPSS, Inc., Chicago, IL).

Results

Study Participants

A total of 384 patients who underwent surgery for resectable NF-PanNETs were included in the study. Among them, 230 (60%) received an appropriate surgical treatment, whereas 129 (34%) experienced potential overtreatment and 25 (6%) were potentially undertreated (**Figure 6)**

Figure 6. Cohort treatment appropriateness. *Patients (n, %) who underwent surgery for nonfunctioning pancreatic neuroendocrine tumours (NF-PanNETs) and received potential overtreatment, appropriate treatment or potential undertreatment.*

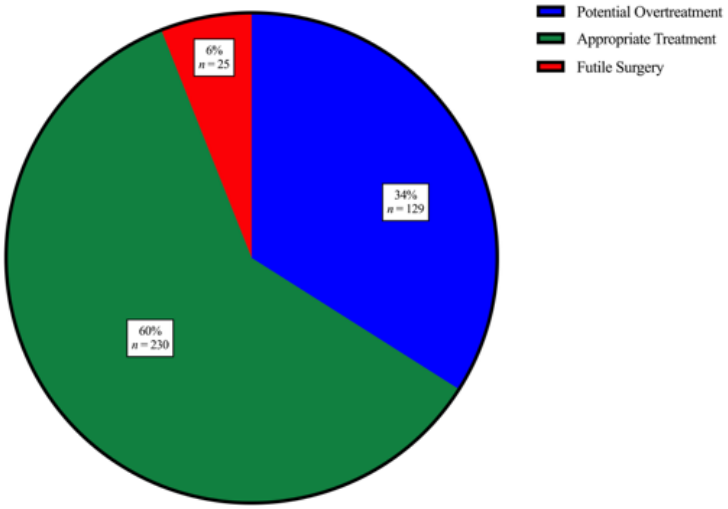

Demographic and Clinico-Radiological Features

Demographics and clinico-radiological characteristics were compared among the three groups, as presented in **Table V**. The analysis revealed a significant association between the type of diagnostic work-up and the appropriateness of surgical treatment (p=0.034). Among the patients within the appropriate surgical treatment group (n=230), the most common diagnostic work-up consisted of a combination of high-quality imaging (CT and/or MRI), EUS and ^{68}Gallium PET (^{68}Ga-PET), performed in 123 patients (54%). A significant difference in the type of diagnostic work-up employed was observed during the study period (p<0.001). Specifically, over the past decade, a more accurate and comprehensive assessment of disease extension through multiple imaging modalities (CT and/or MRI + EUS + ^{68}Ga PET) has been noted (2002-2007: n=2/27, 7%; 2008-2012: n=13/118, 11%; 2013-2017: n=69/121, 57%; 2018-2022: n=94/118, 80%) (**Figure 7**).

Moreover, a significant increase in the interval from diagnosis to surgical resection has been observed throughout the study period (2002-2007: 1 month (i.q.r. 0-2), 2008-2012: 1 month (i.q.r. 1-2.25), 2013-2017: 3 months (i.q.r. 2-7), 2018-2022: 3 months (i.q.r. 2-7.75); $p<0.001$).

Table V. Preoperative characteristics. *Comparison of demographics, clinical, and preoperative characteristics between patients who underwent surgery for nonfunctioning pancreatic neuroendocrine tumours (NF-PanNETs) and received potential overtreatment (n = 129), appropriate treatment (n = 230) and potential undertreatment (n = 25).*

Variable	**OT** *n*=129	**AT** *n*=230	**PU** *n*=25	**Overall** ***p***º	***Adj.* p†** ***PO vs AT***	***Adj.* p‡** ***PO vs PU***	***Adj.* p§** ***AT vs PU***
Sex (female)	57 (44)	100 (44)	14 (56)	0.487	1.000	0.834	0.696
Age at surgery (years)*	60 (48-67)	60 (49-68)	64.5 (48.5-73.7)	0.793	1.000	1.000	1.000
BMI (Kg/m^2)*	25.1 (22.8-28.7)	24.82 (22.8-28.3)	22.4 (19.8- 25.8)	0.155	1.000	0.116	0.245
Symptoms at diagnosis	16 (12)	45 (20)	4 (16)	0.235	0.255	1.000	1.000
N. of imaging examinations				0.068	0.033	1.000	1.000
One imaging modality	28 (22)	37 (16)	4 (16)				
Two imaging modalities	42 (33)	48 (21)	6 (24)				
Three imaging modalities	34 (26)	73 (32)	9 (36)				
Four imaging modalities	25 (19)	72 (31)	6 (24)				
Diagnostic work-up				**0.034**	**0.021**	1.000	1.000
CT or MRI	28 (22)	37 (16)	4 (16)				
CT and MRI	4 (3)	5 (2)	0 (0)				
CT and/or MRI + EUS or ^{68}Ga PET	52 (40)	65 (28)	11 (44)				
CT and/or MRI + EUS + ^{68}Ga PET	45 (35)	123 (54)	10 (40)				
Radiological diameter (mm)*	20 (15-27)	30.5 (24-47.25)	34 (30-63.75)	**< 0.001**	**< 0.001**	**< 0.001**	0.833
Tumour site				**0.012**	**0.009**	0.636	1.000
Head/uncinate process	31 (24)	91 (40)	9 (36)				
Body/tail	98 (76)	139 (60)	16 (64)				

Values are *n (%)* unless otherwise indicated*, BMI*, body mass index; *CT*, computed tomography; *MRI*, magnetic resonance; *PET*, positron emission tomography; *EUS*, endoscopic ultrasound; *Adj,* adjusted; *PO*, potential overtreatment; *AT*, appropriate treatment; *PU*, potential undertreatment. * Expressed as median (i.q.r.).

º PO *versus* AT *versus* PU; † PO *versus* AT, P values with Bonferroni correction for multiple comparisons; ‡ PO *versus* PU, P values with Bonferroni correction for multiple comparisons; §AT *versus* PU, P values with Bonferroni correction for multiple comparisons.

Figure 6. Diagnostic workup over the study period. *Comparison of the diagnostic workup employed in patients who underwent surgery for nonfunctioning pancreatic neuroendocrine tumours (NF-PanNETs) over the study period (2002-2022), categorized into four sub-periods.*

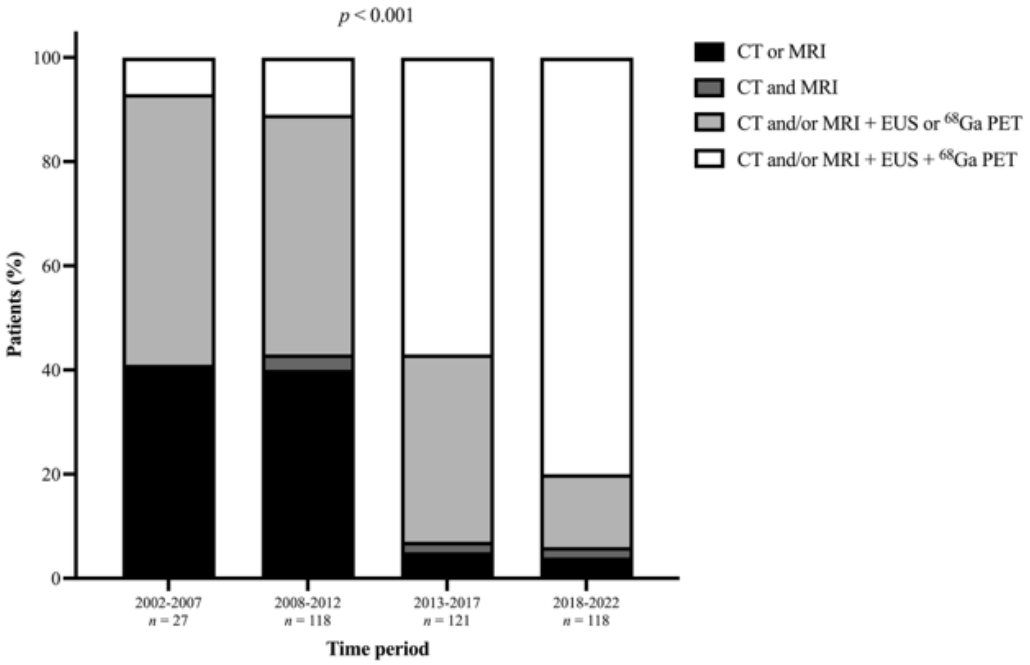

An increase in the rate of appropriately treated patients has been observed after the introduction of institutional multidisciplinary meetings (2018), with a concurrent decrease in potentially overtreated patients (appropriate treatment: *n*=90/119, 76% *vs* *n*=140/265, 53%, potential overtreatment: *n*=21/119, 7% *vs* *n* =108/265, 41%; *p*<0.001). No significant changes in the rate of potentially undertreated patients were reported (*n*=8/119, 7% *vs* *n* =17/265, 6%).

Patients with tumours located in the pancreatic body-tail exhibited a significantly higher frequency of potential overtreatment (39%, *n*=98/253) as compared to patients with pancreatic head lesions (*n*=31/131, 24%; *p*=0.012). Furthermore, a smaller radiological diameter was significantly associated with potential overtreatment [potential overtreatment: 20 mm (i.q.r. 15-27), appropriate treatment: 30 mm (i.q.r. 24-47), potential undertreatment: 34 mm (i.q.r. 30-64); *p*<0.001]. By ROC curve analysis (**Figure 8)**, a radiological tumour size of 25.5 mm was identified as the most accurate cut-off, demonstrating 71% sensitivity and 74% specificity in predicting potential overtreatment.

The global performance of tumour radiological diameter as a predictor of potential overtreament was deemed adequate (AUC 0.783, 95% CI 0.736-0.830, p<0.001).

Figure 8. Receiver operating characteristic (ROC) curve evaluating radiological tumour size (mm) as predictor of treatment appropriateness.

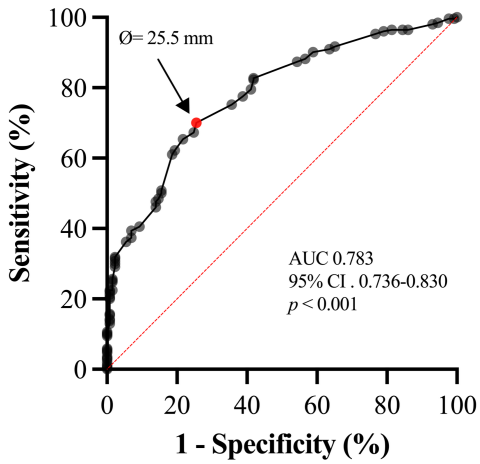

Intraoperative Features and Surgical Outcomes

A comparison of intraoperative features and surgical outcomes among the three groups is reported in **Table VI**. The year of surgical resection demonstrated a strong correlation with treatment appropriateness (p<0.001), revealing a significant increase in the rate of appropriately surgically treated patients during the study period (2002-2007: 48%, 2008-2012: 45%, 2013-2017: 62%, 2018-2022: 75%). Simultaneously, a concurrent decrease in the rate of potentially overtreated patients was reported (2002-2007: 37%, 2008-2012: 51%, 2013-2017: 31%, 2018-2022: 18%) (**Figure 9**).

Table VI. Comparison of intraoperative characteristics and postoperative outcomes. *Comparison of intraoperative characteristics and postoperative outcomes between patients who underwent surgery for nonfunctioning pancreatic neuroendocrine tumours (NF-PanNETs) and received potential overtreatment (n = 129), appropriate treatment (n = 230) and potential undertreatment (n = 25).*

Variable	PO *n*=129	AT *n*=230	PU *n*=25	Overall *p* [o]	*Adj.* p† *PO vs AT*	*Adj.* p[‡] *PO vs PU*	*Adj.* p[§] *AT vs PU*
Date of surgery				**< 0.001**	**< 0.001**	0.102	0.867
2002-2007	10 (8)	13 (6)	4 (16)				
2008-2012	60 (46)	53 (23)	5 (20)				
2013-2017	38 (29)	75 (32)	8 (32)				
2018-2022	21 (16)	89 (39)	8 (32)				
Type of surgery				**< 0.001**	**< 0.001**	0.111	1.000
Pancreatoduodenectomy	18 (14)	84 (37)	8 (32)				
Distal pancreatectomy	74 (57)	127 (55)	15 (60)				
Total pancreatectomy	1 (1)	7 (3)	1 (4)				
Enucleation	30 (23)	10 (4)	1 (4)				
Middle pancreatectomy	6 (5)	2 (1)	0 (0)				
Parenchyma-sparing resection				**< 0.001**	**< 0.001**	**0.039**	1.000
No	93 (72)	218 (95)	24 (96)				
Yes	36 (28)	12 (5)	1 (4)				
Surgical approach				0.209	1.000	0.237	0.396
Laparoscopic	45 (35)	72 (31)	5 (20)				
Open	84 (65)	158 (69)	20 (80)				
Vascular resection	0 (0)	12 (5)	4 (16)	**< 0.001**	**0.015**	**0.003**	0.174
Status of resection margins				**0.002**	0.126	**0.003**	0.087
R0	125 (97)	210 (91)	19 (76)				
R1	4 (3)	20 (9)	6 (24)				
Length of hospital stay (days)* [¥]	9 (6-11)	9 (7-12)	9 (7-11)	0.770	1.000	1.000	1.000
Postoperative complications (Dindo *et al*, 2004)				0.265	0.753	0.462	1.000
No	36 (28)	66 (29)	10 (40)				
Clavien-Dindo I-II	77 (60)	121 (53)	10 (40)				
Clavien-Dindo III-IV-V	16 (12)	43 (19)	5 (20)				
CR-POPF (Bassi et al, 2017)				0.088	0.459	1.000	0.192
No	106 (82)	174 (76)	23 (92)				
Yes							
Grade B	21 (16)	53 (23)	1 (4)				
Grade C	2 (2)	3 (1)	1 (4)				
Exocrine insufficiency	34 (26)	89 (39)	14 (56)	**0.006**	0.054	**0.009**	0.282
Endocrine insufficiency	36 (28)	54 (23)	5 (20)	0.551	1.000	1.000	1.000

Values are *n (%)* unless otherwise indicated**,** *Adj,* adjusted; *CR-POPF*, clinically relevant post-operative pancreatic fistula; *PO*, potential overtreatment; *AT*, appropriate treatment; *PU*, potential undertreatment. * Expressed as median (i.q.r.)
[o] PO *versus* AT *versus* PU; [†] PO *versus* AT, P values with Bonferroni correction for multiple comparisons; [‡] PO *versus* PU, P values with Bonferroni correction for multiple comparisons; [§]AT *versus* PU, P values with Bonferroni correction for multiple comparisons.
[¥] missing data *n* =1 potential overtreatment, *n* =2 appropriate treatment, *n* =1 potential undertreatment

Figure 9. Treatment appropriateness over the study period. *Comparison of rates of potential overtreatment, appropriate treatment and potential undertreatment between patients who underwent surgery for nonfunctioning pancreatic neuroendocrine tumours (NF-PanNETs) over the study period (2002-2022), categorized into four sub-periods.*

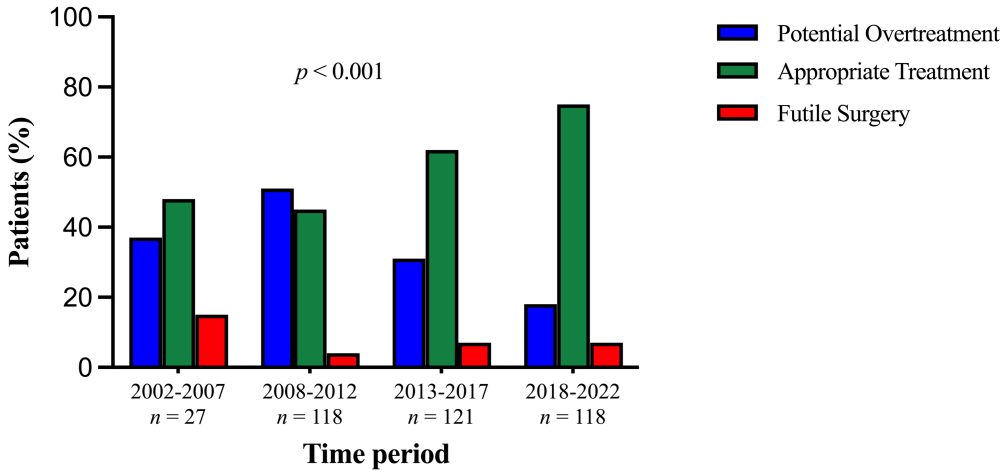

Treatment Appropriateness				
Potential Overtreatment (%)	10 (37)	60 (51)	38 (31)	21 (18)
Appropriate Treatment (%)	13 (48)	53 (45)	75 (62)	89 (75)
Futile Surgery (%)	4 (15)	5 (4)	8 (7)	8 (7)

The type of surgical intervention was significantly associated with treatment appropriateness (p<0.001).

Parenchyma-sparing resections were more common in patients who received potential overtreatment (28%, n=36) compared to patients who experienced appropriate treatment (5%, n=12; p<0.001) or potential undertreatment (4%, n=1; p=0.039). Pancreatoduodenectomy was more frequently performed in the appropriate treatment group (37%, n=84). Patients receiving potential undertreatment underwent vascular resection in 16% of cases (n=4/25), a percentage significantly higher than the one observed in the potentially overtreated patients (0%; p=0.003). Interestingly, among patients undergoing pancreatic resection with vascular reconstruction, 75% (n=12/16) received an appropriate treatment. However, no significant difference was observed between patients within the potential undertreatment group (5%, n=12/130) and those appropriately treated (p=0.174).

R1 resections were more frequent (24%) in the potential undertreatment group. The potential overtreatment group had a significantly higher rate of R0 resections as compared

to the potential undertreatment one (potential overtreatment: 97% *n*=125 *vs* potential undertreatment: 76%, *n*=19; *p*=0.003).

Following surgical resection, the rate of pancreatic exocrine insufficiency progressively increased across the potential overtreatment (26%), appropriate treatment (39%) and potential undertreatment (56%) groups (*p*=0.006). The frequency of pancreatic endocrine insufficiency was similar among the three categories (potential overtreatment: 28%, appropriate treatment: 23%, potential undertreatment: 20%; *p*=0.551).

Pathological Findings

A comparison of pathological features between patients receiving appropriate surgery and potential undertreatment is depicted in **Table VII**.

Table VII. Pathological Characteristics. *Comparison of pathological features at final histology between patients who underwent surgery for nonfunctioning pancreatic neuroendocrine tumours (NF-PanNETs) and received appropriate treatment (n = 230) and potential undertreatment (n = 25).*

Variable	Appropriate Treatment *n*=230	Potential Undertreatment *n*=25	*p value*
Tumour grade (Lloyd *et al*, 2017)			
G2-G3	139 (60)	20 (80)	0.055
G3	4 (2)	4 (16)	**< 0.001**
Ki67 index, %*	3 (2-6)	8 (5-18)	**< 0.001**
T stage, T3-4 (Rindi *et al*, 2006)	81 (35)	16 (64)	**0.005**
N stage, N1 (Rindi *et al*, 2006)	105 (46)	19 (76)	**0.004**
M stage, M1 (Rindi *et al*, 2006)	14 (6)	6 (24)	**0.007**
Microvascular invasion	125 (54)	22 (88)	**0.001**
Perineural invasion	73 (32)	13 (52)	**0.042**
Necrosis	20 (9)	9 (36)	**0.001**
Peripancreatic tissue infiltration	43 (19)	5 (20)	0.793

Values are *n (%)* unless otherwise indicated**,** * Expressed as median (i.q.r.)

Potentially overtreated patients were excluded from this analysis as they showed no signs of aggressiveness by definition. The median Ki67 proliferative index was significantly higher in patients who experienced a potential undertreatment as compared to individuals receiving an appropriate treatment [8 (5-18) *vs* 3 (2-6); *p*<0.001].

Consistently, a significantly higher percentage of G3 tumours was reported in the potential undertreatment group (16% *vs* 2%, $p<0.001$). Patients in the appropriate treatment group had a significantly lower frequency of T3-T4 tumours (64% *vs* 35%, $p=0.005$), nodal metastases (76% *vs* 46%, $p=0.004$), distant metastases (24% *vs* 6%, $p=0.007$), microvascular invasion (88% *vs* 54%, $p=0.001$), perineural invasion (52% *vs* 32%, $p=0.042$) and necrosis (36% *vs* 9%; $p=0.001$) as compared to potentially undertreated subjects. Among the appropriately treated patients with T3-T4 tumours ($n=81/230$), 54% had a G2-3 PanNET ($n=44/81$), 51% showed nodal involvement at histological examination ($n=41/81$), and 28% were positive for both features aggressiveness (G2-3, N1; $n=23/81$). Regarding the potential undertreatment group, G2-3 lesions and lymph node metastases were reported in 75% ($n=12/16$) and 69% ($n=11/16$) of patients with T3-4 tumours, respectively. Both characteristics were observed in 56% of cases ($n=9/16$).

Preoperative Determinants of Potential Overtreatment and Potential Undertreatment

Multivariable regression analyses assessing preoperative predictors of potential surgical overtreatment and undertreatment are reported in **Table VIII**. Surgical resection performed before 2015 (OR 2.580, 95% CI 1.570-4.242; $p<0.001$), radiological tumour size <25.5 mm (OR 6.566, 95% CI 4.010-10.751; $p<0.001$) and tumour location in the pancreatic body/tail (OR 1.908, 95% CI 1.119-3.253; $p=0.018$) were identified as independent predictors of potential overtreatment. Radiological tumour size was the only independent determinant of potential undertreatment (OR 0.291, 95% CI 0.107-0.791; $p=0.016$).

Table VIII. Multivariate analysis of predictors of potential overtreatment and potential undertreatment between patients who underwent surgery for nonfunctioning pancreatic neuroendocrine tumours (NF-PanNETs).

Variable	*Potential Overtreatment*		*Potential Undertreatment*	
	OR (95% CI)	***P value***	**OR (95% CI)**	***P value***
Radiological tumour size		**<0.001**		**0.016**
≥ 25.5 mm	1		1	
< 25.5 mm	6.566 (4.010-10.751)		0.291 (0.107-0.791)	
Diagnostic work-up		0.443		0.417
CT and/or MRI	1		1	
CT and/or MRI + EUS and/or ^{68}Ga PET	0.787 (0.426-1.452)		1.604 (0.513-5.011)	
Time of surgery		**< 0.001**		0.476
2016-2022	1		1	
2002-2015	2.580 (1.570-4.242)		0.739 (0.322-1.697)	
Lesion site		**0.018**		0.924
Head/uncinate process	1		1	
Body/tail	1.908 (1.119-3.253)		0.959 (0.406-2.268)	

OR, odds ratio; CI, confidence interval; CT, computed tomography; *MRI*, magnetic resonance; *PET*, positron emission tomography; *EUS*, endoscopic ultrasound

Survival analysis

After a median follow up of 61 months (i.q.r. 55-66 months), 67 patients (17%) experienced disease recurrence and 29 (7.5%) eventually died due to any cause. Disease relapse was observed in 100% (*n*=25/25), 19% (*n*=42/230) and 0% (*n*=0/129) of patients receiving potential undertreatment, appropriate treatment, and potential overtreatment, respectively ($p<0.001$). Potentially overtreated patients showed a 3-year DFS rate of 100%, as compared to 87% and 0% in patients within the appropriate treatment and potential undertreatment groups, respectively (**Figure 10A**). No significant difference was observed in the site of disease recurrence between patients who received a potential undertreatment with compared to appropriately treated ones (p=0.225). Among the 42 appropriately treated patients who experienced disease recurrence, 17% (n=7) had a nodal relapse and 83% (n=35) developed distant metastases. Similarly, of the 25 patients who received a potential undertreatment, 2 (8%) experienced local recurrence, 5 (20%) developed nodal metastases, and 18 (72%) distant metastases.

Patients who received potential undertreatment had the poorest OS (3-year OS 70%) as compared to appropriately treated (3-year OS 97%) and potentially overtreated patients (3-year OS 99%) (p<0.001). Overall, 14 patients died of disease. No disease-related deaths occurred in the potential overtreatment group. Patients of the potential undertreatment group had also a worse DSS (3-year DSS 70%), as compared to the other groups (3-year DSS 100% for both) (p<0.001) (**Figure 10B**). No statistically significant differences in terms of OS and DSS were reported between potentially overtreated and appropriately treated patients (OS, p=0.129; DSS, p=0.069).

Figure 10. Survival Analyses. *Comparison of (**A**) disease-free survival (DFS) and (**B**) disease-specific survival (DSS) between patients who underwent surgery for nonfunctioning pancreatic neuroendocrine tumours (NF-PanNETs) and received potential overtreatment (n = 129), appropriate treatment (n = 230) and potential undertreatment (n = 25).*

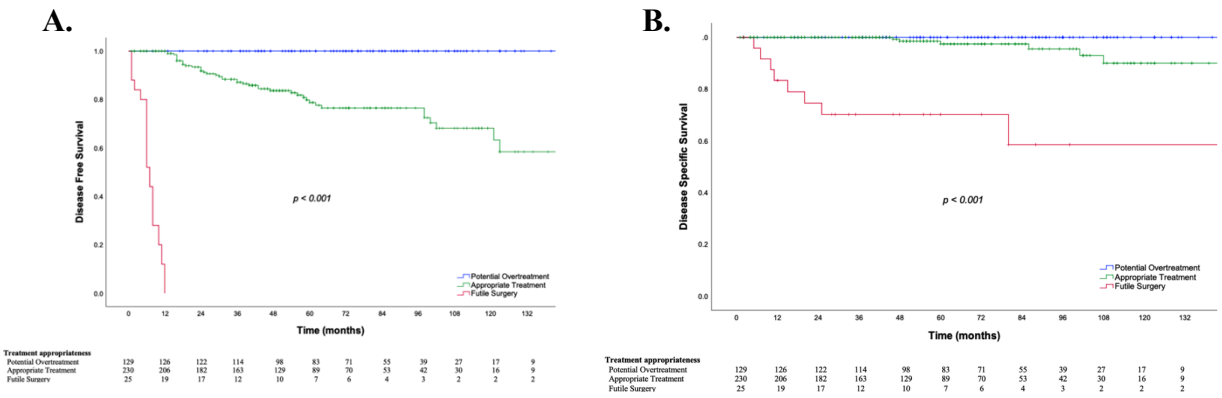

Discussion

The study investigated the appropriateness of surgical treatment and associated factors in patients with resectable NF-PanNETs. Surgery for NF-PanNETs presents numerous challenges due to the unique biological behavior of these tumours. The inherent heterogeneity in aggressiveness poses a significant risk of inadequate surgical resection, resulting in both potential overtreatment and futile interventions.

The present study investigated the suitability of surgical management in a large, single-institution series of 384 patients submitted to curative surgery for NF-PanNET at a tertiary referral center. The decision to proceed with surgery was found to be appropriate in the majority of patients (60%), nevertheless a significant proportion of cases of potential

overtreatment and of futile resection was identified. The rate of potentially overtreated cases decreased over time, which may be attributed to the evolution in the management of small, asymptomatic NF-PanNETs as well as to the advancement in imaging techniques allowing enhanced characterization and identification of these lesions. Indeed, recent studies have shown the feasibility and safety of a "watch and wait" approach for asymptomatic sporadic NF-PanNETs ≤ 2 cm (Gaujoux *et al*, 2013; Partelli *et al*, 2016; Rosenberg *et al*, 2016), leading to a reduction in the risk of overtreatment. Moreover, the current study revealed that patients who underwent surgical resection before 2015 were more likely to experience potential overtreatment. This finding can be attributed to the publication of the ENETS (Falconi *et al*, 2016) consensus guidelines in 2016, which recommended conservative management instead of a surgical approach for this particular subset of patients. These guidelines likely influenced clinical practice and led to a shift in the management of small, asymptomatic NF-PanNETs. Furthermore, the introduction of institutional multidisciplinary meetings in 2018 has likely contributed to the increase in the rate of patients receiving appropriate treatment, ensuring a comprehensive assessment of patients' management. Nevertheless, the rate of cases receiving potential undertreatment remained stable over the study period indicating that there have been no significant advances in the management of localized aggressive lesions in the past 20 years. Patients experiencing early disease relapse after surgery might benefit from multimodal treatment approaches. Previous small series reported promising results in this setting, indicating improved oncological outcomes when patients underwent sequential treatments such as surgery preceded by peptide receptor radionuclide therapy (Bertani *et al*, 2016; Partelli *et al*, 2018a; Li *et al*, 2022). However, larger and more rigorous studies are needed to validate the effectiveness of perioperative medical treatments in this specific context.

The findings of the present study, which identified small tumour diameter and pancreatic body/tail location as independent predictors of potential overtreatment, as well as radiological tumour size as a preoperative determinant of potential undertreatment, are consistent with several prior reports in the literature (Partelli *et al*, 2018b; Rindi *et al*, 2007; Singhi & Klimstra, 2018; Madeira *et al*, 1998). Previous studies (Partelli *et al*, 2016; Ricci *et al*, 2022) have highlighted the challenge of appropriately managing small tumours, particularly those located in the pancreatic body/tail. Importantly, the present

study identified a diameter of 25.5 mm as the optimal cut-off for preoperative assessment, effectively distinguishing patients at high risk of overtreatment. This finding implies that patients with tumours smaller than 25.5 mm should undergo careful evaluation before making treatment decisions. Indeed, such patients could be suitable candidates for active surveillance or potentially benefit from a parenchyma-sparing resection approach.

Furthermore, it is reasonable to speculate that the observed correlation between tumour location and potential overtreatment may be attributed to the fact that surgical resections for tumours situated in the pancreatic body/tail (i.e., distal pancreatectomy) are comparatively less technically challenging and associated with lower postoperative morbidity rates, in contrast to resections required for pancreatic head lesions (i.e., pancreatoduodenectomy)(Townsend *et al*, 2016). Consequently, surgeons may be more inclined to opt for surgical intervention in cases involving pancreatic body-tail lesions, even in the absence of clear preoperative indications of aggressiveness.

Another notable finding from this study pertains to the detrimental consequences of potential unnecessary surgical interventions. Noteworthy is the frequency of post-surgical morbidity among potentially overtreated patients, which has significant implications. Alarmingly, the present results indicate that 25% of potentially overtreated patients experienced postoperative pancreatic impairment, consequently impairing their quality of life (Halloran *et al*, 2011; Phillips, 2015) In addition, potentially undertreated patients showed lower overall survival compared to those reported in literature for patients undergoing curative surgery for locally advanced (Titan *et al*, 2020) and metastatic PanNETs (You *et al*, 2022; Spolverato *et al*, 2017).

The present study has several limitations that should be recognised. The first one is related to its retrospective design. Second, a referral bias might be present, as only patients submitted to surgery in a tertiary center were considered in this series. Moreover, surgical outcomes were not compared with those of non-operative control groups, which does not allow for the validation of the patients' classification. In addition, variables as tumour growth and patients' choice could not be included in the analysis, thereby precluding an assessment of their impact on surgical indications. Finally, the study developed over a long period, during which significant evolutions in PanNETs assessment and management as well as advances in surgical techniques occurred.

In conclusion, the study provides insights into the treatment appropriateness for surgically managed NF-PanNETs over a 20-year period. Potential overtreatment remains a concern, but the rate of appropriately treated patients has been increasing. Surgeons could enhance their clinical judgment and tailor treatment approaches to improve treatment's selection, especially in presence of tumours located in the pancreatic body-tail and/or with a radiological diameter < 25.5 mm. Further research is needed to increase current ability to preoperatively predict tumour aggressiveness.

2) Preoperative Predictors of New-Onset Diabetes Mellitus Following Distal Pancreatectomy for Non-functioning Pancreatic Neuroendocrine Tumours (Battistella et al, 2025)

Aim: to evaluated postoperative morbidity associated with surgical resections, focusing on patients undergoing distal pancreatectomy, to evaluate current standards of care and identifying areas in which biological insights may refine patient selection.

Materials and Methods

Study Design and Participants

The present retrospective observational study adhered to the Strengthening the Reporting of Observational Studies in Epidemiology (STROBE) guidelines (von Elm *et al*, 2014). All consecutive patients who underwent curative DP for localized NF-PanNETs at San Raffaele Hospital (Milan, Italy) from 2015 to 2022 were considered. Inclusion criteria were: 1) NF-PanNET diagnosis confirmed at final postoperative histology, ii) availability of pre-operative morphological imaging (contrast-enhanced computed tomography [CE-CT] or magnetic resonance imaging [MRI]). Exclusion criteria encompassed patients with multifocal or metastatic disease, preoperative diagnosis of diabetes mellitus, islet auto transplantation, or postoperative follow-up shorter than 24 months. Given the retrospective nature of the study, ethical committee approval was waved.

Data Collection

A comprehensive collection of preoperative, intraoperative and postoperative data was conducted by retrospectively retrieving information from a prospectively maintained institutional database. Preoperative variables, including demographic characteristics (age and sex), BMI, glycated haemoglobin A1c (HbA1c) and glycaemia levels, were reviewed. The following pathological characteristics were recorded: tumour size, tumour grade, T/N stages, microvascular and perineural invasion, and presence of necrosis. Tumour grade was determined based on the 2017 World Health Organization (WHO) classification into G1 (Ki67<3%), G2 (Ki67 3-20%) and G3 (Ki67 >20%)(Lloyd *et al*, 2017). The Ki67 proliferative index was assessed by MIB1 antibody staining and expressed as the percentage of cells with nuclear staining in 2000 cells, counted in the area of highest

nuclear labelling (Klimstra *et al*, 2010). Tumour stage was categorized following the current European Neuroendocrine Tumour Society (ENETS) TNM staging system(Rindi *et al*, 2006). The presence of microvascular invasion, perineural invasion and necrosis were reviewed. Potential overtreatment was defined as surgical resection of patients with histologically confirmed T1–T2 tumours, Ki-67 index <10%, node-negative status (N0), and absence of vascular or perineural invasion and tumour necrosis(Partelli et al, 2024).

Postoperative complications were classified according to the Clavien-Dindo classification of surgical complications(Dindo *et al*, 2004). Postoperative pancreatic fistula (POPF) was graded according to the 2016 definition proposed by the International Study Group on Pancreatic Surgery (ISGPS)(Bassi *et al*, 2017).

Radiological Evaluation

Preoperative radiological evaluation included CE-CT or MRI scans. In the absence of available CE-CT images, MRI scans were used. Pancreatic measurements (mm) were obtained in the axial and coronal planes using standard radiological PACS software (AGFA Enterprise Imaging, AGFA HealthCare, Mortsel, Belgium) with multi-planar reconstruction (MPR), and included: distance from the tumour to the pancreatic tail, greatest tumour diameter along the longitudinal axis of the pancreas, distance from the tumour to the confluence of the superior mesenteric vein (SMVc), and distance from the SMVc to the pancreatic head (**Figure 1)**. The lengths of pancreatic parenchyma proximal and distal to the tumour were considered healthy pancreatic parenchyma (HPP). To ensure maximum reproducibility of all the above measurements, a curved line following the course of the Wirsung duct from the tip of the tail to the papilla, was used. When the duct was not visible or in cases of anatomical variants (e.g., pancreas divisum), the line was drawn through the center of the pancreatic gland using MPR. From these measurements, additional derived variables were calculated.

Pancreatic parenchymal consistency was also evaluated radiologically, with atrophy defined as a reduction in parenchymal thickness, a loss of the normal lobulated contour and fatty infiltration. Radiological assessments were independently reviewed by two radiologists blinded to postoperative outcomes, with discrepancies resolved by consensus.

Body composition parameters were extracted using SliceOmatic software (version 5.0, Tomovision, Montreal, Canada) based on axial CT/MRI images at the level of the third lumbar vertebra. Total muscle area (TMA), total fat area (TFA), visceral fat area (VFA), and subcutaneous fat area (SFA) were measured (**Figure 17**). Total abdominal muscle area (TAMA) was calculated. Detailed methodology for body composition assessment has been previously published (Pecorelli *et al*, 2016, 2023). All body composition metrics were expressed as absolute areas in square centimetres (cm^2).

Figure 17. Radiological assessment of body composition parameters on axial CT at the level of the third lumbar vertebra.

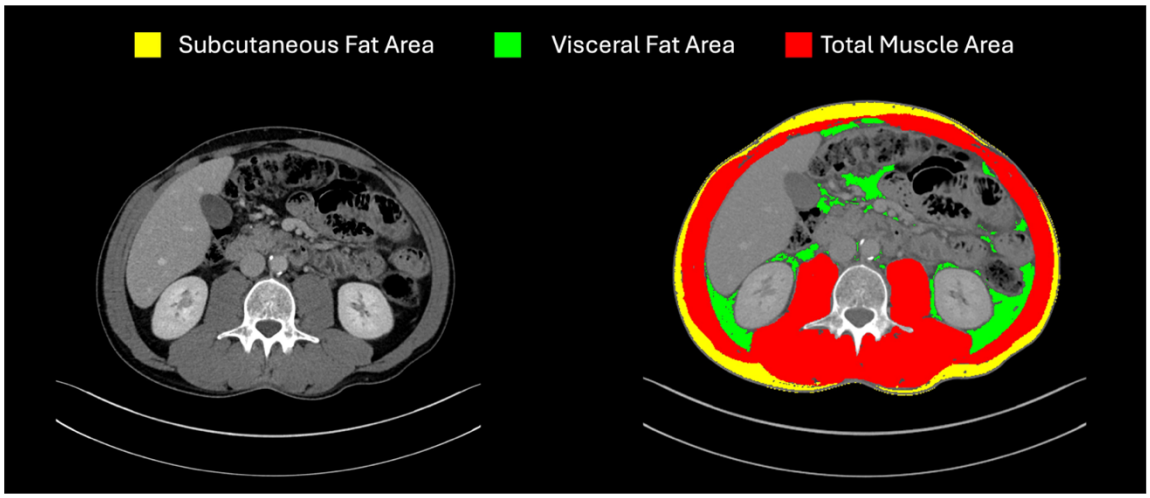

Long-term Outcomes Definition

Postoperative NO-DM and exocrine insufficiency were recorded. According to the American Diabetes Association diagnostic criteria(*Standards of Medical Care in Diabetes—2022* Abridged for Primary Care Providers, 2022), PONO-DM was defined when HbA1c was equal to or greater than 6.5% and/or in the presence of a fasting plasma glucose (FPG) equal to or greater than 126 mg/dL and/or in a patient with classic symptoms of hyperglycemia or hyperglycemic crisis associated to a random plasma glucose equal to or greater than 200mg/dL. Exocrine pancreatic insufficiency was defined as the requirement for pancreatic enzyme replacement therapy due to clinical evidence of malabsorption (steatorrhea, weight loss, and abdominal distention), with recurrence of symptoms upon withdrawal of therapy. DFS was defined as the time from surgery to any

kind of disease recurrence. OS was defined as the time from surgery to death from any cause. In the absence of events, DFS and OS were censored at the date of last follow-up.

Statistical Analysis

Categorical variables were presented as absolute numbers with corresponding percentages (%) and compared using the the χ^2 or Fisher exact test, as appropriate. Continuous variables were reported as median with interquartile ranges (IQR) for skewed distribution, or as mean ± standard deviation (SD) for normal distributions. The normality of continuous variables was assessed using the Kolmogorov-Smirnov test. Continuous variables were compared between two groups by using Student's t test or Mann-Whitney U test, as appropriate based on the variables' distribution. Cox regression analysis was employed to model the time to development of PONO-DM and to identify independent preoperative predictors associated with its occurrence. Variables with significant associations in univariate analysis, or those deemed clinically relevant, were included in multivariable models. The discriminative performance of the final Cox regression model was evaluated using receiver operating characteristic (ROC) curve based on the linear predictor (Xβ). Model discrimination was quantified by calculating the area under the curve (AUC). A nomogram and online risk calculators were developed based on the final Cox model, to visually estimate the individual risk of developing PONO-DM at 1, 3, and 5 years following surgery. Survival probability was estimated using the Kaplan-Meier method. The log-rank test was employed to compare DFS and OS between patients with and without PONO-DM. Statistical significance was set at a p-value less than 0.05. Statistical analyses were performed using SPSS software, version 29.0.2 for Mac (IBM Corp., Armonk, NY, USA) and R software, version 4.5.0 (R Foundation for Statistical Computing, Vienna, Austria), using *survival*, *rms*, and *shiny* libraries.

Results

Patient Demographics and Preoperative Metabolic Profiles

A total of 65 patients who underwent distal pancreatectomy for localized NF-PanNETs were included in the study. Mean age was 59 (±12) years and 37% (n=24) of patients were female. After a median follow up of 58 months [IQR 49-67 months], 27 patients (41%) developed PONO-DM. Among those who developed PONO-DM, the median time to diagnoses was 9 months. The cumulative incidence was 22% (n=14/65) at 1 year, 28% (n=18/65) at 3 years, and 38% (n=25/65) at 5 years.

There were no significant differences between patients who did and did not develop PONO-DM in terms of gender distribution (p=0.987) or age (p=0.714). BMI was significantly higher in the diabetes group (26.22 kg/m^2 [IQR 24.49-30.69 kg/m^2] vs. 23.96 kg/m^2 [IQR 22-27 kg/m^2], p=0.016). Preoperative glycemia and glycated haemoglobin (HbA1c) levels were not significantly different between groups, although trends were observed. Glycemia ≥100 mg/dL was more prevalent in the PONO-DM group (41% vs. 21%, p=0.085), and a higher proportion of these patients had HbA1c ≥42 mmol/mol (14% vs. 0%, p=0.084) (**Table IX**).

Table IX: Patients demographic and preoperative metabolic characteristics

Variable	**Overall** ***n*= 65**	**No PONO-DM** ***n*= 38**	**PONO-DM** ***n*= 27**	***p*** **value**
Sex, female	24 (37)	14 (37)	10 (37)	0.987
Age, yr *	59 (±12)	59 (±14)	60 (±10)	0.714
Age >60yr	33 (51)	20 (53)	13 (48)	0.722
BMI, kg/m^2 †	25.39 [22.59-28.78]	23.96 [22-27]	26.22 [24.49 -30.69]	**0.016**
BMI >25 kg/m^2	34 (52)	17 (45)	17 (63)	0.147
Glycaemia, mg/dL †	92 [83.5-102]	91 [82-98.25]	97 [87-106]	0.103
Glycaemia ≥100 mg/dL	19 (29)	8 (21)	11 (41)	0.085
HbA1c, mmol/mol *§	36.40 (±5)	35.44 (±3.36)	37.59 (±6.37)	0.137
HbA1c ≥42 mmol/mol§	3 (6)	0 (0)	3 (14)	0.084

PONO-DM, postoperative new-onset diabetes mellitus*; BMI,* body mass index; *HbA1c,* haemoglobin A1c. Data are expressed as *n* (%) unless otherwise specified

* Expressed as mean (± standard deviation)

† Expressed as median (interquartile range)

§ *n*= 16 missing

Radiological Parameters

All examined radiological parameters are summarized in **Table X**. CE-CT was available for 57 patients, while MRI scans were analyzed for the remaining 8 patients.

Radiological evaluation of body composition revealed that TFA was significantly higher in patients who developed PONO-DM (343cm^2 [IQR 254.4-482.3cm^2] vs. 275.3cm^2 [IQR 157.7-375.6cm^2], p=0.014). Specifically, a greater VFA was observed in the PONO-DM group (192.7cm^2 [IQR 102-258cm^2] vs. 104cm^2 [IQR 45.9-193.3cm^2], p=0.021). SFA approached statistical significance (*PONO-DM*; 177.2cm^2 [IQR 127.9-252.5cm^2] vs. *no PONO-DM;* 146.5cm^2 [IQR 106.64-194.075cm^2], p=0.052). No differences were observed in TMA (p=0.567) or TAMA (p=0.405) between the two groups. Notably, the VFA/TAMA ratio was significantly elevated in patients who developed PONO-DM (2.40 [IQR 1.44-2.71] vs. 1.39 [IQR 0.72-2.10], p=0.021).

In terms of pancreatic morphology and quantitative measurements, radiological pancreatic texture differed significantly between the two groups, with pancreatic atrophy being more frequent among patients who developed PONO-DM (44% vs. 21%, p=0.044). A trend toward a longer tumour-to-tail distance was observed in the PONO-DM group (55mm vs. 33.25mm, p=0.064). Notably, the proportion of healthy tail parenchyma, measured as percentage of HPP distal to the tumour relative to the total pancreas, was significantly higher in the PONO-DM group (32% vs. 17%, p=0.046) (**Figures 11A-B**).

Additional proportional metrics assessing the relationship between the tumour location, tumour size, and the distribution of HPP also demonstrated suggestive but non-significant associations with postoperative diabetes (**Table X)**.

Figure 11. Contrast-enhanced computed tomography images from (A) two patients with non-atrophic and (B) two patients with atrophic pancreatic parenchyma *. Lesions located in the distal tail of the pancreas are shown in panels* ***a*** *(coronal view) and panels* ***c*** *(axial view). Lesions located in the body/proximal tail of the pancreas are shown in panels* ***b*** *(coronal view) and panels* ***d*** *(axial view). yellow area: proximal pancreatic parenchyma; red area: tumour; red dots, distal pancreatic parenchyma*

A)

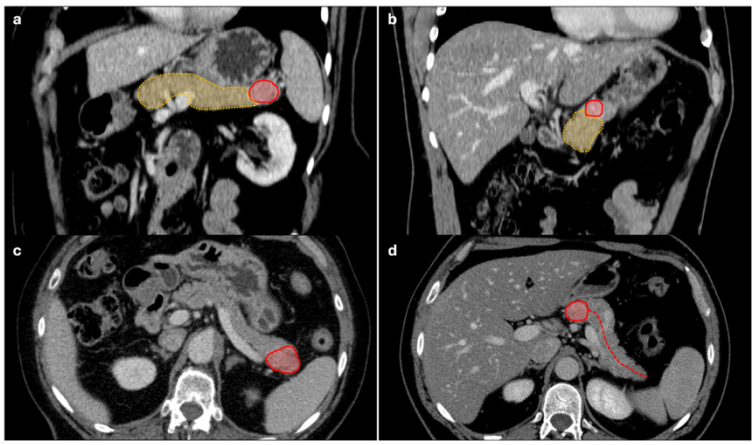

B)

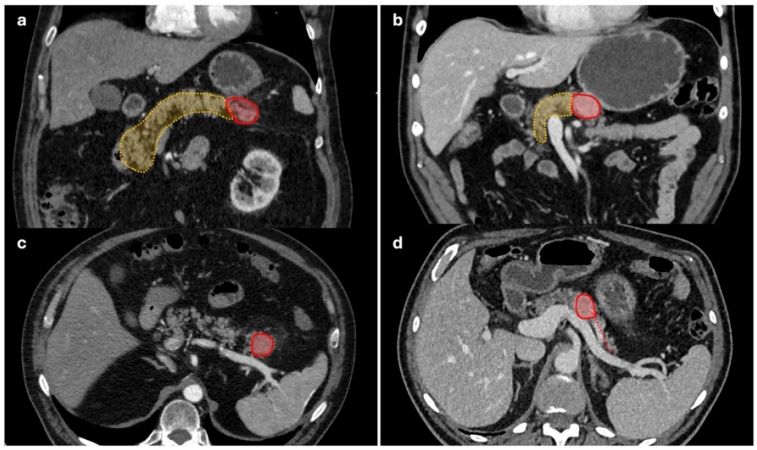

Table X: Patients' radiological parameters extracted from preoperative imaging

Variable	Overall *n*= 65	No PONO-DM *n*= 38	PONO-DM *n*= 27	*p* value
TMA, cm^{2} *	135 [99.43-158.5]	131.65 [98.53-156.87]	137.8 [107.3-161.7]	0.567
TAMA, cm^2/m^{2} *	77.83[60.61-89.60]	75.46 [60.30-88.46]	80.31[62.29-95.12]	0.405
TFA, cm^{2} *	312.4 [222-435.35]	275.31 [157.72-375.65]	343 [254.4-482.3]	**0.014**
SFA, cm^{2} *	162 [117-219.6]	146.5 [106.64-194.075]	177.2 [127.9-252.5]	0.052
VFA, cm^{2} *	148.1 [61.4-212]	104 [45.9-193.27]	192.7 [102-258]	**0.021**
VFA/TAMA ratio	1.64 [0.92-2.59]	1.39 [0.72-2.10]	2.40 [1.44-2.71]	**0.021**
Atrophic parenchyma, yes	20 (31)	8 (21)	12 (44)	**0.044**
Total pancreas, mm†	184.05 (±28.27)	183.48 (±32.04)	184.86 (±22.49)	0.839
Tail–tumor, mm*	38.2 [0-67.25]	33.25 [0-57.75]	55 [0-75.6]	0.064
Tumor, mm*	27 [19.7-38.3]	28.6 [21.52-38.42]	26 [17.7-39]	0.345
SMVc–tumor, mm*	48 [22.75-74.55]	54.25 [24.5-74.57]	40 [21.5-75]	0.401
Pancreatic head–SMVc, mm†	61.93 (±23.11)	64.82 (±26.31)	57.86 (±17.31)	0.235
Total HPP, mm†	149.48 (±31.24)	148.79 (±31.48)	150.44 (±31.47)	0.836
HPP distal to the SMVc, mm*	93.1 [72.05-109.85]	85.25 [62.7-107.37]	99.3 [91-110]	0.152
HPP prox to the tumor, mm†	111.88 (±40.80)	118.08 (±39.75)	103.14 (±41.40)	0.147
HPP / total pancreas, %*	85 [76-89]	85 [74.5-88]	85 [79-91]	0.320
tumor/ total pancreas, %*	15 [11-24]	15 [12-25.5]	15 [9-21]	0.320
tumor/pancreas distal SMVc, %*	23 [16-37]	24 [18.75-41]	21 [15-29]	0.114
HPP/ pancreas distal SMVc, %*	77 [63-84]	76 [59-81.25]	79 [71-85]	0.114
HPP distal SMVc / total HPP, %*	60 [52.5-65]	58.5 [50.25-64.25]	64 [56-70]	0.096
HPP prox tumor / total HPP, %*	75 [56.5-100]	78 [63.75-100]	65 [44-100]	0.082
HPP prox tumor / total pancreas, %†	60 (±20)	64 (±18)	55 (±20)	0.076
HPP tail / total HPP, %*	25 [0-43.5]	22 [0-36.25]	35 [0-56]	0.082
HPP tail / total pancreas, %*	22 [0-36.5]	17 [0-29.25]	32 [0-43]	**0.046**
HPP prox SMVc / total HPP, %*	40 [35-47.5]	41.5 [37.75-49.75]	36 [30-44]	0.093
HPP prox SMVc / total pancreas, %*	33 [26.5-37]	34.5 [29.25-39]	30 [25-35]	0.089

PONO-DM, postoperative new-onset diabetes mellitus*; TMA,* Total Muscle Area*; TAMA*, Total Abdominal Muscle Area*; TFA,* Total Fat Area*; SFA,* Subcutaneous Fat Area*, VFA,* Visceral Fat Area*; SMVc,* superior mesenteric vein confluence*; HPP,* healthy pancreatic parenchyma*; Prox,* proximal
Data are expressed as *n* (%) unless otherwise specified
* Expressed as median (IQR)
† Expressed as mean (± SD)

Histological Findings

Pathological examinations revealed a median specimen length of 100 mm, with most tumours graded G2–G3 (60%), staged as T1–T2 (74%), and no nodal involvement (N0, 68%).

Patients who developed PONO-DM had a significantly greater length of pancreas removed (surgical specimen, 12mm [IQR 100-130mm] vs. 99mm [IQR 80-120mm], p=0.022). Other pathological variables, including tumour size (p=0.464), lymph node involvement (p=0.078), grade (p=0.918), presence of vascular (p=0.258) or perineural invasion (p=0.249), and necrosis (p=0.389) were not significantly different between groups (**Table XI**). Overall, 15 out of 65 patients (23%) were classified as having undergone potential surgical overtreatment. Among these, 40% (6/15) developed PONO-DM.

Table XI: Patients' pathological characteristics at histological examination

Variable	Overall *n*= 65	No PONO-DM *n*= 38	PONO-DM *n*= 27	*p* value
Surgical specimen, mm*	100 [90-120]	99 [80-120]	120 [100-130]	**0.022**
Resection margin, mm*	26 [15-44.5]	30 [18-45]	25 [10-40]	0.519
Tumour dimension, mm*	28 [22-45]	28 [23-47]	27 [18-45]	0.464
T stage, T3-4 (Rindi *et al*, 2006)	17 (26)	10 (26)	7 (26)	0.972
N stage, N1(Rindi *et al*, 2006)	21 (32)	9 (24)	12 (44)	0.078
Grading, G2-3 (Lloyd *et al*, 2017)	39 (60)	23 (61)	16 (59)	0.918
Ki-67, %*	3 [1.5-6]	3 [1.75-6.25]	3 [1-6]	0.919
Ki-67 >10%	7 (11)	5 (13)	2 (7)	0.690
ELN*	20 [14-31]	21 [14-33]	19 [15-28]	0.540
Vascular invasion, yes	38 (58)	20 (53)	18 (67)	0.258
Perineural invasion, yes	21 (32)	10 (26)	11 (41)	0.249
Necrosis, yes	5 (8)	2 (5)	3 (11)	0.389

ELN, examined lymph nodes, *PONO-DM,* post-operative new onset diabetes mellitus
Data are expressed as *n* (%) unless otherwise specified
* Expressed as median (IQR)

Postoperative Outcomes

A higher rate of major postoperative complications (Clavien-Dindo grade ≥III) (30% vs. 16%, *p*=0.181) and hospital readmissions (30% vs. 11%, p=0.061) was reported in the PONO-DM group compared to the non-diabetic group, although these differences did not reach statistical significance (**Table XII**). A positive correlation between exocrine insufficiency and the development of PONO-DM was observed (33% vs. 8%, *p*= 0.020). Furthermore, exocrine insufficiency was significantly associated with a shorter length of HPP proximal to the tumour. Patients who did not develop exocrine insufficiency exhibited a significantly longer proximal segment compared to those who did (121 mm [i.q.r. 86–144 mm] vs. 89.9 mm [i.q.r. 49–114 mm], *p*= 0.043).

Table XII: Postoperative details of patients undergoing distal pancreatectomy for NF-PanNET

Variable	Overall *n*= 65	No PONO-DM *n*= 38	PONO-DM *n*= 27	*p* value
Postoperative complications, CD ≥3 (Dindo *et al*, 2004)	14 (21)	6 (16)	8 (30)	0.181
POPF, yes (Bassi *et al*, 2017)	39 (60)	22 (58)	17 (63)	0.681
CR-POPF, yes	30 (46)	18 (47)	12 (44)	0.516
Lymphatic leakage, yes	2 (3)	1 (3)	1 (4)	1.000
Abdominal collections, yes	18 (28)	10 (26)	8 (30)	0.769
PPH, yes	2 (3)	1 (3)	1 (4)	1.000
Exocrine insufficiency, yes	12 (19)	3 (8)	9 (33)	**0.020**
Hospital readmission, yes	12 (19)	4 (11)	8 (30)	0.061

PONO-DM, postoperative new-onset diabetes mellitus*; CD,* Clavien-Dindo*; POPF,* postoperative pancreatic fistula; *CR-POPF,* clinically relevant postoperative pancreatic fistula*; PPH,* postoperative pancreatic haemorrhage
Data are expressed as *n* (%)

With regards to survival analysis, no significant difference in OS was observed between the two groups (p=0.269). A trend toward a higher relapse rate was reported among patients who developed PONO-DM (p=0.062) (**Figure 13**).

Figure 13. Survival Analyses. *Comparison of Overall survival (**a**) and Disease-free survival (**b**) between patients who underwent distal pancreatectomy for localized nonfunctioning pancreatic neuroendocrine tumours (NF-PanNETs) and developed new-onset diabetes mellitus (n=27) and those who did not (n=38). PONO-DM, postoperative new-onset diabetes mellitus*

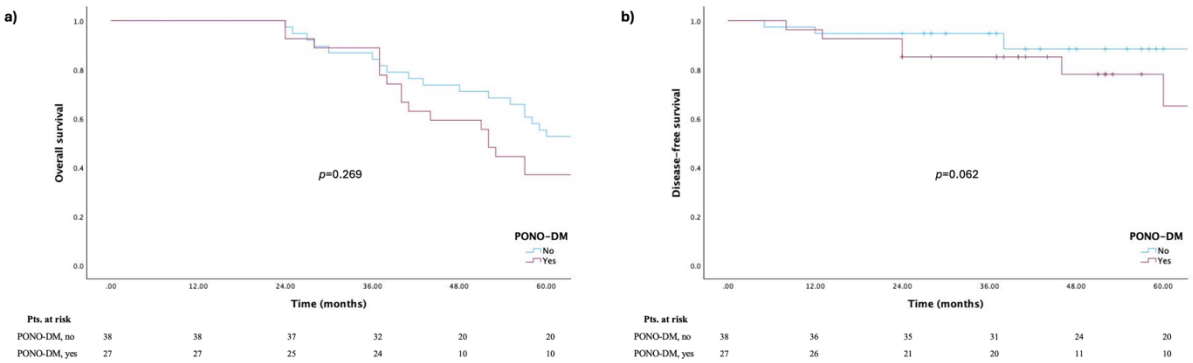

Preoperative Prediction of Postoperative New-Onset Diabetes Mellitus

At Cox regression analysis (**Figure 14**), BMI (Kg/m^2, HR 1.187, 95% C.I. 1.072-1.315, *p*=0.001), HbA1c (mmol/mol, HR 1.169, 95% C.I. 1.064-1.283, *p*=0.001) and the percentage of HPP distal to the tumour relative to total pancreatic length (HR 1.030, 95% C.I. 1.005-1.055, *p*=0.018) emerged as independent factors associated with an increased risk of developing PONO-DM. The composite model incorporating these variables demonstrated good predictive accuracy, with an AUC of 0.766 (95% CI: 0.627–0.905, *p*<0.001) (**Figure 15**).

Figure 14. Cox regression analysis with corresponding forest plot of preoperative factors associated with risk of developing new-onset diabetes mellitus over the study period. *Hazard ratios (HR) with corresponding 95% confidence intervals (CI) are presented. BMI, body mass index; HbA1c, haemoglobin A1c; TFA, total fat area; VFA visceral fat area; TAMA, total abdominal muscle area; HPP, healthy pancreatic parenchyma*

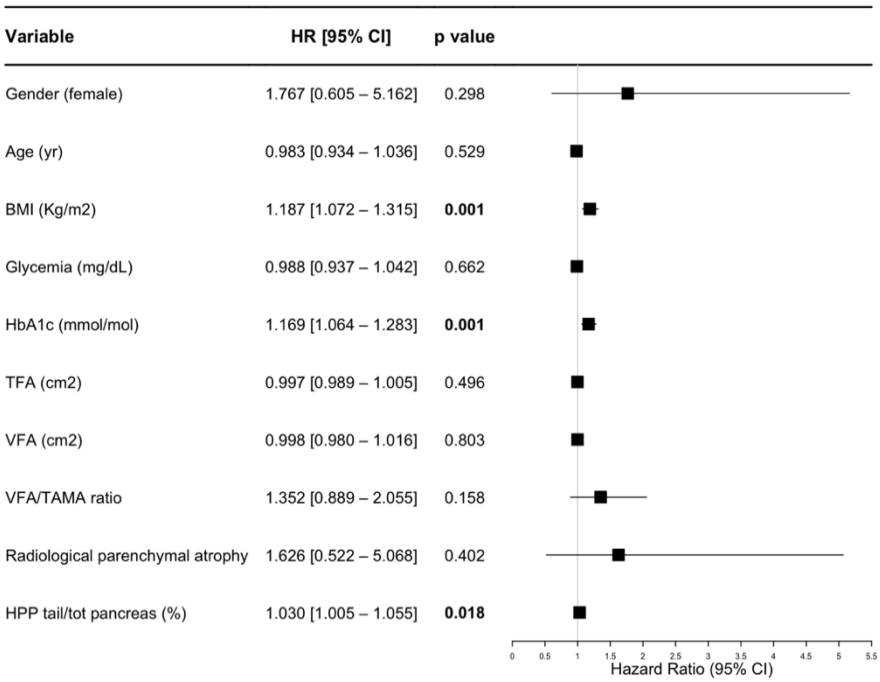

Figure 15. Receiver operating characteristic (ROC) curve assessing the predictive performance of the Cox regression model (based on linear predictor, Xβ) for postoperative new-onset diabetes mellitus.

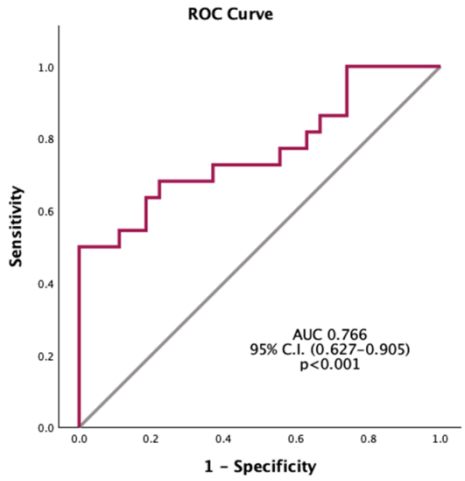

The nomogram based on the final Cox regression model is depicted in **Figure 16**, estimating the individual probability of developing PONO-DM at 1-, 3-, and 5 years following DP. The nomogram was further implemented into a web-based risk calculator, which can allow clinicians to directly derive the risk probability of PONO-DM after imputing data of the variables (https://net-distal-pancreatectomy.shinyapps.io/postoperative-diabetes-risk-calculator/).

Figure 16. Nomogram for predicting postoperative new-onset diabetes mellitus (PONO-DM) after distal pancreatectomy for localized nonfunctioning pancreatic neuroendocrine tumours. *The length of each variable line segment in the nomogram reflects the influence of the variable on the occurrence of PONO-DM. The total score is the sum of the score values of each variable, and the scale value corresponding to the total score is the predicted risk probability of PONO-DM occurrence. HPP, healthy pancreatic tissue; HbA1c, glycated haemoglobin; BMI, body mass index*

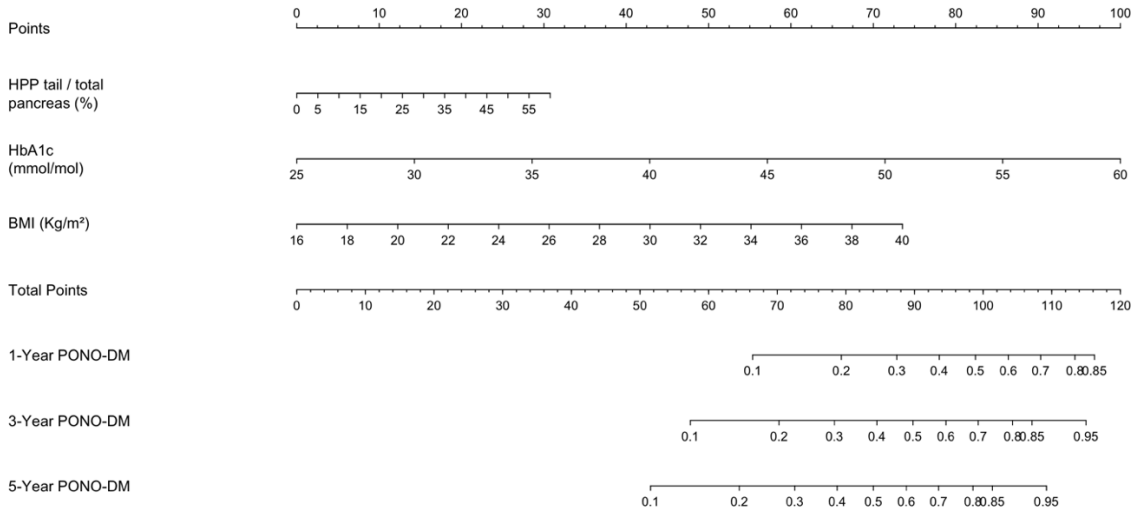

Discussion

NF-PanNETs are frequently characterized by indolent biological behaviour and favourable long-term prognosis(Dasari *et al*, 2017). For patients with localized NF-PanNETs, surgical resection remains the only potentially curative treatment option. However, recent guidelines(Kos-Kudła *et al*, 2023) suggest that a watch-and-wait strategy may be appropriate in selected cases, in presence of small, low-grade tumours. In this scenario, the long-term metabolic consequences of surgery, especially the development of PONO-DM, warrant careful consideration (De Mestier *et al*, 2020; Andreasi *et al*, 2019; Yu *et al*, 2020; Shen *et al*, 2023). Despite increasing awareness, no accurate and validated tools currently exist to predict PONO-DM in the context of NF-PanNETs.

The present study evaluated the incidence and preoperative predictors of PONO-DM in patients undergoing DP for localized NF-PanNETs. PONO-DM occurred in the 41% of the cohort, which is consistent with the incidence rates reported in previous studies involving non-malignant pancreatic conditions(Shirakawa *et al*, 2012; Burkhart *et al*, 2015; Dai *et al*, 2020; Imamura *et al*, 2024; Falconi *et al*, 2008). Of note, nearly one-quarter of patients who developed PONO-DM met criteria for potential overtreatment (Partelli et al, 2024), underscoring the pressing clinical need for improved preoperative risk-benefit stratification in this setting.

Clinical and radiological features were systematically assessed, and distinct preoperative metabolic and anatomical parameters emerged as significant factors associated with an increased risk of PONO-DM. From a metabolic standpoint, elevated preoperative BMI and HbA1c were independently associated with an increased risk of developing PONO-DM over time, corroborating findings from prior studies conducted in broader, heterogeneous surgical populations (Dai *et al*, 2020; Imamura *et al*, 2024; Chen *et al*, 2023; Tariq *et al*, 2020). Importantly, our results highlight the potential role of surgical prehabilitation (De Luca *et al*, 2023; D'Amico *et al*, 2025) in patients with PanNETs. Indeed, targeted preoperative strategies, such as preoperative weight reduction and glycaemic optimization, may reduce the risk of postoperative endocrine dysfunction and contribute to improved long-term clinical outcomes.

About radiologically-derived parameters, an association between preoperative body composition and the risk of PONO-DM was observed. Patients with increase fat-related measures, specifically TFA, VFA, VFA/TAMA ratio, reported a higher incidence of PONO-DM. Similarly, pancreatic parenchymal atrophy on imaging was more common among affected individuals. However, these findings did not retain significance as independent predictors in multivariable analysis. In contrast, anatomical measurements related to pancreatic parenchyma demonstrated that the proportion of healthy pancreatic parenchyma resected distal to the tumour, resulting in smaller functional remnants, was significantly and independently associated with the development of PONO-DM. This finding aligns with previous reports by *Shirakawa et al.*(Shirakawa *et al*, 2012), *Shen et al.*(Shen *et al*, 2023), and *Izumo et al*.(Izumo *et al*, 2020), which demonstrated that a smaller residual pancreatic parenchymal volume correlates with an increased risk of

postoperative endocrine insufficiency. These data highlight the importance of preserving functional pancreatic parenchyma whenever oncologically appropriate and support the consideration of parenchyma-sparing resections or non-operative management (i.e., active surveillance) in well-selected cases. Notably, the present study employed a simplified radiological approach based on linear pancreatic measurements, offering a pragmatic alternative to the labour-intensive volumetric techniques used in previous cohorts (Shirakawa *et al*, 2012; Izumo *et al*, 2020; Shen *et al*, 2023). This method demonstrated good reproducibility and may be readily integrated into routine preoperative imaging assessments.

Based on all significant preoperative predictors of PONO-DM (HbA1c, BMI, percentage of distal HPP/total pancreas) a nomogram and an online risk calculator were established to estimate the risk for PONO-DM at 1, 3, and 5 years postoperatively, on an individual base. The newly developed prediction model demonstrated good discriminative performance and represent valuable tool to support preoperative counselling and guide personalized surgical planning.

Finally, no association was found between PONO-DM and pathological features of aggressiveness, such as tumour dimension and grade, lymph node metastases, vascular or perineural invasion. Nevertheless, a trend toward higher recurrence rates was observed among patients who developed PONO-DM, consistent with findings by *De Mestier et al*.(De Mestier *et al*, 2020). This observation further reinforces the importance of preventing PONO-DM, particularly in patients with otherwise favourable oncologic profiles. Indeed, metabolic disturbances associated with PONO-DM (i.e., hyperglycaemia, insulin resistance, and chronic low-grade inflammation), may promote a pro-tumourigenic environment, contributing to disease progression and recurrence(Gallo *et al*, 2018).

Several limitations must be acknowledged. First, the retrospective design of the study. Consequently, radiological parameters were extracted through post-hoc review, and preoperative biochemical data were not consistently available. Second, the sample size of the cohort was relatively small due to strict inclusion criteria and involvement of a single Institution. Nevertheless, the long-term follow-up ensured and strengthened the reliability

of outcome assessments. Third, the timing and modality of preoperative imaging were not uniform across the cohort. However, all scans were performed within one year prior to surgery as part of standard preoperative staging, and measurements were performed employing standardized protocols and validated software to minimize variability. Finally, although the newly developed nomogram demonstrated good internal discrimination, external validation in larger, independent cohorts is required.

In conclusion, the present study assesses the risk of developing PONO-DM in patients submitted to DP for NF-PanNET. Elevated BMI, HbA1c, and a higher proportion of healthy pancreatic parenchyma resected distal to the tumour emerged as independent preoperative predictors of PONO-DM. By integrating metabolic and radiological parameters, a practical nomogram and web-based risk calculator were constructed to estimate individual patient risk. This tool may assist in anticipating the risk of postoperative endocrine complications and support the implementation of targeted prehabilitation strategies and personalized surgical decision-making. Nonetheless, biologically informed criteria for surgical indication are urgently needed to better identify patients who are likely to derive meaningful benefit from resection and for whom the risk of long-term morbidity is justified, particularly given the often indolent course of this disease.

3) Personalized preclinical models

Aim: to evaluated PDTs from PanNETs spanning grades G1–G3, determining their validity as ex vivo platforms for personalised drug testing and to developed and optimize the protocol for generation PCTSs from primary PanNETs specimens, ensuring preservation of native tissue architecture, vasculature, and stromal composition.

Materials and Methods

Patient-derived tumoroids Patient Collective

Fresh human PanNET tissue was obtained from patients diagnosed with NF-PanNET undergoing surgery at the Pancreatic Surgery Unit, San Raffaele Hospital, Milan, Italy and Inselspital Bern, Switzerland (2018 and 2020). All patient materials were used according to the human research act and had signed an institutional form of broad consent. Upon surgical resection a pathologist processed one mirror block of the tumour tissue to 1cm^3 blocks under sterile conditions avoiding necrotic regions. These blocks were suspended in recovery cell culture freezing medium (Thermo Fisher Scientific, USA), cryopreserved using an isopropyl alcohol freezing container (Nalgene, USA) and stored in liquid nitrogen.

Primary Cell Isolation and Culture

Cells were isolated and culture according to previously published protocol (April-Monn *et al*, 2021). Cryopreserved tumour pieces of 1 mm3 were thawed and dissociated in digestion medium (10 mg/mL collagenase IV (Worthington, USA), 0.25% Trypsin-EDTA (Sigma-Aldrich, Switzerland), and 0.2 mg/mL DNase (Roche, Switzerland) in advanced DMEM-F12, Hepes 10 mM, 1% L-glutamine, 1% penicillin-streptomycin-amphotericin B) using a gentle MACS TM dissociator (Miltenyi Biotec, Switzerland). Cells were filtered through a 70 µm strainer to remove collagen debris, and red blood cells were lysed with ACK lysis buffer (Thermo Fisher, Scientific, USA). After mechanical fibroblast removal and single-cell dissociation, cells were resuspended and maintained in AdvDMEM + GF medium (DMEM- F12, 5% FBS, Hepes 10 mM, 1% L-glutamine (200 mM), 1% penicillin (100 IU/mL), 1% streptomycin (0.1 mg/mL), 1% amphotericin B (0.25 mg/mL) (Merck, Switzerland), 20 ng/mL EGF, 10 ng/mL bFGF (Thermo Fisher Scientific, USA), 100 ng/mL PlGF, 769 ng/mL IGF-1 (Selleckchem,

USA)). After 2 days of recovery phase, cells were counted and resuspended in fresh AdvDMEM + GF medium supplemented with 123 µg/mL growth-factor-reduced Matrigel® (Corning, USA) and plated in 96-well ULA plates (50 µL/well, 3–4 $\times 10^3$ cells/well).

Patient-derived tumoroids Drug Preparation

Compounds sunitinib (S1042, Selleckchem), everolimus (S1120, Selleckchem) and temozolomide (S1237, Selleckchem) were obtained from commercial vendors and stored as stock aliquots at –80 ° C. A 5-point, 625-fold concentration range was used for all compounds. Sunitinib: 0.0256 uM, 0.1280 uM, 0.6400 uM, 3.200 uM, 16.000 uM. Everolimus: 0.0008 uM, 0.004 uM, 0.02 uM, 0.1 uM, 0.5 uM. Temozolomide: 0.46 uM, 2.3 uM, 11.52 uM, 57.6 uM, 288 uM.

Patient-derived tumoroids Viability Measurement

The RealTime-Glo™ MT Cell Viability (RTG) assay (Promega, Switzerland) was used to continually monitor cell viability of 3D human primary PanNET cultures. The RTG assay was performed according to the manufacturer's instructions, and luminescence was measured in an Infinite® 200 PRO plate reader (Tecan, Switzerland).

Patient-derived tumoroids Micro-Cell-Blocks (MCBs)

Islet-like tumoroids corresponding to 3-5 ×104 cells were collected (either directly on the day of isolation (D0) or from the 96-well ULA plate at the end of drug screening (D12)). Cells were captured in plasma-thrombin clots and fixed, counterstained with Hematoxylin, and embedded in paraffin. 2.5µm-thick serial sections were stained for synaptophysin (Cat. No. 27G12, Novocastra, Leica Biosystem, USA, 1:100). Slides were counterstained with hematoxylin. Scans were acquired with a Panoramic 250 (3DHistech, Hungary) automated slide scanner at 20×magnification. Images were acquired using QuPath software (Bankhead *et al*, 2017).

Precision-cut tumour slices Patient Collective

Patients submitted to surgery for PanNET at HSR between 2022 and 2025 were enrolled (*3DPanNET protocol*). Fresh pancreatic surgical specimens not required for diagnostic purposes were retrieved immediately after resection from the pathology unit and transported to the laboratory on ice (4 °C). From each specimen, approximately 0.5

cm^3 tissue blocks were prepared and either processed immediately (fresh protocol) or cryopreserved.

For cryopreservation, samples were immersed in cell-culture freezing medium (Thermo Fisher Scientific, USA), placed in an isopropyl alcohol–based controlled-rate freezing container (Nalgene, USA), and stored in liquid nitrogen.

Precision-cut tumour slices Generation and Culture

Tumour samples were embedded in 4% low-temperature agarose to ensure structural stability during slicing. Cryopreserved samples were first thawed for 45–60 seconds in a 37 °C water bath. PCTS were generated under sterile conditions using a Leica VT1200 S vibrating microtome (Leica Biosystems, Nussloch, Germany). Slices of 350 µm thickness were obtained using continuous blade oscillation while specimens were fully submerged in DPBS (Thermo Fisher Scientific, USA) supplemented with 1% penicillin (100 IU/mL) and 1% streptomycin (0.1 mg/mL).

Following slicing, tissues were transferred to 24-well ultra-low attachment plates (Corning® Costar®, USA) and cultured in 1 mL/well of tumour-slice medium (AdvDMEM + GF), consisting of: DMEM/F12, 5% FBS, 10 mM HEPES, 1% L-glutamine (200 mM), 1% penicillin (100 IU/mL), 1% streptomycin (0.1 mg/mL), 1% amphotericin B (0.25 mg/mL; Merck, Switzerland), 20 ng/mL EGF, 10 ng/mL bFGF (Thermo Fisher Scientific, USA), 100 ng/mL PlGF and 769 ng/mL IGF-1 (Selleckchem, USA). Cultures were maintained at 37 °C, 5% CO_2, and 21% O_2 in a humidified incubator.

Precision-cut tumour slices Viability

Alamar Blue assay (Cat. No. DAL1025; Thermo Fisher Scientific, Massachusetts, USA) was performed on the slices to assess cellular viability. The reagent was diluted 1:10 in the appropriate culture medium added to the slices and incubated at 37◦C with 5% CO2 for 4 h. As a control for background fluorescence, an empty well was filled with both medium and Alamar Blue solution. After incubation, 100 µL of the mixture was transferred to a 96-well light-screened plate, and relative fluorescence units (RFU) were measured using the Victor3 multilabel plate reader (PerkinElmer, Buckinghamshire, UK). Background fluorescence was subtracted from the absolute RFU values. After 24 hours from slices culture, for Alamar blue reagent was added to each well, for baseline viability

assessment. After baseline viability reading, two slices were snap-frozen on dry ice for HE evaluation. The remaining slices were stratified based on baseline viability. Slices were then allocated to treatment conditions such that each drug concentration contained a comparable distribution of baseline viabilities.

Precision-cut tumour slices Drug Preparation and Testing

After a 48-hour recovery phase (baseline viability), drug treatments were initiated and tested for 7 days. Drug-containing medium was replenished every 48 hours, and Alamar Blue assays were performed 24 hours after each drug exposure. The following agents were tested at five serial concentrations each: Everolimus (S1120, Selleckchem) and Sunitinib (S1042, Selleckchem), as previously described for patient-derived tumoroids. Drug conditions were plated in duplicate to triplicate per concentration. Each experimental plate included 2-4 DMSO-treated slices as positive viability controls. At the end of the culture period, all remaining slices were snap-frozen on dry ice and stored at -80 °C for downstream immunofluorescence and HE analyses.

Curve Fitting and Drug Sensitivity Data

Drug-response curve data consisted of 1) PDTs: six DMSO-positive controls and five drug-response points and 2) PCTSs: two to four DMSO-positive controls, and five drug-response points. A 5-point, 625-fold concentration range was used. Values obtained from 7 days treatment were weighted and normalized to each individual baseline control value at baseline for the same well: drug effect estimates were obtained by adjusting normalized luminescence measurements to the growth rate (GR) of the control treated sample using GRmetrics v1.16.0 (Hafner *et al*, 2016). Drug sensitivity was then calculated as the area over this GR value curve (GR AOC) with larger GR AOC values indicating a stronger inhibition of cell growth. Samples with an GR AOC above the median of the distribution were considered responders and samples with an GR OAC below the median distribution were considered non-responders(Hafner *et al*, 2016). For PDTs sensitivity, additional stratification was performed based on absolute GR AOC cut-offs defined as median ± 0.25: lower vs intermediate vs higher sensitivity.

Histochemistry

For hematoxylin and eosin staining, tissue sections were rehydrated in distilled water and stained with hematoxylin (Cat. No. 05–06002; BioOptica S.p.A., Milan, Italy),

followed by rinsing under running water and soaked in 95% ethanol. Sections were subsequently counterstained with eosin (Cat. No. 05–10007; BioOptica S.p.A., Milan, Italy), washed, and dehydrated through graded ethanol solutions (95%, 100%) and xylene. Histological images were acquired using an Aperio AT2 scanner (Leica, Wetzlar, Germany), and analyzed with QuPath (Bankhead *et al*, 2017).

Immunofluorescence Analyses and Acquisition

For immunofluorescence staining, slices were permeabilized and blocked using a solution containing 10% FBS, 0.3% Triton X-100 (Cat. No. A4975; AppliChem GmbH, Darmstadt, Germany), and 1 mg/mL BSA (Cat. No. A2153; Sigma-Aldrich, Missouri, USA). Sections were incubated with primary antibodies overnight at 4°C, followed by secondary antibody incubation for 2 h at room temperature. The following primary antibodies were used: anti-CD31 (Cat. No. ab32457; Abcam, Cambridge, UK, 1:100), anti-CD45 (Cat. No. 14-9457-82, Thermo Fisher Scientific, Massachusetts, USA, 1:100), anti-collagen IV (Cat. No. 53-9871-82; Thermo Fisher Scientific, Massachusetts, USA, 1:50), anti-collagen IV (Cat. No. ab236640; Abcam, Cambridge, UK, 1:100), anti-chromogranin A (Cat. No. ab283265, Abcam, Cambridge, UK, 1:100), anti-synaptophysin (Cat. No. ab8049, Abcam, Cambridge, UK, 1:100). Secondary antibodies used: Alexa Fluor 488 (Cat. No. A32790 and A32766; Thermo Fisher Scientific, Massachusetts, USA, 1:500), Alexa Fluor 647 (Cat. No. A32733 and A32728; Thermo Fisher Scientific, Massachusetts, USA, 1:500), Streptavidin Alexa Fluor 647 Conjugate (Cat. No. S32357; Thermo Fisher Scientific, Massachusetts, USA, 1:500). Actin was stained using Alexa Fluor 568 Phalloidin, added with secondary antibodies (Cat. No. 94072; Sigma-Aldrich, Missouri, USA, 1:250). Nuclei were stained with hoechst 33342 (Cat. No. 23491-52-3; Merck KGaA, Darmstadt, Germany) at a 1:1000 dilution for 10 min at room temperature. Immunofluorescence images were acquired as single images or as z stack reconstructions using Olympus FluoVIEW 3000 RS confocal microscope (Olympus, Tokyo, Japan). Images were analyzed with Fiji (Schindelin *et al*, 2012) software.

Tissue Immunohistochemistry

2.5 µm sections from next generation TMAs were used for immunohistochemistry. Immunostainings were performed on an automated staining system (Leica Bond RX; Leica Biosystems, Nunningen, Switzerland). The following antibodies were employed: anti-synaptophysin (Cat. No. 27G12, Novocastra, 1:100), anti-MCT-4 (Cat. No. ab15086, Abcam, 1:500), anti-CD-34 class II antibody (Cat. No. M7165, Dako, 1:100), anti-DAXX (polyclonal rabbit, Sigma, 1:40), anti-ATRX (polyclonal rabbit, Sigma, 1:400), and ant-ARX (Cat. No. AF7068, R&D Systems, 1:1500). Antibody detection was performed with the Bond Polymer Refine Detection kit (Leica Biosystems, DS9800) using 3,3-diaminobenzidine (DAB) as brown chromogen and following the manufacturer's instructions. The samples were counterstained with haematoxylin, dehydrated and mounted with Pertex (Sakura). Slides were scanned on Panoramic 250 Flash (3DHISTECH), enabling their teleconsultation by means of 3DHistech CaseViewer software. For MCT-4, each sample was scored as negative, heterogeneous positive or homogeneous positive. DAXX and ATRX stainings were scored as previously described (Marinoni et al, 2014). CD-34 staining was performed to calculate MVD. In each TMA punch (diameter 0.6 mm), microvessels with a clearly defined lumen or a well-defined linear shape were manually counted, employing the counting tool from QuPath open-source software. Each microvessel was recognized by eye based on the aforementioned criteria. MVD was expressed as number of microvessels per 1 mm^2.

Patients Data Collection

Preoperative and postoperative data were retrospectively retrieved from appropriate database. Preoperative variables, including demographic characteristics (age and sex), and BMI were reviewed. The following pathological characteristics were recorded: tumour site, tumour size, tumour grade, T/N/M stages, microvascular and perineural invasion, and presence of necrosis. Tumour grade was determined based on the 2017 World Health Organization (WHO) classification into G1 (Ki67<3%), G2 (Ki67 3-20%) and G3 (Ki67 >20%)(Lloyd *et al*, 2017). The Ki67 proliferative index was assessed by MIB1 antibody staining and expressed as the percentage of cells with nuclear staining in 2000 cells, counted in the area of highest nuclear labelling(Klimstra *et al*, 2010). Tumour stage was categorized following the current European Neuroendocrine Tumour Society (ENETS) TNM staging system(Rindi *et al*, 2006). Pre- and post-surgical therapeutic

management was reviewed, and treatment responses were recorded. Clinical response evaluation was performed according to investigator-assessed RECIST criteria (Eisenhauer *et al*, 2009).

Statistical Analysis

Categorical variables were presented as absolute numbers with corresponding percentages (%) and compared using the the χ^2 or Fisher exact test, as appropriate. Continuous variables were reported as median with interquartile ranges (IQR) for skewed distribution, or as mean ± standard deviation (SD) for normal distributions. The normality of continuous variables was assessed using the Kolmogorov-Smirnov test. Continuous variables were compared between two groups by using Student's t test or Mann-Whitney U test, as appropriate based on the variables' distribution. Statistical significance was set at a p-value less than 0.05. Statistical analyses were performed using SPSS software, version 29.0.2 for Mac (IBM Corp., Armonk, NY, USA) and R software, version 4.5.0 (R Foundation for Statistical Computing, Vienna, Austria), using *ggplot2*, *GRmetrics* libraries.

Results

Patient-derived tumoroids

Patient Cohort

Patients who underwent surgical resection for PanNETs between 2018 and 2020 at HSR (Italy) or the University of Bern (UniBE, Switzerland) and for whom cryopreserved tumour tissue was available were included in this study. A total of 22 patients met inclusion criteria, comprising 15 individuals treated at HSR and 7 treated at UniBE. Comprehensive demographic, clinical, and pathological data, along with longitudinal clinical follow-up, were available for all cases.

Demographics and Pre-operative Characteristics

Baseline demographic and pre-operative variables are summarized in **Table XIII**. The mean age at surgery was 54 years (±15), and female patients represented the majority of the cohort (16/22, 73%). Four patients (18%) received systemic therapy prior to surgical resection. Specifically, one patient was treated with FOLFOX, one with capecitabine–temozolomide, one underwent peptide receptor radionuclide therapy (PRRT), and one received sunitinib followed by PRRT.

Patient _ID	Sex, female	Age, yrs	Treatment prior to tissue sampling	Specify
aP321m	0	55	0	
aP455m	0	48	0	
aP471m	1	48	0	
aP476m	0	65	0	
aP479p	1	46	0	
aP487p	1	56	0	
aP499p	1	69	0	
mP036p	1	59	1	FOLFOX
mP038p	1	59	0	
mP044p	1	19	0	
mP045p	1	78	0	
mP049p	1	66	0	
mP050p	0	58	0	
mP051p	1	25	0	
mP057p	0	73	0	
mP058p	0	51	0	
mP063m	1	33	0	
mP068p	1	61	1	CAPTEM
mP074p	1	48	1	PRRT
mP077p	1	52	1	SUN – PRRT
mP078p	1	46	0	
mP080m	1	75	0	

FOLFOX, Folinic acid, 5-Fluorouracil, and Oxaliplatin; *CAPTEM*, Capecitabine, Temozolomide; *PRRT*, Peptide receptor radionuclide therapy; *SUN*, Sunitinib

Table XIII. Patients' demographic and preoperative characteristics

Histopathological characteristics

Pathological features are depicted in **Table XIV**. At the time of surgery, 12 patients (54%) had metastatic disease. The median Ki-67 index was 6.5% (i.q.r. 2–17%), resulting in grade distribution as follows: G1 in six cases, G2 in fourteen cases, and G3 in two cases. Alterations in DAXX/ATRX were identified in 15 tumours (68%). Expression of the hypoxia-associated transporter MCT-4 was observed in seven tumours (32%), including five with heterogeneous and two with homogeneous staining patterns. The median microvascular density (MVD) was 136 vessels/mm² (i.q.r. 68–274).

Table XIV. Patients' pathological characteristics at histological examinations *TNM staging* (Rindi *et al*, 2006)*; G, grading (ki67) (Lloyd et al, 2017); Sample site: M*, liver metastasis; *P*, primary tumour. *Het*, heterogeneous; *Hom*, homogeneous; *MVD*, microvascular density

Patient _ID	T	N	M	Sample site	G	Ki 67(%)	PDX1	ARX	DAXX/ATRX mut	MCT-4	MVD (n/mm2)
aP321m	3	1	1	M	3	75	Positive	Negative	1	Het	90.14
aP455m	3	1	1	M	2	15	Positive	Negative	0	Negative	155.37
aP471m	3	0	1	M	2	5	Positive	Negative	1	Negative	372.70
aP476m	-	-	1	M	2	15	Positive	Positive	1	Negative	87.43
aP479p	1	0	0	P	2	5	Negative	Positive	0	Negative	157.39
aP487p	3	1	0	P	2	7	Positive	Negative	1	Het	106.19
aP499p	3	1	0	P	2	20	-	-	1	-	-
mP036p	2	0	0	P	2	6	-	-	1	Negative	64.44
mP038p	3	1	1	P	2	4	Positive	Negative	1	Negative	49.11
mP044p	3	1	0	P	2	18	Negative	Positive	1	Het	135.92
mP045p	3	0	1	P	2	17	Positive	Negative	1	Negative	57.55
mP049p	2	0	0	P	1	2	Positive	Negative	0	Negative	607.50
mP050p	2	1	0	P	1	<1	-	-	-	Negative	122.73
mP051p	3	0	0	P	1	<1	Positive	Negative	0	Negative	214.29
mP057p	4	1	1	P	2	19	-	-	0	Het	58.36
mP058p	2	0	0	P	1	1	Negative	Positive	1	Negative	325.97
mP063m	3	1	1	M	2	5	Positive	Negative	1	Negative	222.22
mP068p	2	1	1	M	1	1	Positive	Negative	1	Negative	195.53
mP074p	3	0	1	P	2	10	Positive	Negative	1	Hom	528.09
mP077p	3	1	1	P	3	65	Negative	Positive	0	Hom	43.60
mP078p	2	0	0	P	1	2	Negative	Positive	1	Negative	637.14
mP080m	1	0	1	M	2	10	Negative	Positive	1	Het	72.51

Patient-derived tumoroids Generation

In collaboration with University of Bern, Institute of Tissue Medicine and Pathology (Dr. Ilaria Marinoni), patient-derived tumoroids (PDTs) cultures were successfully generated from all cryopreserved tumour samples using a previously established protocol (April Monn et al. 2021). In total, 22 PDTs were obtained: 15 derived from primary pancreatic tumours and 7 from liver metastases. Histomorphology and immunophenotyping analyses demonstrated that PDTs maintained key neuroendocrine tumour features. PDTs retained neuroendocrine morphology, architecture and expression of diagnostic neuroendocrine biomarker synaptophysin, based on cytology of micro-cell-block staining from cultured cells (**Figure 18**). The proportion of tumour cell remained high throughout the culture period. As expected, non-tumour stromal and immune components were not retained in culture.

Figure 18. Representative Hematoxylin and eosin (HE) staining and neuroendocrine diagnostic marker synaptophysin (SYN) immunolabeling in original tumour tissue (a, c) and tissue-matched patient-derived tumoroids (b, d) after 10 days of culture. *Scale bar, 25um.*

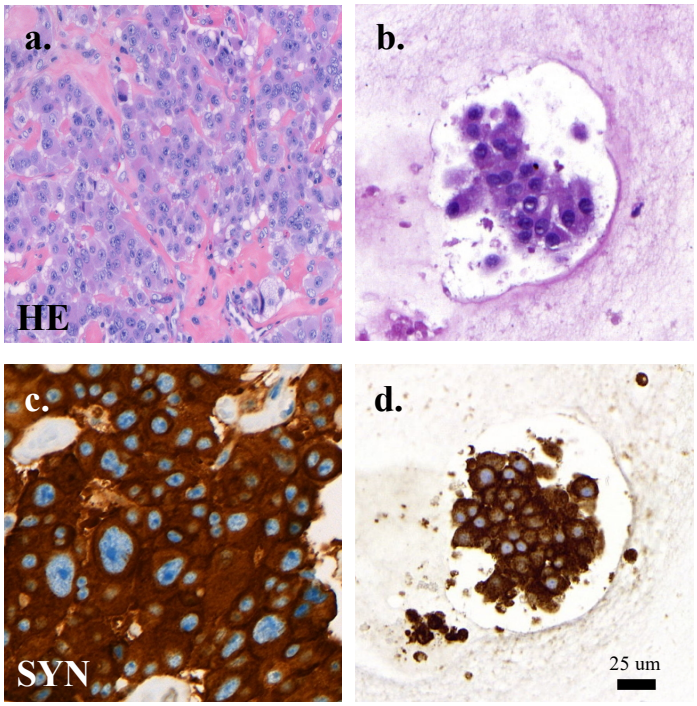

Patient-derived tumoroids Drug Sensitivity

After two days recovery period, PDTs were exposed for 10 days to three clinically approved agents used in PanNET management: sunitinib, everolimus, and temozolomide, using a five-point 625-fold serial dilution scheme. Drug responses were quantified relative to DMSO-treated controls, and growth-rate-adjusted drug sensitivity metrics (GR-metrics) were applied to classify PDTs into sensitivity categories (**Figure 19**). Everolimus testing was performed in 19 PDTs, sunitinib in 20, and temozolomide in 14. Among these, thirteen PDT lines were evaluable for all three agents; one for everolimus and temozolomide; and six for everolimus and sunitinib.

Figure 19. Drug response of tumoroids to sunitinib, everolimus, temozolomide treatment*, generated in collaboration with the University of Bern (Dr Ilaria Marinoni). **A)** Tumoroid drug sensitivity classified into higher and lower responders using the cohort median growth rate area over the curve (GR AOC) value as the threshold. **B)** Tumoroid drug sensitivity further stratified into higher, intermediate, and lower responders based on absolute GR AOC cut-offs defined as median ± 0.25. GR*, growth rate; *AOC*, area over the curve; *blue dots*: lower sensitivity, *red dots*: higher sensitivity, *yellow dots*: intermediate sensitivity

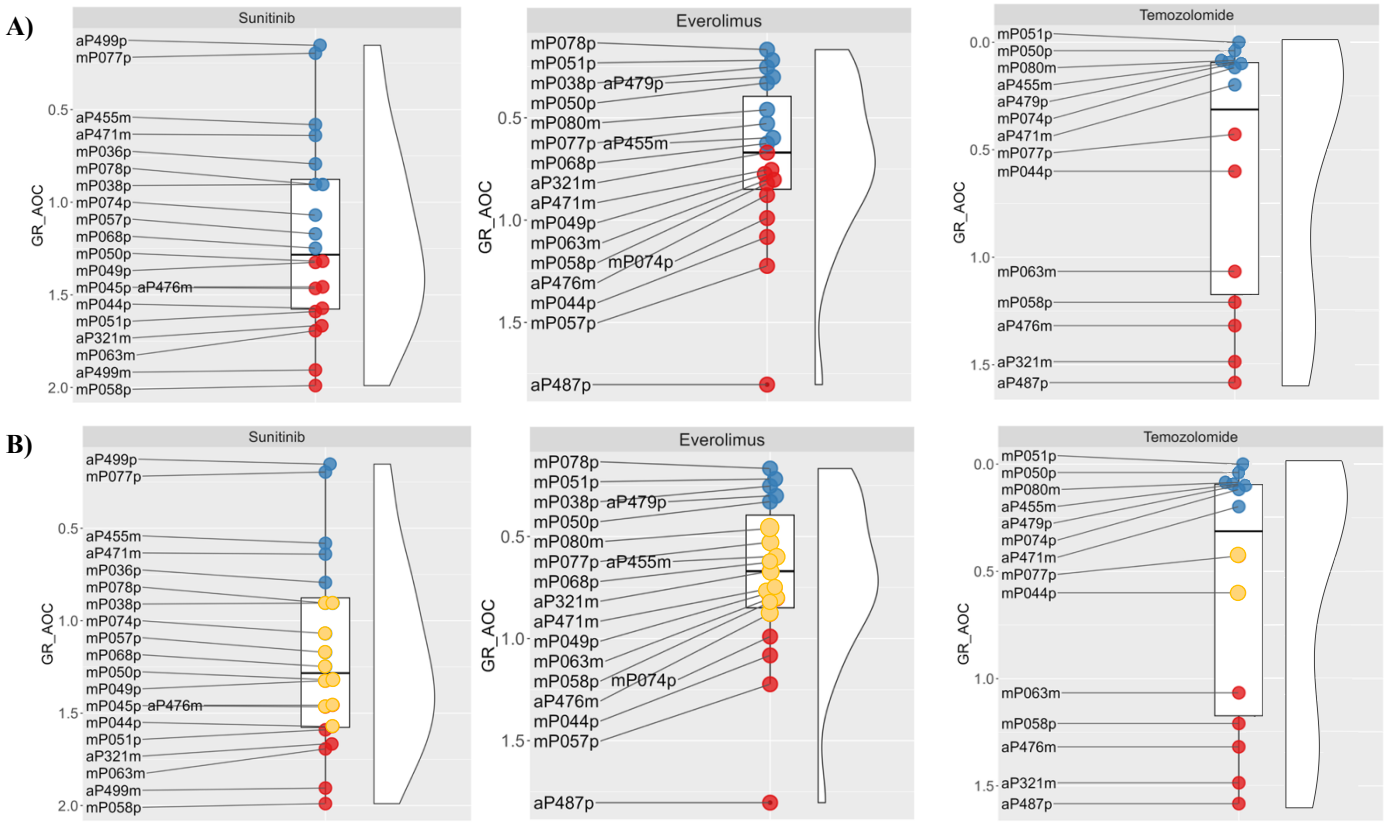

To evaluate the heterogeneity of therapeutic response, PDTs were first dichotomized according to the median GR-value as the sensitivity cut-off, for each drug. Using this binary classification, 50% (10/20) of PDTs demonstrated relative sensitivity to sunitinib and 50% (7/14) to temozolomide. Everolimus showed a similarly balanced response pattern, with 10/19 PDTs exhibiting higher sensitivity and 9/19 lower sensitivity.

Subsequently, a more granular three-tiered stratification was applied, defining an intermediate sensitivity group as the interval between the median ± 0.25 threshold. Under this system, sunitinib sensitivity distributed as follows: five PDTs demonstrated high sensitivity, ten intermediate sensitivity, and five low sensitivity. Temozolomide produced an asymmetric distribution, with five PDTs classified as highly sensitive, two as intermediately sensitive, and seven as lower-sensitivity. Lastly, for everolimus, four PDT

lines demonstrated higher sensitivity, ten fell within the intermediate category, and five exhibited lower sensitivity.

Tumour Histopathological Characteristics and Patient-derived tumoroids Sensitivity

Histopathological characteristics of the corresponding tumour specimen were examined for each PDT line. No statistically significant associations were identified between PDT sensitivity to sunitinib (**Tables XVa**) or temozolomide (**Tables XVc**) and the histopathological characteristics of the corresponding tumour tissues. In contrast, everolimus response demonstrated a significant association with specific tissue-based features (**Tables XVb)**. PDTs derived from tumours with heterogeneous MCT-4 expression exhibited reduced sensitivity to everolimus, with no sensitive cases observed in this subgroup (0/4, 0%), whereas 75% (3/4) of PDTs from tumours lacking MCT-4 heterogeneity were classified as sensitive ($p = 0.008$). Moreover, a higher proliferative index in the original tumour correlated with increased ex-vivo sensitivity to everolimus. Tumours associated with everolimus-sensitive PDTs exhibited a median Ki-67 index of 14% (i.q.r. 7.75–18.75%), compared with 2% (i.q.r. 1–4.5%) in those associated with low sensitivity ($p = 0.014$). A significant association between Ki67 index and MCT4 status was observed, with MCT4-heterogeneous tumours exhibiting higher Ki67 values ($p = 0.035$).

Table XV. Comparison between patient-derived tumoroids (PDTs) drug responses (lower vs intermediate vs higher sensitivity) and tumour histopathological characteristics. a) *Sunitinib treated PDTs.* ***b)*** *Everolimus treated PDTs.* ***c)*** *Temozolomide treated PDTs. TNM staging* (Rindi *et al*, 2006); *Grading* (Lloyd *et al*, 2017)

a) Sunitinib

Variables	Low sensitivity (n=7)	High + int sensitivity (n=14)	High sensitivity (n=5)	P value low *vs* high+int sensitivity	P value low *vs* high sensitivity
T stage, T1-2	2 (29)	5 (38)	1 (20)	1.000	1.000
N stage, N1	4 (57)	7 (54)	3 (60)	1.000	1.000
M stage, M1	3 (43)	8 (57)	2 (40)	0.659	1.000
Grading, G1-2	6 (86)	13 (93)	4 (80)	1.000	1.000
Ki67 (%)	7 [5-20]	5 [1-17.5]	5 [1-46]	0.294	0.514
Ki67> 5%	5 (71)	6 (43)	2 (40)	0.361	0.558
Ki67>10%	3 (43)	5 (36)	2 (40)	1.000	1.000
DAXX/ATRX mut	5 (71)	9 (69)	4 (80)	1.000	1.000
MVD (n/mm^2)	130 [59-438]	146 [80-248]	214 [113-274]	0.934	0.715
MCT4*				1.000	1.000
Neg	4 (57)	10 (71)	3 (60)		
Het	1 (14)	3 (21)	2 (40)		
Hom	1 (14)	1 (7)	0 (0)		

**n*=1 missing (low sensitivity)
Int, intermediate; *MVD*, microvascular density

b) Everolimus

Variables	Low sensitivity (n=5)	High+ int sensitivity (n=14)	High sensitivity (n=4)	P value low *vs* high + int sensitivity	P value low *vs* high sensitivity
T stage, T1-2°	3 (60)	4 (29)	0 (0)	0.326	0.167
N stage, N1°	2 (40)	8 (57)	3 (75)	0.608	0.524
M stage, M1	1 (20)	10 (71)	2 (50)	0.111	0.524
Grading, G1-2	5 (100)	12 (86)	4 (100)	1.000	–
Ki67 (%)	2 [1-4.5]	10 [4.25-18.25]	14 [7.75-18.75]	**0.028**	**0.014**
Ki67> 5%	0 (0)	9 (64)	4 (100)	**0.033**	**0.008**
Ki67>10%	0 (0)	6 (43)	2 (50)	0.128	0.167
DAXX/ATRX mut*	2 (40)	10 (71)	3 (75)	0.569	1.000
MVD (n/mm^2)	157 [85-425]	145 [83-337]	121 [70-430]	0.781	0.624
MCT-4				0.210	**0.008**
Neg	5 (100)	7 (50)	0 (0)		
Het	0 (0)	5 (36)	3 (75)		
Hom	0 (0)	2 (14)	1 (25)		

°*n*=1 missing (low sensitivity)
**n*=1 missing (high + int sensitivity)
Int, intermediate; *MVD*, microvascular density

c) Temozolomide

Variables	Low sensitivity (n=7)	High + int sensitivity (n=7)	High sensitivity (n=5)	P value low *vs* high+int sensitivity	P value low *vs* high sensitivity
T stage, T1-2*	3 (43)	1 (14)	1 (20)	0.559	1.000
N stage, N1*	2 (29)	5 (71)	3 (60)	0.103	0.242
M stage, M1	4 (57)	4 (57)	3 (60)	1.000	1.000
Grading, G1-2	7 (100)	5 (71)	4 (80)	0.462	0.417
Ki67 (%)	5 [1-10]	15 [5-65]	7 [3-45]	0.155	0.508
Ki67> 5%	3 (43)	5 (71)	3 (60)	0.592	1.000
Ki67>10%	1 (14)	4 (57)	2 (40)	0.226	0.523
DAXX/ATRX mut*	3 (43)	6 (86)	5 (100)	0.226	0.182
MVD (n/mm^2)	157 [122-372]	106 [87-222]	106 [88-274]	0.225	0.465
MCT4				0.755	0.735
Neg	5 (72)	3 (43)	3 (60)		
Het	1 (14)	3 (43)	2 (40)		
Hom	1 (14)	1(14)	0 (0)		

°*n*=1 missing (high/high + int sensitivity)
**n*=1 missing (low sensitivity)
Int, intermediate; *MVD*, microvascular density

Patient-derived tumoroids Drug Sensitivity versus Clinical Outcomes

Ex-vivo drug sensitivity results were subsequently compared with systemic therapies administered after surgical resection and with corresponding clinical outcomes (**Figure 20, Table XVI**). Concordance was evaluated by categorizing PDTs as lower *versus* intermediate/higher sensitivity and relating these classifications to clinical disease progression (DP) *versus* stable disease (SD).

Among the three patients who received sunitinib following tumour resection, concordance between PDT sensitivity and clinical response was observed in two cases (67%), with one discordant case in which disease progression occurred despite intermediate/high ex-vivo sensitivity. For everolimus, concordance was noted in two of four patients (50%). Interpretation of everolimus agreement rates, however, is limited by intervening therapy. One patient who had undergone PRRT prior to everolimus treatment demonstrated concordance with ex-vivo results, whereas the other, who received CAP-TEM before starting everolimus, exhibited discordance.

Notably, temozolomide yielded complete concordance between ex-vivo PDT sensitivity profiles and subsequent clinical outcomes, with all six post-operatively treated patients exhibiting responses aligned with their tumoroid-derived drug-sensitivity classification (100%). Of these, four patients experienced disease progression, while two maintained stable disease.

Fgure 20. Comparison of clinical response and ex-vivo patient-derived tumoroids drug sensitivity in patients with pancreatic neuroendocrine tumours. *DP, disease progression; PR, partial response*

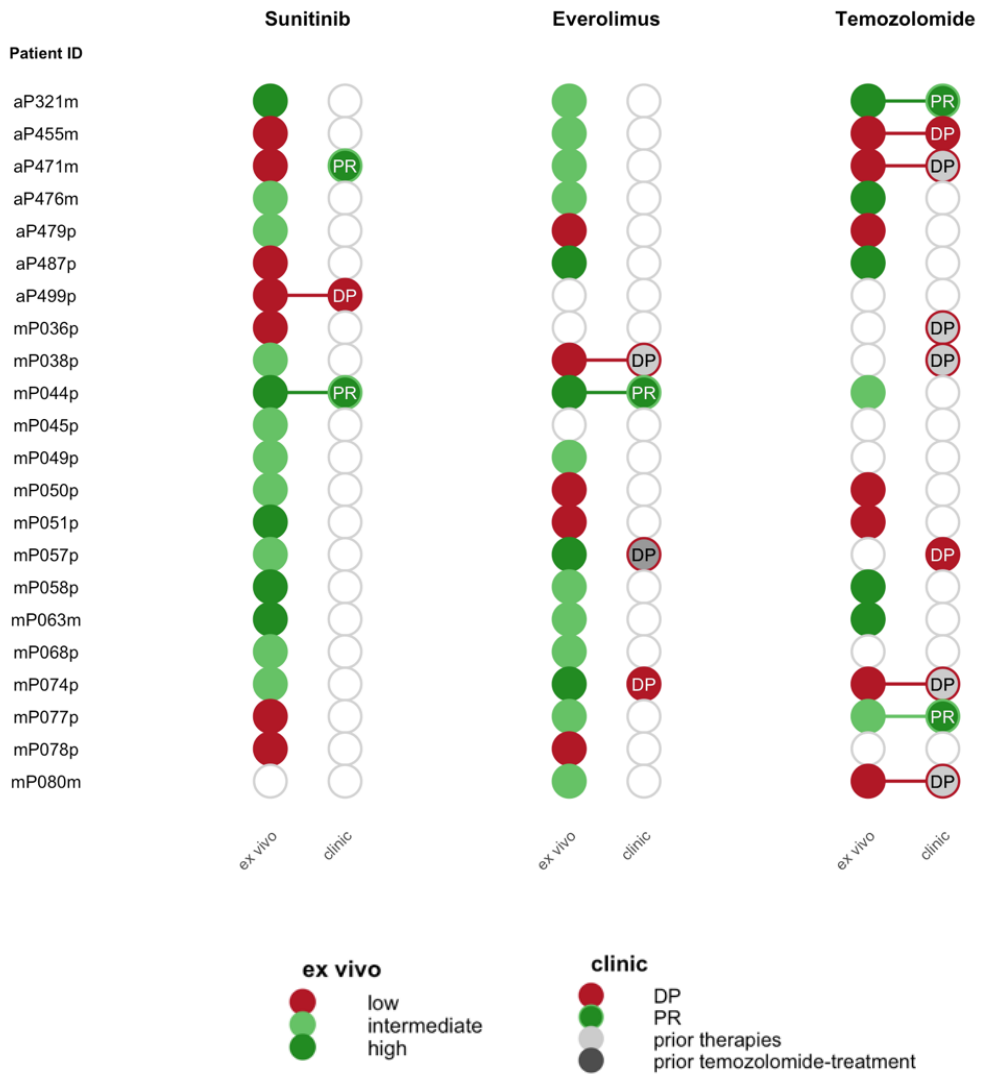

Table XVI. Patient post-operative treatment and drug response

Patient ID	Treatment after surgery (therapy response)
aP321m	TEM (*PR*)
aP455m	CAPTEM (*DP*) – PRRT (*DP*) – surgery (*DP*)
aP471m	Microwave ablation (*DP*) – PRRT (*DP*) – TEM (*DP*) – RNT (*PR*)
aP476m	CARBOPLATIN (*DP*) – microwave ablation + surgery
aP479p	–
aP487p	SSA (*PR*)
aP499p	SUN (*DP*) – irinotecan + lurbinectedin (*PR*) – surgery
mP036p	PRRT + SSA (*DP*) – RT (*DP*) – PRRT + CAP (*DP*) – CAP-TEM (*DP*)
mP038p	PRRT + SSA (*DP*) – EVE (*DP*) – TEM (*DP*) – CAP (*PR*)
mP044p	SSA (*DP*) – EVE (*PR*) – SUN + SSA (*DP*)
mP045p	SSA (*DP*)
mP049p	–
mP050p	–
mP051p	–
mP057p	SSA + CAPTEM (*DP*) – EVE (*DP*)
mP058p	–
mP063m	SURGERY – SSA (*DP*) – PRRT
mP068p	TACE + SSA (*DP*) – thermoablation + SSA (*DP*) – PRRT (*DP*) – surgery
mP074p	EVE (*DP*) – CAP-TEM + SSA (*DP*) – PRRT (*DP*) – SSA
mP077p	CAP-TEM (*PR*)
mP078p	–
mP080m	TACE + SSA (*DP*) – PRRT + SSA (*DP*) – TACE (*DP*) – surgery – CAP-TEM (*DP*)

TEM, temozolomide; *CAP,* capecitabine; *TEM*, temozolomide *PRRT*, peptide receptor radionuclide therapy; *SUN*, sunitinib; *SSA*, somatostatin analogues; *EVE*, everolimus; *TACE*, trans-arterial chemoembolization
DP, disease progression; *PR*, partial response

Precision-cut tumour slices

Given the limited concordance observed between ex-vivo responses to targeted therapies and patient outcomes, and in light of the growing recognition of the critical role played by the tumour microenvironment in cancer biology and therapeutic response, we subsequently sought to develop a complementary ex-vivo model capable of preserving native tissue architecture, cellular heterogeneity, and stromal–immune components. Initial attempts involved generating punches (diameter, 2mm) from primary tumours (**Figure 21**). The small size of available specimens yielded only a limited number of punches, preventing meaningful comparative analyses. Technical reproducibility was low, and substantial inter-sample variability was observed.

Figure 21. Graphical representation of the punch-based strategy for obtaining uniform tumour tissue cores for ex vivo culture. *(created with BioRender)*

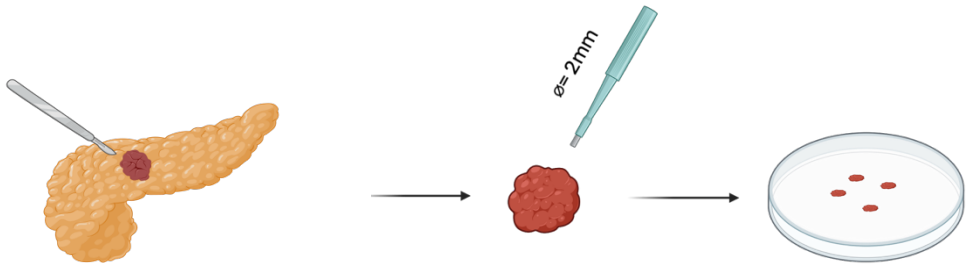

To address these limitations, patient-derived precision-cut tissue slices were subsequently established. A dedicated research workflow (3DPanNET protocol, CET 26-2023, P.I. Battistella A.) was implemented, enabling enrolment of all patients undergoing surgery for NF-PanNETs at HSR from 2023 onwards and biobanking of tumour material in cryopreservation medium. Fresh surgical specimens were initially utilized for protocol optimization. Building upon established tissue-slice protocols previously developed for pancreatic adenocarcinoma (Braun et al. 2021), optimization experiments were performed to tailor the methodology for pancreatic neuroendocrine tumours. This process identified the following settings as optimal for slice generation: frequency 70 Hz, amplitude 1.5, slicing speed 0.175 mm/s, and slice thickness 350 µm. Given the marked inter-patient heterogeneity in tissue composition, vascularity, fibrosis, and tumour architecture characteristic of PanNETs, minor procedural adjustments were occasionally required on a case-by-case basis to ensure optimal cutting performance and slice integrity.

Once the protocol was fully established, each specimen consistently yielded approximately 30–40 slices.

Following sectioning, slices were transferred into 24-well culture plates and maintained in culture using the same defined medium formulation previously optimized for patient-derived tumoroid culture (**Figure 22**).

Figure 22. Culture of precision-cut slices derived from primary PanNET samples in ULA 24-well plates following the optimized vibratome protocol.

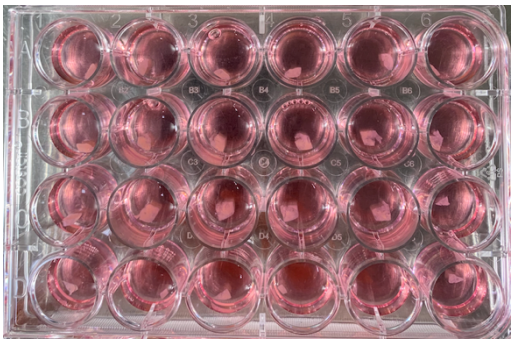

Tissue morphology and structural integrity were subsequently verified by hematoxylin and eosin staining and immunofluorescence analysis, demonstrating preservation of cytoarchitecture, compartmental organization, and key components of the tumour microenvironment (**Figure 23**).

Figure 23. Generation and validation of precision-cut pancreatic neuroendocrine tumour slices. Schematic representation of precision-cut tumour slices generation *(**A**). Representative pancreatic neuroendocrine tumour specimen obtained at surgical resection (**B1**), followed by low-melting agarose embedding (**B2**), vibratome cutting (**B3**) and generation of precision-cut tissue slices (white arrow, **B4**). Haematoxylin and eosin staining (**C**) and immunofluorescence stainings (**D**) of a 350-µm slice demonstrates preservation of tumour cytoarchitecture confirming maintenance of tissue integrity and microenvironment components (endothelial CD34 positive cells, immune CD45 positive cells, CgA positive tumour cells, collagen-IV reach extra cellular matrix), following ex-vivo preparation after 10 days of culture.*

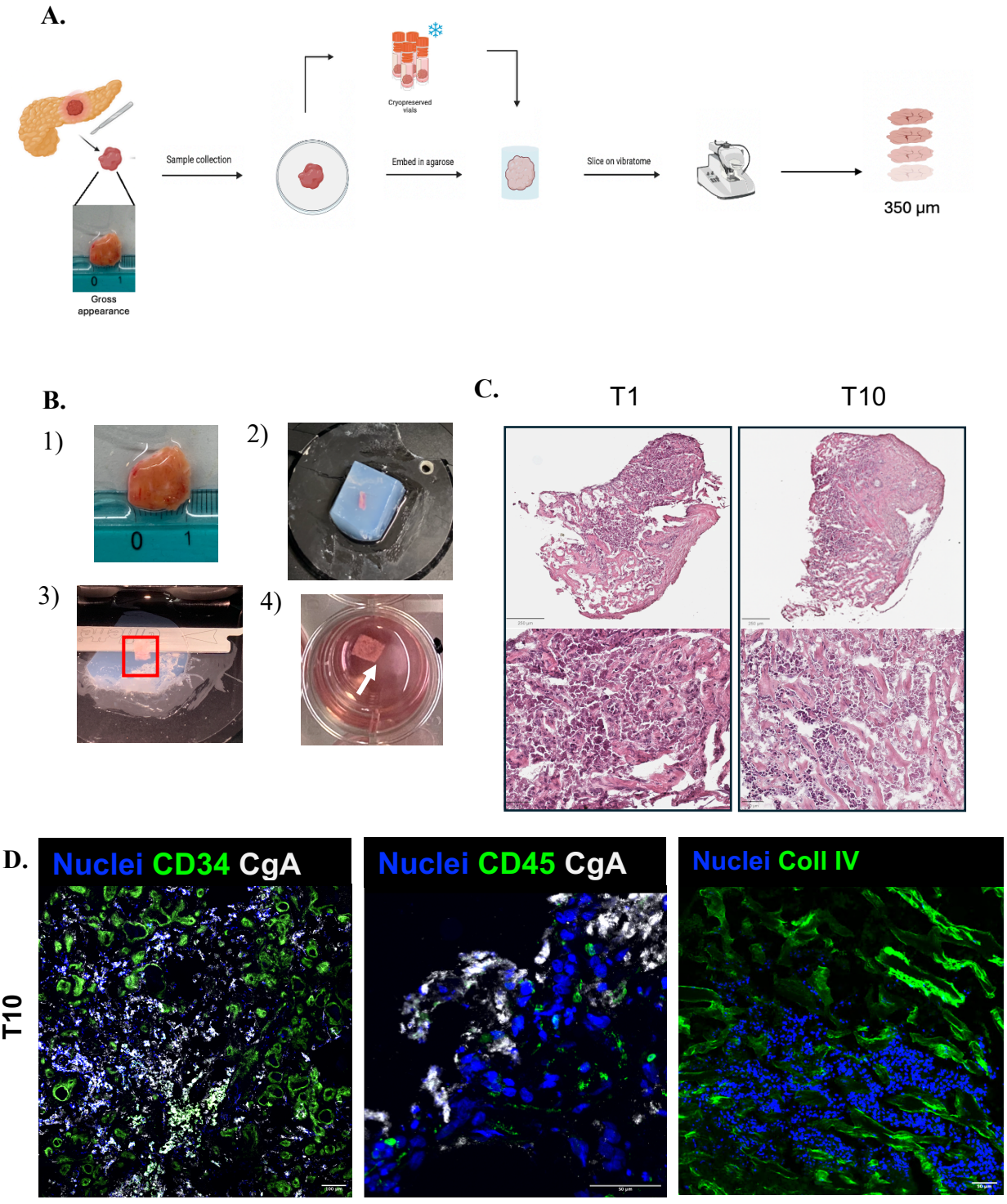

In particular, the tissue slices demonstrated preserved microenvironmental complexity, including CD34-positive endothelial cells, collagen IV–rich stromal matrix, and CD45-positive immune infiltrates, in addition to chromogranin A–positive tumour cells. To evaluate tissue viability and functional maintenance ex vivo, metabolic activity through Alamar Blue assay was monitored in both freshly obtained and cryopreserved precision-cut tumour slices over a 10-day culture period (**Figure 24**). Immediately following vibratome sectioning, a transient decline in metabolic activity was observed in both conditions, consistent with tissue adaptation to ex-vivo culture. However, activity subsequently recovered within 48 hours and remained stable thereafter, demonstrating that both fresh and cryopreserved slices retain metabolic competence and viability for at least 10 days in culture. No significant differences in metabolic trajectories were detected between fresh and previously cryopreserved, supporting the feasibility of this approach for downstream studies.

Figure 24. Metabolic assay (Alamar Blue Assay) of (a) fresh and (b) cryopreserved slices. *An initial decline in metabolic activity was observed during the first day post-sectioning, consistent with tissue adaptation to ex-vivo conditions. Thereafter, metabolic activity recovered and remained stable for up to 10 days in culture in both fresh (4 patients) and cryopreserved slices (3 patients).*

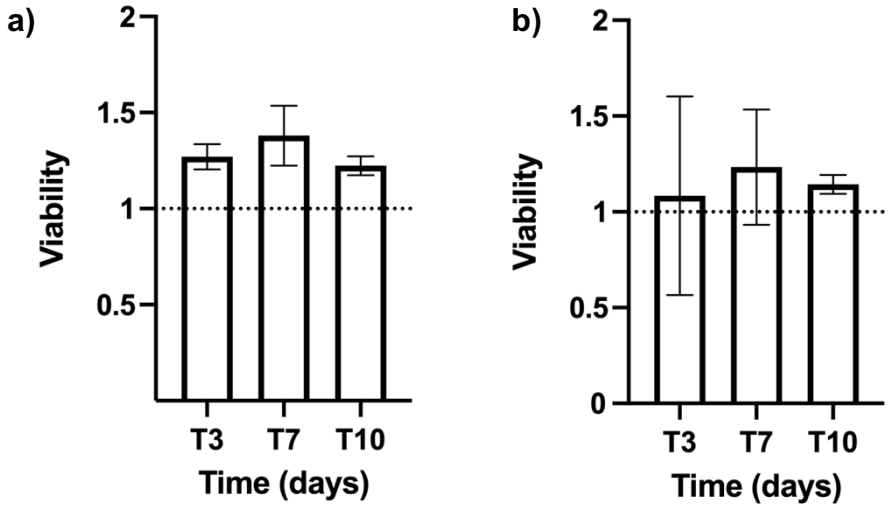

Drug Sensitivity Profiles in Precision-cut tumour slices versus Patient-derived tumoroids

To examine the influence of tissue architecture and the tumour microenvironment on drug response, precision-cut tumour slices were generated and analyzed in parallel with matched patient-derived tumoroids (**Figure 25)**. Drug sensitivity assays for sunitinib and everolimus were performed across both platforms using a five-point, 625-fold serial dilution scheme. Drug responses were normalized relative to DMSO controls, and GR-metrics were calculated independently for PDTs and for precision-cut slices. Sensitivity classification was performed within each model, avoiding cross-model normalization.

Figure 25. Histopathological comparison of primary tumour tissue, precision-cut slices, and patient-derived tumoroids. *Representative haematoxylin and eosin (HE) staining of the primary pancreatic neuroendocrine tumour and corresponding precision-cut tissue slices demonstrates preservation of cytoarchitecture. Patient-derived tumoroids were successfully generated from matched PanNET samples. SYN, synaptophysin*

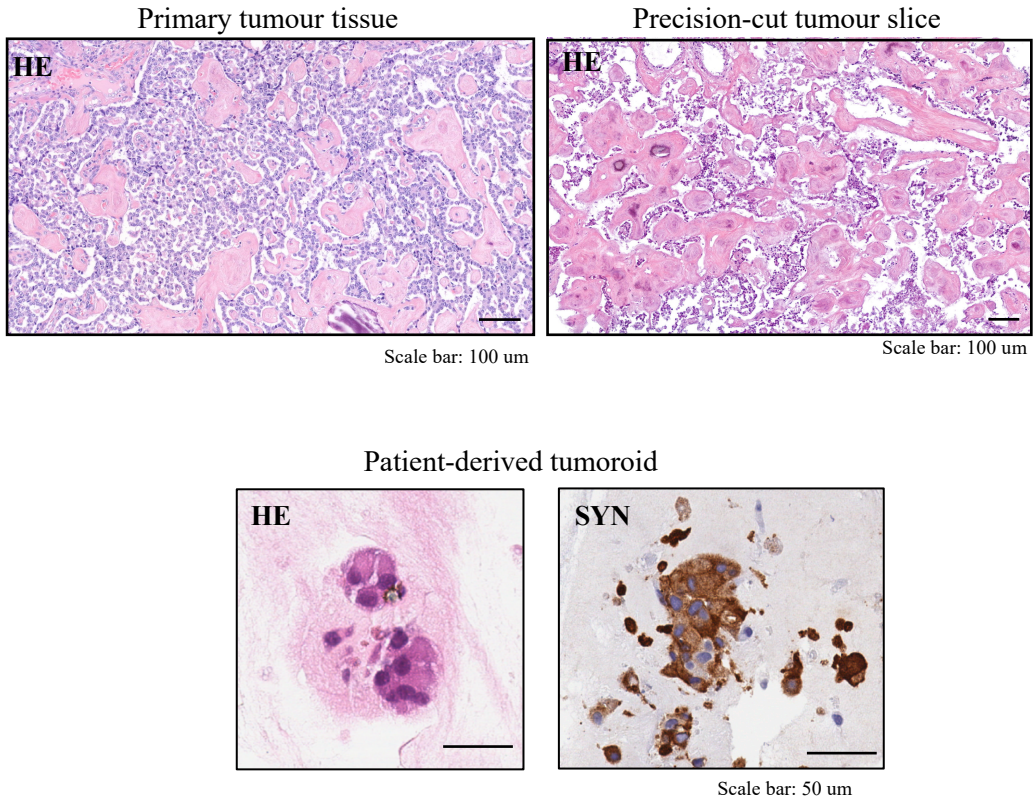

.

Cryopreserved tumour specimens from nine patients submitted to surgery at HSR for localized PanNET were included in this analysis. In cases with limited tissue availability, priority was given to slice preparation; likewise, when drug testing could not be conducted for both agents, priority was given to sunitinib. Precision-cut tumour slices were successfully established from all patients, with seven samples exposed to sunitinib and six to everolimus. PDTs were similarly generated from all eight specimens, with sunitinib and everolimus testing performed in eight and five cases, respectively (**Table XVII**).

Table XVII. Summary of cohort generation for precision-cut tumour slices and matched patient-derived tumoroids

Patient ID	Precision-cut tumour slices	Patient-derived tumoroids
3DPanNET_19	1 no drug testing	1 Sun, Eve
3DPanNET_32	1 Sun, Eve	1 Sun, Eve
3DPanNET_14	1 Sun, Eve	1 Sun
3DPanNET_24	1 Sun, Eve	1 Sun
3DPanNET_27	1 Sun, Eve	1 Sun, Eve
3DPanNET_34	1 Sun, Eve	0
3DPanNET_35	1 Sun, Eve	1 Sun, Eve
3DPanNET_36	1 Sun	1 Sun, Eve
3DPanNET_31	0	1 Sun

Sun, Sunitinib; *Eve*, Everolimus

Across the cohort, divergent drug-response profiles were observed between precision-cut slices and matched tumoroids (**Figure 26**). Concordance for sunitinib between the two experimental models was observed in 2 of 6 (33%) patients, and in 1 of 3 (33%) for everolimus.

Figure 26. Drug response to everolimus and sunitinib in precision-cut tumour slices and corresponding patient-derived tumoroids. *Drug-response profiling was performed in paired precision-cut tumour slices and patient-derived tumoroids from the same surgical specimens. Violin plots show growth-rate–adjusted area-over-the-curve (GR-AOC) values computed using GRmetrics. Responses were stratified into higher and lower sensitivity groups using the cohort median GR-AOC as the threshold. Sensitivity classification was performed independently for each model, without cross-platform normalization GR, growth rate; AOC, area over the curve; blue dots: lower sensitivity, red dots: higher sensitivity.*

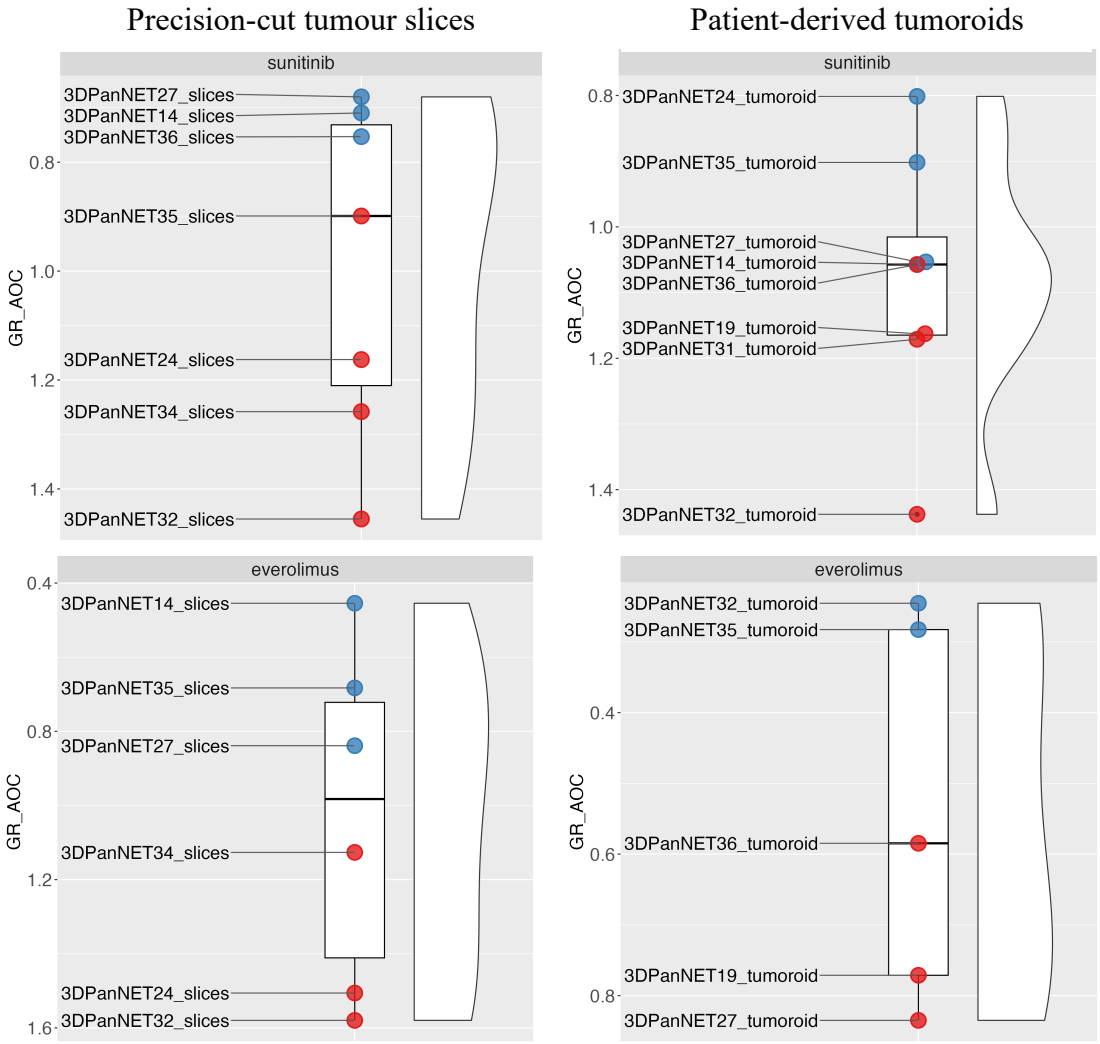

Tumour Histopathological Characteristics and Ex Vivo Models Sensitivity

Histopathological features of tumours corresponding to precision-cut slices and PDTs were compared according to ex-vivo sunitinib sensitivity (**Table XVIII-a**). Among precision-cut slices, no significant associations were observed between sunitinib response and tumour stage, size, nodal status, or grade. A trend toward lower Ki-67 proliferative index was noted in the high-sensitivity slice group (median 3.75% vs. 6.33%, $p = 0.057$). Microvascular invasion was significantly more frequent in tumours yielding low-sensitivity slices (100% vs. 0%, $p = 0.008$). Microvascular density (MVD), evaluated both as a continuous variable and as categorical strata (low/intermediate/high), did not differ between slice sensitivity groups.

Similarly, in tumoroids, sunitinib sensitivity was not significantly associated with tumour stage, grade, size, nodal involvement, Ki-67 index, or MVD.

Tumours were stratified according to concordance in sunitinib response between precision-cut slices and matched tumoroids. Concordant cases were significantly enriched for T2 tumours (100% vs. 0%, $p = 0.028$), whereas discordant cases were exclusively T3. In addition, MVD differed between groups, with discordant cases demonstrating either low or high MVD, while concordant cases uniformly showed intermediate values ($p = 0.048$) (**Figure 27**). No other histopathological parameters showed significant association with concordance status.

In contrast, everolimus showed no statistically significant correlation with tumour histopathology in either precision-cut slices or PDTs. and concordance assessments similarly failed to identify any discriminative tissue characteristics between concordant and discordant cases (**Table XVIII-b**). Notably, a trend toward an association between microvascular density (MVD) and concordance was observed: mean MVD was higher in discordant cases (121.5 ± 2.1 vessels/mm²) compared with concordant cases (83.0 vessels/mm²). However, given the very limited sample size ($n = 3$), these observations remain descriptive only, and formal statistical testing could not be meaningfully conducted.

Table XVIII. Histopathological features of pancreatic neuroendocrine tumour specimens corresponding to precision-cut slices and patient-derived tumoroids tested with sunitinib (a) and everolimus (b). *TNM staging* (Rindi *et al*, 2006); *Grading* (Lloyd *et al*, 2017)

a) Sunitinib

Variable	PC-slices SUN low sensitivity n=3	PC-slices SUN high sensitivity n=4	P value	PDTs SUN low sensitivity n=3	PDTs SUN high sensitivity n=5	P value	Negative SUN correlation n=4	Positive SUN correlation n=2	P value
T stage			1.000			1.000			**0.028**
T2	2 (67)	3 (75)		2 (67)	4 (80)		4 (100)	0 (0)	
T3	1 (33)	1 (25)		1 (33)	1 (20)		0 (0)	2 (100)	
Tumour dimension (mm)	30.33 (±2.517)	34.25 (±10.874)	0.576	28 (±1.735)	34.20 (±9.039)	0.203	28.75 (±2.872)	40.0 (±14.142)	0.460
N stage, N1	1 (33)	1 (25)	0.381	2 (67)	3 (60)	1.000	2 (50)	0 (0)	0.524
Grading			1.000			0.444			1.000
G1	0 (0)	1 (25)		1 (33)	0 (0)		1 (25)	0 (0)	
G2	3 (100)	3 (75)		2 (67)	5 (100)		3 (75)	2 (100)	
Ki67 (%)	6.33 (±1.528)	3.75 (±1.258)	0.057	3.67 (±1.528)	6.60 (±2.408)	0.081	5 (±2.582)	5 (±0)	1.000
Microvascular invasion, yes	3 (100)	0 (0)	**0.008**	1 (33)	4 (80)	0.286	2 (50)	1 (50)	1.000
Perineural invasion, yes	3 (100)	4 (100)	–	3 (100)	5 (100)	–	0 (0)	0 (0)	–
MVD, vessels/mm^{2*}	135 (±64)	129 (±82)	0.914	89 (±29)	114 (±61)	0.537	108 (±66)	121 (±2)	0.798
MVD			1.000			0.762			0.276
Low	1 (33)	2 (50)		2 (67)	2 (40)		3 (75)	0 (0)	
Intermediate	1 (33)	1 (25)		1 (33)	2 (40)		0 (0)	2 (100)	
High	1 (33)	1(25)		0 (0)	1 (20)		1 (25)	0 (0)	
MVD, intermediate	2 (67)	3 (75)	1.000	2 (67)	3 (60)	1.000	0 (0)	2 (100)	**0.048**

PC, precision-cut*; PDTs,* patient-derived tumoroids*; SUN,* sunitinib
Expressed as n (%) unless otherwise specified
* expressed as mean (± SD)

b) Everolimus

Variable	PC- slices EVE low sensitivity n=3	PC-slices EVE high sensitivity n=3	P value	PDTs EVE low sensitivity n=2	PDTs EVE high sensitivity n=3	P value	Negative EVE correlation n=2	Positive EVE correlation n=1	P value
T stage			1.000			0.444			0.028
T2	2 (67)	2 (67)		1 (50)	2 (67)		0 (0)	1 (100)	
T3	1 (33)	1 (2533		1 (50)	1 (33)		2 (100)	0 (0)	
Tumour dimension (mm)	30 (±3)	36.67 (±11.93)	0.401	38 (±16)	29 (±1)	0.560	40 (±14.142)	27	–
N stage, N1	2 (67)	0 (0)	0.357	1 (50)	1 (33)	1.000	0 (0)	1 (100)	0.444
Grading			1.000			1.000			1.000
G1	0 (0)	1 (33)		0 (0)	0 (0)		0 (0)	0 (0)	
G2	3 (100)	2 (67)		2 (100)	3 (100)		2 (100)	1 (100)	
Ki67 (%)	5 (±1)	3.67 (±1.528)	0.275	4.50 (±0.707)	5.67 (±2.082)	0.518	5	4	–
Microvascular invasion, yes	2 (67)	0 (0)	0.143	0 (0)	3 (100)	0.127	1 (50)	0 (0)	0.683
Perineural invasion, yes	3 (100)	3 (100)	–	2 (100)	3 (100)	–	0 (0)	0 (0)	–
MVD, vessels/mm^{2*}	94 (±22)	144 (±93)	0.420	103 (±28)	123 (±82)	0.775	121.50 (±2.121)	83	0.043
MVD			1.000			1.000			0.310
Low	2 (67)	1 (33)		1 (50)	1 (33)		0 (0)	1 (100)	
Intermediate	1 (33)	1 (33)		1 (50)	1 (33)		2 (100)	0 (0)	
High	0 (0)	1(33)		0 (0)	0 (0)		0 (0)	0 (0)	
MVD, intermediate	2 (67)	2 (67)	1.000	1 (50)	2 (67)	1.000	2 (100)	0 (0)	0.083

PC, precision-cut*; PDTs,* patient-derived tumoroids*; EVE,* everolimus
Expressed as n (%) unless otherwise specified
* expressed as mean (± SD)

Figure 27. Assessment of microvascular density (MVD) in the sunitinib cohort. *CD34 immunohistochemistry illustrating MVD in primary pancreatic neuroendocrine tumour tissue used to generate precision-cut slices and patient-derived tumoroids (**a**). CD34 IHC showing tumours with 1) intermediate MVD (118-123 vessels/mm^2), 2) high MVD (206-246 vessels/mm^2), and 3) low MVD (42-83 vessels/mm^2). Black boxes indicate regions shown at higher magnification. Scale bar: 250um; magnification scale bar: 100um. (**b**) Distribution of MVD values across the precision-cut slices cohort and correlation with sunitinib response in matched patient-derived tumoroids. Red dots, discordant slices-tumoroids correlation; blue dots, concordant slices-tumoroids correlation*

a)

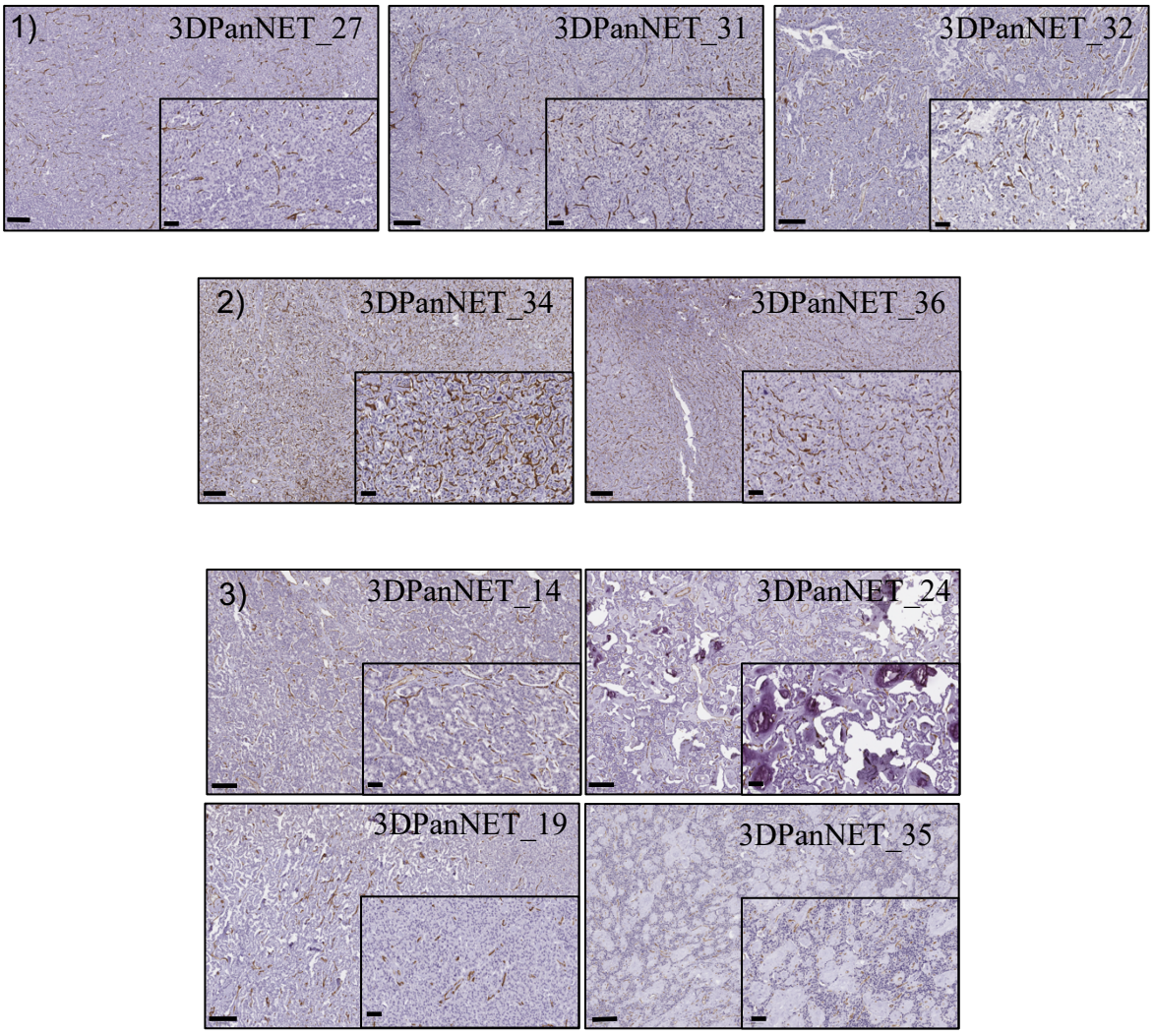

b)

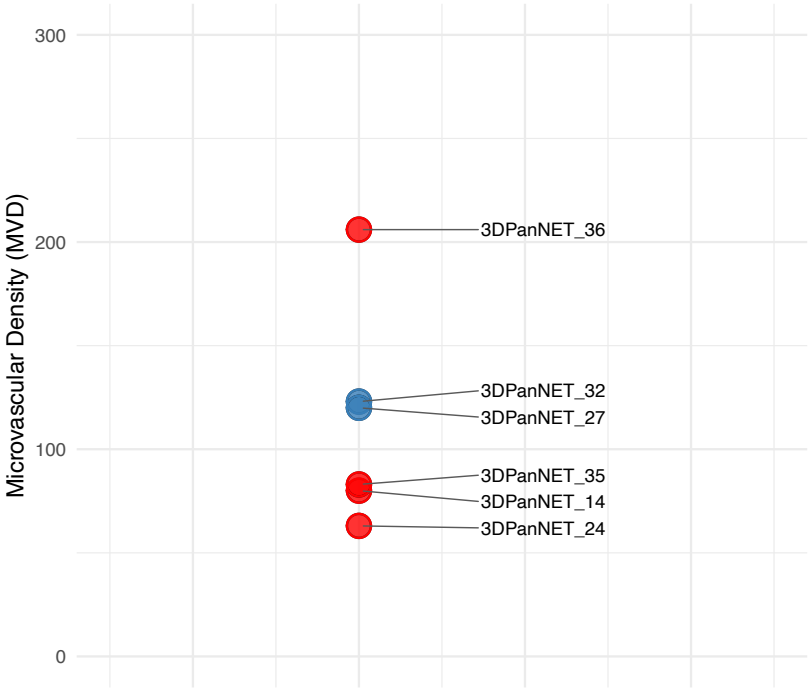

Discussion

Despite substantial advances in understanding PanNET (epi)genomics and the microenvironmental cues that shape tumour behaviour (Scarpa *et al*, 2017; Di Domenico *et al*, 2020; Cives *et al*, 2019), the field still lacks validated predictive biomarkers capable of guiding chemotherapy or targeted therapy selection. This persistent unmet clinical need largely reflects the limited availability of preclinical models that faithfully recapitulate the complexity of PanNET biology. Robust, scalable systems that preserve both tumour-intrinsic features and key components of the tumour microenvironment remain poor, constraining efforts to elucidate disease mechanisms and to evaluate therapeutic vulnerabilities in biologically relevant contexts (Ear *et al*, 2024; Kos-Kudła *et al*, 2023).

PDTs offer a scalable, patient-specific platform that preserves essential tumour-intrinsic characteristics while enabling controlled experimental manipulation. In this study, PDTs were successfully generated from 22 available cryopreserved G1-G3 NF-PanNET specimens, encompassing both primary and metastatic lesions. PDTs demonstrated stable tumour-cell content and viability over culture period, enabling robust quantitative pharmacotyping, approach previously applied on high-grade

PanNET/PanNEC PDTs (April-Monn *et al*, 2024). PDTs exhibited marked inter-patient heterogeneity in drug sensitivity, mirroring the biological variability characteristic of PanNETs. Sensitivity distributions were relatively broad for everolimus and sunitinib, and more skewed for temozolomide. This pattern is consistent with the predominantly tumour-intrinsic determinants of response to alkylating chemotherapy, such as proliferation rate and MGMT-mediated DNA repair (Rinke *et al*, 2021; Brighi *et al*, 2023). In contrast, responses to targeted agents reflect more complex, multifactorial mechanisms, aligning with multicentre clinical data showing wide dispersion in progression-free survival under targeted therapies (Medici *et al*, 2025; Panzuto *et al*, 2024; Fazio *et al*, 2021). A central mechanistic insight derived from our PDT platform was the association between histopathological markers of metabolic adaptation and everolimus sensitivity. In out cohort, heterogeneous MCT-4 expression, reflecting hypoxia, was associated with greater *ex vivo* sensitivity to everolimus. These findings highlight the intricate crosstalk between cellular metabolic programmes and mTORC signalling (Mossmann *et al*, 2018). In this regard, Cros et al. (Cros *et al*, 2025a) recently reported that patient-derived tumour slices exhibiting glycolytic (GLUT-1) and hypoxic (CA-9) signatures were less responsive to everolimus. The apparent discrepancy with our findings may reflect fundamental differences between the two experimental platforms: PCTSs maintain the native TME, including stromal and vascular elements that shape metabolic gradients and influence drug response, whereas PDTs capture primarily tumour-intrinsic phenotypes in the absence of microenvironmental cues. Additionally, hypoxic status in the *ex vivo* models may not fully retain that of original tumour tissue or may evolve dynamically during culture, further complicating interpretation of metabolic correlates of drug response. Controlled experiments integrating oxygen-regulated culture systems will therefore be essential to disentangle the mechanistic contribution of metabolic adaptation to mTOR inhibitor sensitivity.

Moreover, in our cohort, an association between higher Ki-67 indices and enhanced PDT responsiveness to mTOR inhibition was observed, suggesting that more proliferative PanNETs, characterized by hypoxic metabolic phenotype, may depend more heavily on PI3K/mTOR signaling.

Despite these promising results, PDT-derived sensitivities to targeted therapies only partially recapitulated clinical outcomes. Temozolomide sensitivity showed full concordance with clinical response in evaluable cases, reinforcing the predictive validity of DNA-alkylator testing in tumour-only neuroendocrine tumour models, consistent with findings from the April Monn *et al*. (April-Monn *et al*, 2024), further supporting the robustness of PDTs as platform for modelling cytotoxic chemotherapy response.

By contrast, correlations for everolimus and sunitinib were modest, likely reflecting the intrinsic limitations of PDTs, which lack stromal, vascular, and immune compartments. As VEGFR inhibitors such as sunitinib act primarily on endothelial and pericyte networks and on angiogenic signalling loops, epithelial-only models cannot fully capture their pharmacodynamic behaviour (Huang *et al*, 2010; Raymond *et al*, 2011a; Vinik & Raymond, 2013). Similarly, mTOR inhibitor efficacy is shaped by microenvironmental features, including oxygen gradients, nutrient fluxes, fibroblast-derived cytokines, and ECM-mediated signalling, that are absent in isolated tumoroids (Zanini *et al*, 2020). These limitations are increasingly acknowledged within the neuroendocrine field. While PDTs remain crucial for modelling tumour-intrinsic biology, they cannot reproduce the complex interplay between endothelial cells, fibroblasts, and immune populations that define PanNET evolution and drug response to therapies that engage the broader TME (Cives *et al*, 2019; Lee *et al*, 2023). This underscores the need for complementary, microenvironment-aware models, to achieve a more comprehensive and clinically relevant translational framework.

In line with this rationale, **PCTSs** from primary PanNET tissues were successfully generated. Through systematic adjustments of slicing frequency, speed, and vibration amplitude, the protocol achieved robust reproducibility. PCTSs retained cytoarchitectural integrity, endocrine morphology, and metabolic viability for at least 10 days ex vivo. The preservation of native vasculature, extracellular matrix architecture, and intact endothelial–tumour interfaces enabled pharmacodynamic assessment within a physiologically relevant microenvironment, as previously demonstrated for liver-derived slices (Doornebal *et al*, 2022). PCTS-based pharmacotyping revealed divergent sensitivity patterns compared with matched PDTs, highlighting the impact of microenvironmental context. Importantly, concordance between PDTs and slices was

highest in tumours with intermediate MVD, whereas discordance was observed at both extremes of vascularity, emphasizing the importance of the TME in modulating sunitinib response. Furthermore, an association between microvascular invasion, a recognized adverse prognostic factor in NF-PanNETs (Izumo *et al*, 2024), and reduced sunitinib sensitivity was observed. Nevertheless, further studies are required to elucidate the underlying mechanisms and their implications for therapeutic resistance.

Several limitations must be acknowledged. First, the rarity of PanNETs, the limited availability of tumour samples and of corresponding clinical response data, largely a consequence of the indolent course of the disease, reduce the statistical power and restrict the depth of clinico-biological correlations that can be drawn. Validation in larger, multicentric cohorts with comprehensive clinical therapeutic response data will be essential to refine and substantiate our findings. Second, these models were generated exclusively from primary surgical resections and may therefore not fully capture the biological diversity observed in recurrent or metastatic disease. Nonetheless, recent evidence from the University of Bern (*ENETS Conference 2025*, Avanthay S.) demonstrating highly conserved epigenetic signatures between matched primary and metastatic PanNET lesions supports the use of resection-derived tissue for *ex vivo* drug-response testing, particularly when aiming to inform adjuvant therapeutic strategies prior to overt progression. Third, it should be noted that patients may have received additional systemic therapy (i.e., temozolomide-base therapy) following surgery, which may alter tumour biology (Mosalem *et al*, 2025); consequently, the subsequent clinical response may not accurately reflect the behaviour of the untreated tumour population from which the *ex vivo* models were originally derived. Finally, mechanistic studies aimed at elucidating the molecular pathways underlying tumour sensitivity and resistance within these *ex vivo* models are required to confirm the present observations and to provide a deeper understanding of the microenvironmental determinants that shape therapeutic responses in PanNETs.

Collectively, PDTs and PCTS constitute complementary *ex vivo* platforms that together delineate the tumour-intrinsic and microenvironmental determinants of drug sensitivity in non-functioning PanNETs. PDTs serve as a reductionist system ideally suited for dissecting tumour-specific signalling dependencies, enabling precise evaluation

of pathways that govern epithelial cell autonomy. In contrast, PCTS preserve the architectural, vascular, stromal, and immune components of the native tumour microenvironment, thereby capturing regulatory cues that cannot be recapitulated in organoid systems alone. When considered together, these models generate a more integrated understanding of therapeutic vulnerabilities. PDT-derived responses to agents that primarily target tumour-cell signalling pathways are contextualised by PCTS, which model constraints imposed by vasculature, extracellular matrix organisation, and immune-cell interactions. This layered approach is increasingly important as therapeutic strategies for PanNETs shift toward agents acting at the tumour-microenvironment interface (Cives *et al*, 2019), such as cabozantinib (Chan *et al*, 2025) and immunomodulatory therapies (Al-Toubah *et al*, 2020; Mandriani *et al*, 2022; Lauricella *et al*, 2022).

4) 3D bioprinted models

Aim: To develop advanced three-dimensional preclinical models able to recapitulate PanNET architecture and its microenvironment on which to perform downstream functional studies, with particular emphasis on reconstructing the tumour–endothelial interface.

Materials and Methods

Cell Cultures

PanNET cell lines: The BON1 cell line was provided by C. Sette, Cattolica University, Rome, Italy in 2022. The NT3, NT-18P and NT18LM cell lines were a kind gift from J. Schrader and F. Viol (Viol *et al*, 2022) . For NT3, NT-18P and NT-18LM the cell culture flasks were coated with collagen IV for better attachment of the cells. BON1 cells were cultured in DMEM/F12 medium (Sigma), whereas NT3, NT-18P and NT-18LM cells were cultured in RPMI 1640 medium (Sigma). For all cell lines, the medium was supplemented with 10% FBS, 100 IU/mL penicillin, and 0.1 mg/mL streptomycin, and cells were kept in a humidified incubator at 5% CO2 and 37 ◦C. Additionally, growth factors EGF (Gibco PHG0314) and FGF2 (Gibco PHG0024) were added to NT3, NT-18P and NT-18LM growth medium.

Human Umbilical Vein Endothelial Cells : Human Umbilical Vein Endothelial Cells (HUVEC) (Lonza, Basel, Switzerland) were cultured in EGM-2 medium (EuroClone, Pero, Italy) at 37◦C with 5% CO2 , and used between passage 1 and 5. Before plating the cells, standard culture flasks were coated with 1.8% type B gelatine from bovine skin (Sigma-Aldrich, Missouri, USA).

Human Mesenchymal Stell Cells: Immortalized mesenchymal stem cells (hMSC-TERT292) were obtained from Evercyte (Cat. No. CHT-063-0292; Evercyte GmbH, Vienna, Austria). Cells were cultured at 37°C with 5% CO2 in complete medium using the MesenCult-ACF Plus Culture Kit (Cat. No. 05445; StemCell Technologies, Vancouver, Canada). Culture flasks were pre-coated with the coating reagent provided in the kit (Cat. No. G9391; Sigma-Aldrich, Missouri, USA) and incubated for 2 h at room temperature.

Human Pancreatic Stellate Cells : Human Pancreatic Stellate Cells (hPSC) (Innoprot, P10474) were cultured at 37◦C with 5% CO2, with Stellate Cell Medium-PLUS (Innoprot, P60126-PLUS). Culture flasks were pre-coated with poly-L-lysine (Cat. No. P4707; Sigma-Aldrich, Missouri, USA) at a dilution of 15µL in 10mL of sterile water and incubated over night at 37°C.

Biomaterials

Compatibility assays were performed to evaluate the behaviour of different cellular populations within various biomaterials. The following bioinks were tested: GelXA LAMININK 411 (CELLINK AB, Gothenburg, Sweden), PureCol (Collagen I; Cat. No. 5005, Advanced Biomatrix), and GelMA–Fibrin (CELLINK AB, Gothenburg, Sweden). GelXA LAMININK 411 consists of gelatin, alginate, and xanthan gum, which together enhance printability, and incorporates laminin-411 to support cell adhesion and migration. This bioink is crosslinked via UV photopolymerization. GelMA–Fibrin contains fibrinogen, a glycoprotein that is enzymatically converted to fibrin by thrombin, thereby promoting endothelial cell functionality; the material crosslinks through a combination of photocuring and thrombin–fibrinogen interactions. PureCol, a collagen type I–based matrix, required pH neutralization with 0.1 M NaOH prior to cell incorporation. The material was crosslinked through temperature-induced gelation at 37 °C. Casting and bioprinting approaches were employed for mono-biomaterial scaffolds generation, according to bioinks properties. Casted models are referred as droplets. Bioprinted models are referred as constructs.

Figure 46. Schematic representation of the biomaterials tested, highlighting their casting or bioprinting compatibility, and the cell types employed. *HUVEC, human umbilical vein endothelial cells; hMSC, human mesenchymal stem cells; hPSCs, human pancreatic stellate cells.*

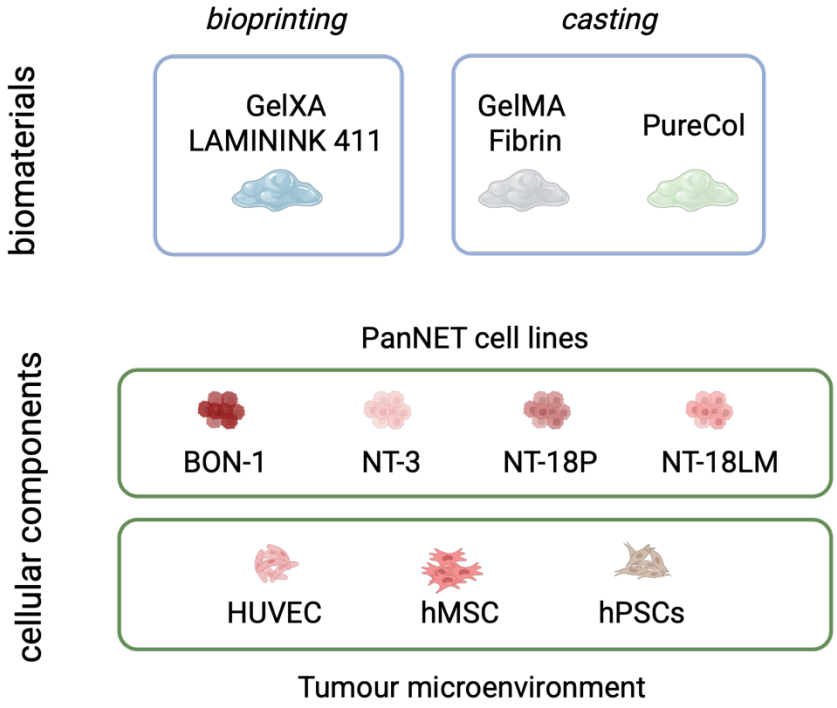

Bioprinted Constructs Generation

GelXA LAMININK 411-based constructs were bioprinted with the BIO X bioprinter (CELLINK AB, Gothenburg, Sweden) to generate 5x5x1mm^3 scaffolds employing the following bioprinting set-up: blue nozzle (0.41 mm), 20/25Kpa pressure, 5mm/s speed, 0.25mm Layer height, 30% rectilinear infill, 300ms Preflow delay, 100ms postflow delay.

Figure 47. Graphical representation of GelXA LAMININK 411 –based constructs generation. *(A) GelXA LAMININK 411 is mixed with the cell line of interest. (B) The mixture is subsequently bioprinted using an extrusion-based system (BIO X bioprinter). (C) The material is deposited into the predefined construct geometry (5×5×1 mm³).*

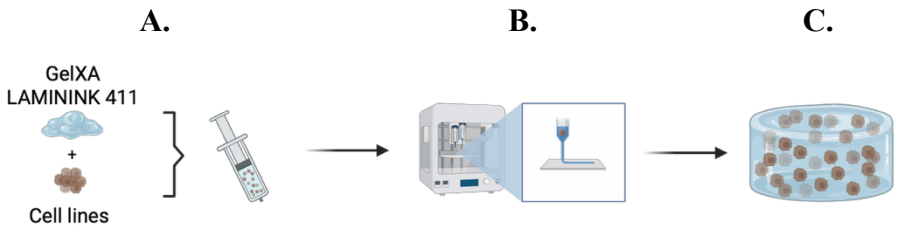

Casted Droplets Generation

PureCol- and GelMA–Fibrin–based droplets were generated by casting 50–100 µL of each hydrogel into 96-well round-bottom plates (Corning®, US), crosslinked, and subsequently transferred to 24-well plates for culture.

Figure 48. Graphical representation of casting procedure of mono- and multi- cellular droplets generation. ***A****) GelMA Fibrin-based droplets.* ***B****) PureCol-based droplets. Multicellular droplets were obtained by mixing the two cell lines within the hydrogel prior to casting.*

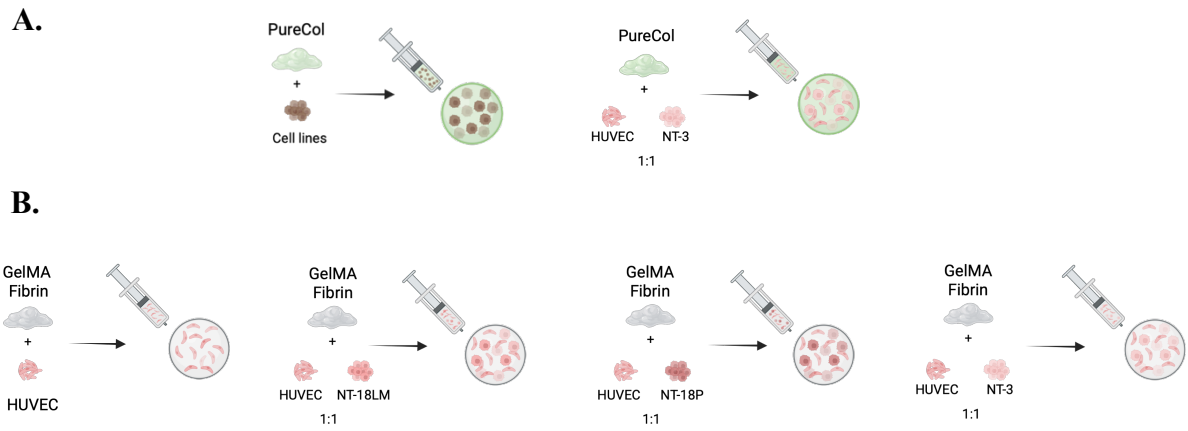

Vessel-like Construct Fabrication

Vessel-like constructs were generated employing a hybrid technique, combining 3D bioprinting and casting methods. Briefly, GelXA LAMININK 411 (CELLINK AB, Gothenburg, Sweden) was mixed with PanNET cell lines ($10x10^6$ cells/mL) and bioprinted with the BIO X bioprinter (CELLINK AB, Gothenburg, Sweden) to generate a $7x7x6mm^3$ scaffold, with a 5.5mm in diameter central channel. Printing specifics: blue nozzle (0.41 mm), 20/25Kpa pressure, 5mm/s speed, 0.25mm Layer height, 30% rectilinear infill, 300ms Preflow delay, 100ms Postflow delay. GelMA Fibrin (CELLINK AB, Gothenburg, Sweden) was heated up at 37°C in a laboratory bath until complete dissolution, mixed with HUVEC and hMSC (2:1 ratio, final cell concentration $10x10^6$ cells/mL) and manually cast to fill the hollow cavity. Immediately, a 3D printed tool (diameter 2.5mm, **Figure 49**) was placed inside the casted material and photo-crosslinked with 405nM UV light for 60 seconds. The tool was subsequently removed, generating a 2 mm lumen in diameter. Further cross-linking with $CaCl_2$ 50mM for 4minutes was performed.

Figure 49. 3D-printed tool for lumen-cavity generation. *The device consists of a cylindrical central body (2.5 mm in diameter) used to create hollow scaffolds, supported by three stabilizing legs that allow the pin to stand upright during casting.*

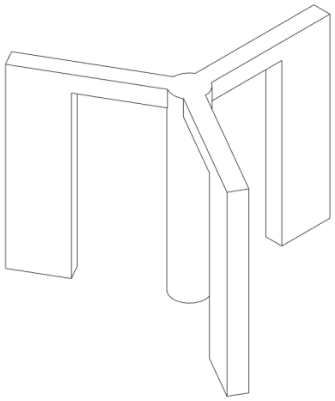

The scaffolds were incubated overnight at 37 °C and 5% CO_2 in EGM-2 medium supplemented with 10 U/mL thrombin (Merck, New Jersey, USA). The following day, the medium was replaced with fresh culture medium (EGM-2 + RPMI supplemented with growth factors medium, 2:1) and the constructs were maintained under static conditions in multiwell plates, with medium changed every two days. After 14 days of static maturation, the scaffolds were transferred into the VesselBox system. To assemble the device, the scaffold was carefully positioned into the bioreactor base, and secured by fastening the adapters to align with the scaffold lumen. The chamber was then filled with the EGM-2 + RPMI supplemented with growth factor medium (2:1), and the lid was closed to seal the system. Perfusion was set at at 100 µL/min and ensured by the R100-1J peristaltic pump (React4Life, Vimodrone, Italy; **Figure 50**). Continuous fresh medium circulation during dynamic culture was ensured through an external reservoir containing 8 mL of the same medium formulation. In dynamic settings, half medium was changed every 2 days. A scaffold in a multiwell plate (static condition) was used as a control.

***Figure 50. Illustration of the dynamic culture system**. The bioreactor (red arrow) connected to a media reservoir (green arrow) and perfused through a milli-fluidic peristaltic pump (R100-1J, yellow arrow)*

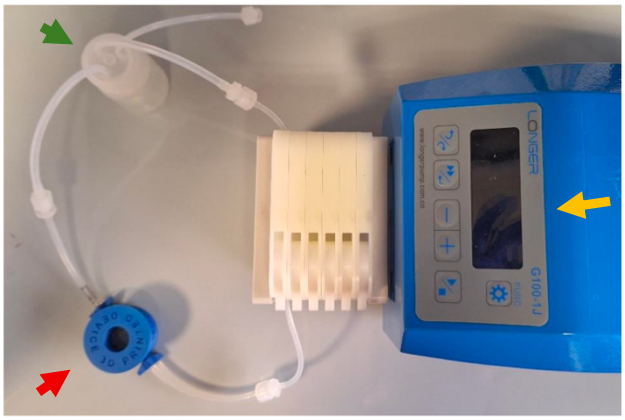

Bioreactor Fabrication

The bioreactor (VesselBox) was designed using Fusion 360 (Autodesk, California, USA), and all components were fabricated by FDM 3D printing (**Figure 51**) using a biocompatible filament (Extrudr, Lauterach, Austria). Larger components of the bioreactor were sterilized by autoclaving, whereas smaller or more delicate elements were disinfected by immersion in 80% ethanol, followed by rinsing with sterile water prior to use.

Figure 51. Creality 3D printer. Extrusion based 3D printer.

Live/Dead Assay

To assess embedded cells viability after manufacturing and before scaffold perfusion (days 14 post-printing), we used the LIVE/DEAD® Cell Imaging Kit (Thermo Fisher Scientific, Massachusetts, USA), which allows for the visualization of live (green) and dead (red) cells. The scaffolds were washed with DMEM without serum and phenol red (Thermo Fisher Scientific, Massachusetts, USA) and Live/Dead reagent was added in a 1:3 ratio (reagent:medium). After 30 minutes of incubation at 37°C, 5% CO_2 the constructs were washed with DMEM without serum and phenol red and observed with the Olympus FluoVIEW 3000 RS confocal microscope and then processed using FIJI (ImageJ) software (Schindelin *et al*, 2012).

Immunofluorescence

For immunofluorescence, cell-laden scaffolds were fixed with 4% PFA in Phosphate Buffered Saline (PBS) (Santa Cruz Biotechnology, Texas, USA) 2h at RT. After fixation, the scaffolds were washed twice with Hank's Balanced Salt Solution (HBSS) (Euroclone, Pero, Italy) for 5 minutes RT, and stained for the markers of interest. The scaffolds were permeabilized and blocked (1mg/mL BSA, 10% FBS and 0.3% Triton X in PBS) for 30 minutes at room temperature and then stained overnight 4°C with primary antibodies and subsequently with secondary antibodies for 2h. The following primary antibodies were used: anti-CD31 (Cat. No. ab32457; Abcam, Cambridge, UK, 1:100), anti-Von Willebrand Factor (Cat. No. sc-365712, Santa Cruz Biotechnology, Texas, USA, diluted 1:50), anti-chromogranin A (Cat. No. ab283265, Abcam, Cambridge, UK, 1:100), anti-synaptophysin (Cat. No. ab8049, Abcam, Cambridge, UK, 1:100). Secondary antibodies used: Alexa Fluor 488 (Cat. No. A32790 and A32766; Thermo Fisher Scientific, Massachusetts, USA, 1:500), Alexa Fluor 647 (Cat. No. A32733 and A32728; Thermo Fisher Scientific, Massachusetts, USA, 1:500). Actin was stained using Alexa Fluor 568 Phalloidin, added with secondary antibodies (Cat. No. 94072; Sigma-Aldrich, Missouri, USA, 1:250). Nuclei were stained with hoechst 33342 (Cat. No. 23491-52-3; Merck KGaA, Darmstadt, Germany) at a 1:1000 dilution for 10 min at room temperature. Immunofluorescence images were acquired as single images or as z stack reconstructions using Olympus FluoVIEW 3000 RS confocal microscope (Olympus, Tokyo, Japan).

Images were analyzed with Fiji (Schindelin *et al*, 2012) software and R software, version 4.5.0 (R Foundation for Statistical Computing, Vienna, Austria), using *ggplot2*, *cowplot* libraries.

2D Migration Assay

Cell migration assays were carried out for NT-3, NT-18P, and NT-18LM cells using the ibidi Culture-Insert 2 Well system (ibidi GmbH, Germany). Silicone inserts were first removed, and the wells were coated with collagen IV for 30 minutes at room temperature; the inserts were then repositioned onto the coated surface. Cells were seeded at a density of 3×10^5 cells per well in 70 µL RPMI supplemented with growth factors, as previously described, and allowed to adhere for 12 hours. Following attachment, the inserts were gently removed to create a 500-µm cell-free gap. Gap closure was used as the quantitative readout of migratory capacity and was monitored by phase-contrast microscopy at 6-hour intervals until complete closure was observed in at least one experimental condition.

Results

The printability of individual cell lines was first evaluated to determine the optimal cellular concentration, assess cell morphology within the bioink matrix, and evaluate post-inclusion viability.

4.1. Simple Models

4.1.1. GelXA LAMININK 411

GelXA LAMININK 411 was initially selected as the primary biomaterial, as our prior experience with a wide variety of cell types has demonstrated its compatibility with multiple cell lines in our laboratory. Indeed, GelXA LAMININK 411 shows favourable rheological properties and its ability to support delicate tissues, including cells from the pancreatic, vascular, immune, nervous and hematopoietic systems. Bioprinted 5x5x1mm^3 constructs were generated.

PanNEN cell lines

We initially evaluated the baseline performance of GelXA LAMININK 411 in supporting neuroendocrine tumour cell viability and self-organization.

BON-1 Constructs

BON-1 cells, a highly proliferating PanNEN cell line, printability with GelXA LAMININK 411 was tested. A cell density of 10×10^6 cells/mL, previously optimized in comparable bioprinting systems, was selected. Constructs were maintained under static conditions in DMEM/F-12 medium to evaluate baseline viability and self-organization within this matrix. Live/dead staining performed at days 1, 7, and 14 demonstrated consistently high viability, with only negligible non-viable cells at later stages (**Figure 28A**). Over time, BON-1 cells underwent progressive self-aggregation into compact, islet-like structures, indicating active intercellular adhesion and adaptation to the 3D microenvironment (**Figure 28B**). By day 14, cohesive spheroidal aggregates resembling pancreatic islet-like architectures were evident. Immunofluorescence for nuclei (hoechst) and Chromogranin A (CgA) confirmed preservation of neuroendocrine differentiation, demonstrating that GelXA LAMININK 411 provides a stable and biocompatible matrix for BON-1 cell proliferation and morphogenesis.

Figure 28. BON-1 cells viability and behaviour in GelXA LAMININK 411 *Panel (**A**) shows live/dead staining at days 1, 7, and 14. Panel (**B**) presents immunofluorescence staining for hoechst (blue) and chromogranin A (CgA, white). White boxes indicate regions shown at higher magnification.*

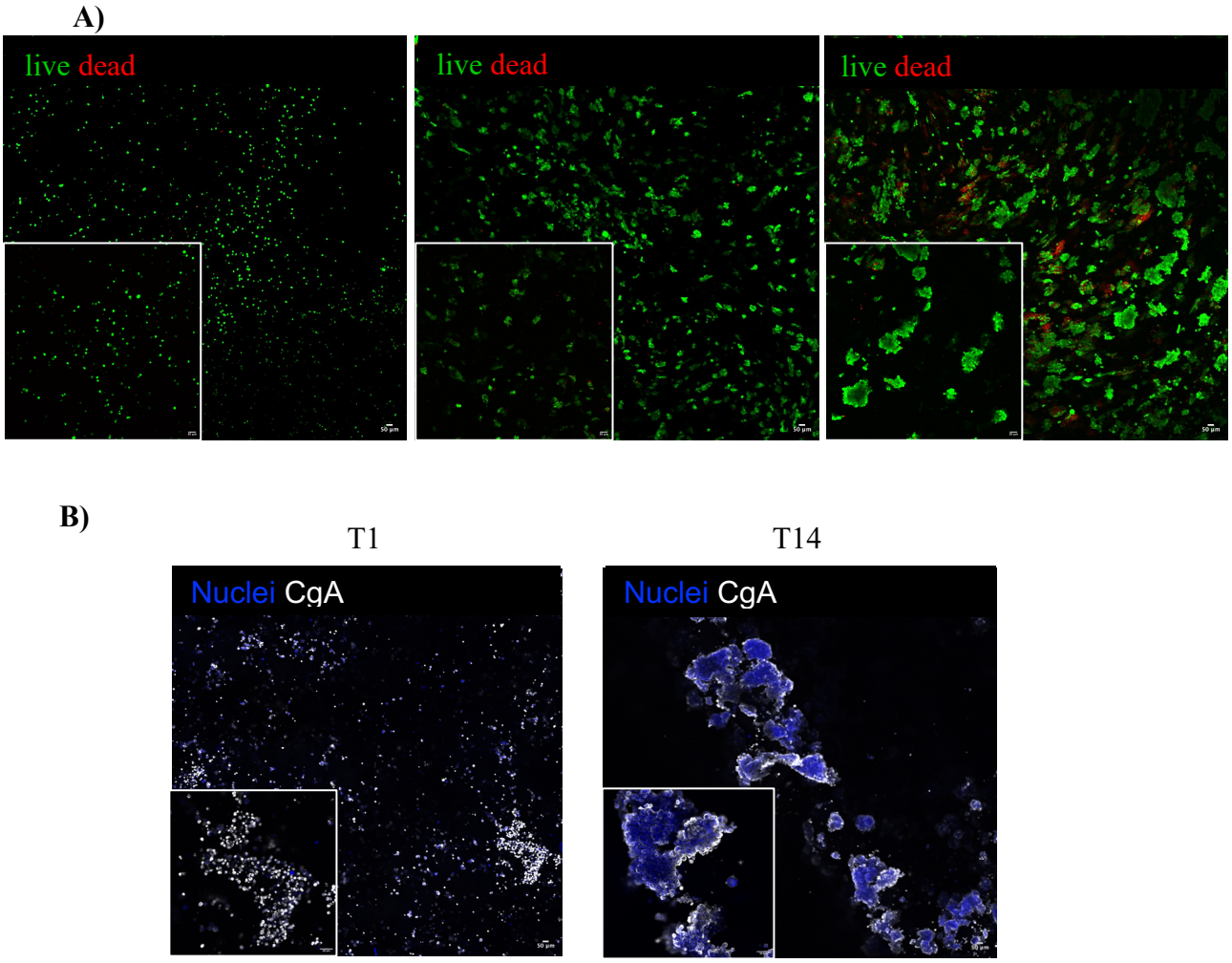

NT-3 Constructs

To assess a more differentiated and less proliferative PanNET model, NT-3 cells were bioprinted in GelXA LAMININK 411 and cultured for up to 21 days in RPMI medium supplemented with EGF (20 ng/mL) and FGF (10 ng/mL). $10x10^6$ cells/mL concentration was selected. Live/dead assays confirmed excellent viability throughout the culture period (**Figure 29A**). Cells exhibited a time-dependent increase in cohesion and organization within the matrix. By day 14, NT-3 cells displayed rounded micro-aggregates with an organized actin cytoskeleton and strong CgA expression, confirming preserved differentiation. By day 21, enhanced cellular compaction and alignment were

observed, indicating active cell–cell communication (**Figure 29B**). Compared with BON-1, NT-3 required longer culture periods to achieve similar levels of aggregation, reflecting its lower intrinsic proliferative rate (ki67 14.6% ± 1.0% vs 80.6% ± 3.3%).

Figure 29. NT-3 cells viability and behaviour in GelXA LAMININK 411. *(**A**) Live/dead staining throughout the culture period, and (**B**) immunofluorescence staining for hoechst (blue), phalloidin (red), and chromogranin A (CgA, white) at day 21. White boxes indicate regions shown at higher magnification.*

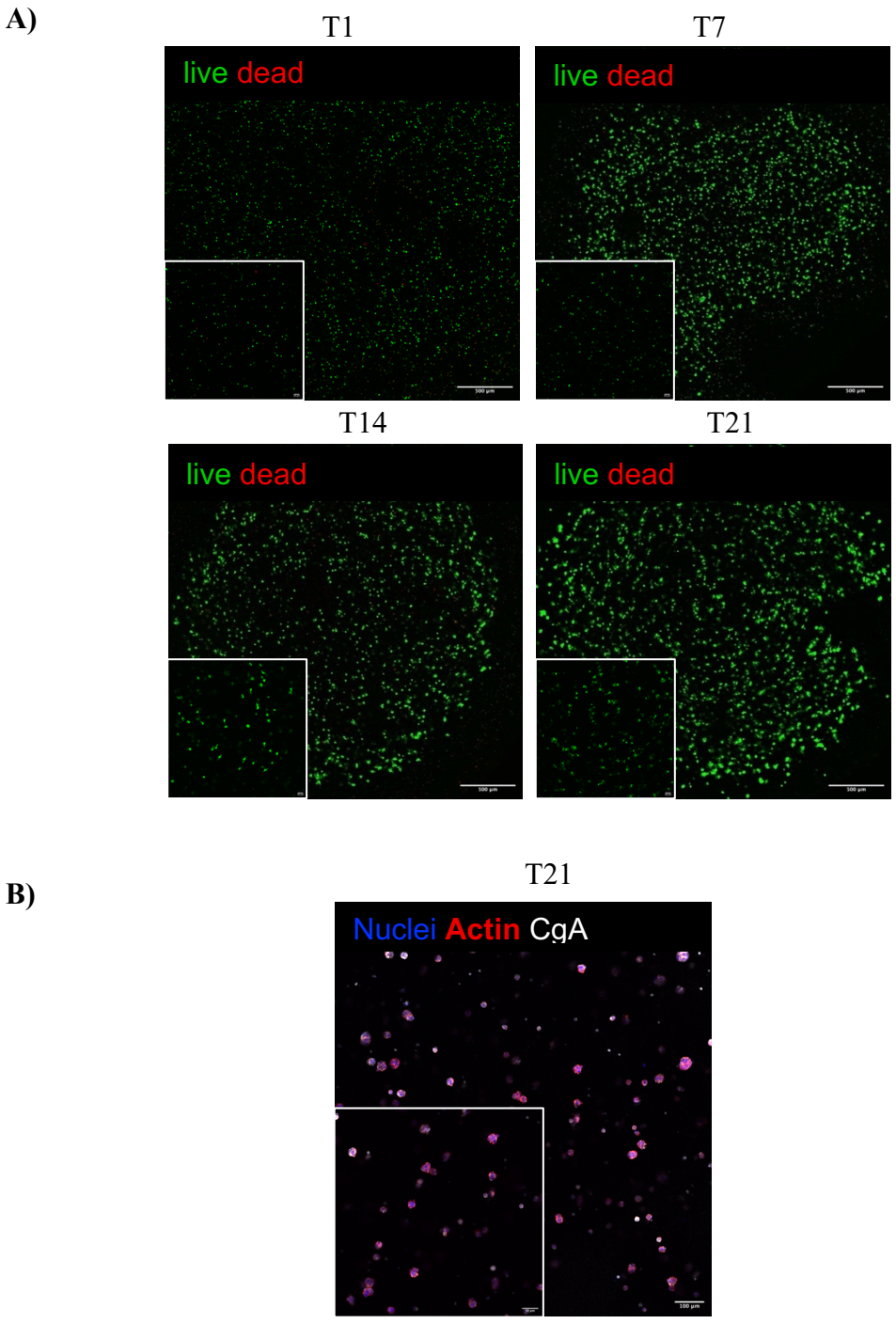

NT-18P and NT-18LM Constructs

The ability of GelXA LAMININK 411 to sustain *in between* PanNET phenotypes was subsequently evaluated using NT-18P (**Figure 30A,** ki67 25.18% ± 2.35%) and NT-18LM (**Figure 30B,** ki 67 25.57% ± 1.59%) cell lines. Both cell lines were bioprinted at 10 × 10^6 cells/mL and cultured for up to 21 days in RPMI medium supplemented with EGF (20 ng/mL) and FGF (10 ng/mL). Live/dead stainings confirmed persistent viability for both lines across all time points (days 7, 14, and 21), indicating that the hydrogel provided a stable, non-cytotoxic environment (**Figure 30C-D**). Despite robust survival, limited polycellular organization was observed, particularly in NT-18P constructs, where cells remained largely dispersed.

Figure 30. NT-18P and NT-18LM cells viability and behaviour in GelXA LAMININK 411. *Both NT-18P (**A-C**) and NT-18LM (**B-D**) cell lines were maintained under static conditions for 21 days in GelXA LAMININK 411. Live/dead staining demonstrated sustained viability throughout the culture period (**A-B**). Immunofluorescence staining for hoechst (blue), phalloidin (red), and chromogranin A (CgA, white) in NT-18P and NT-18LM culture after 21 days is shown in panels I and (**D**), respectively. White boxes indicate regions shown at higher magnification.*

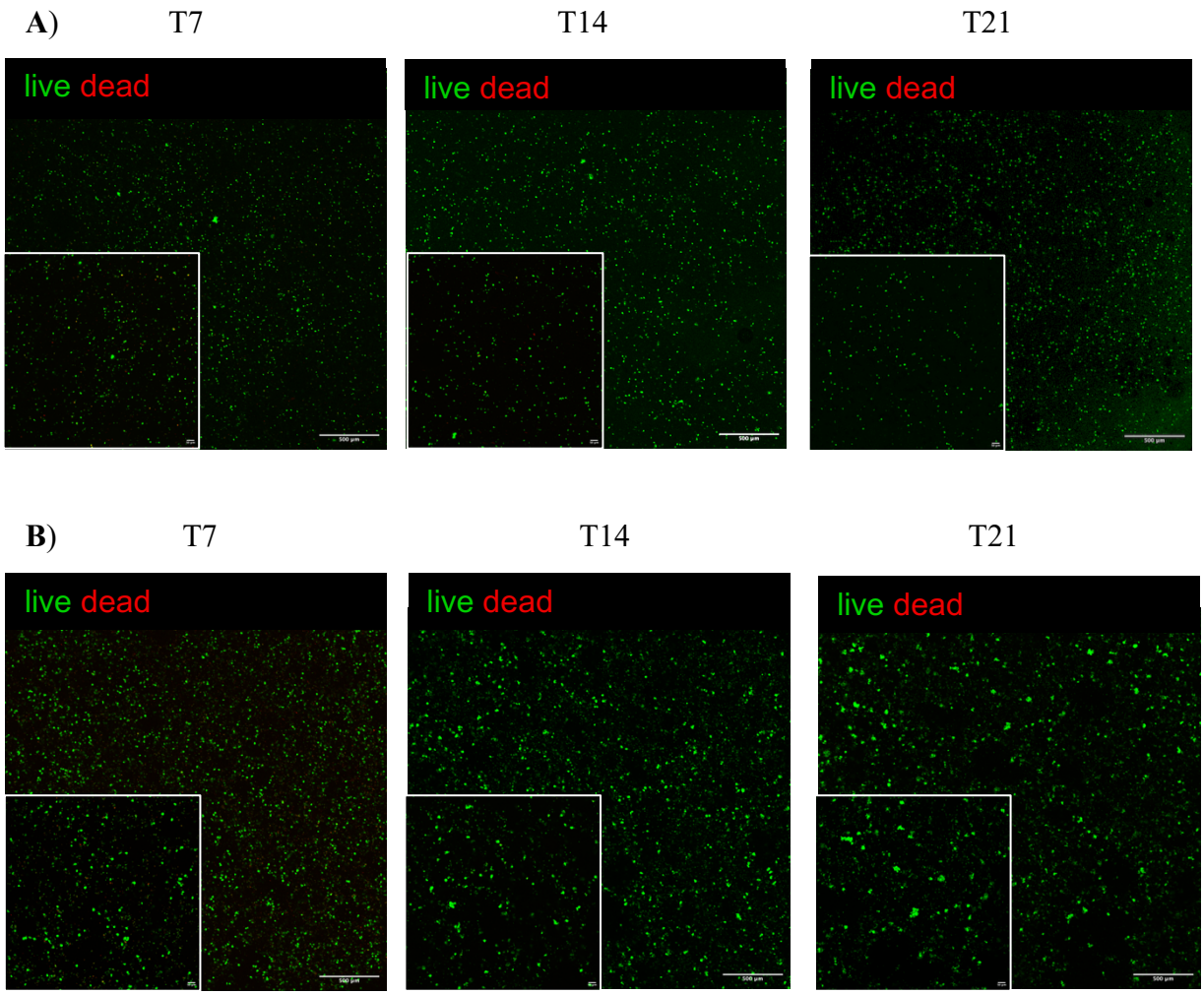

C) T21 **D)** T21

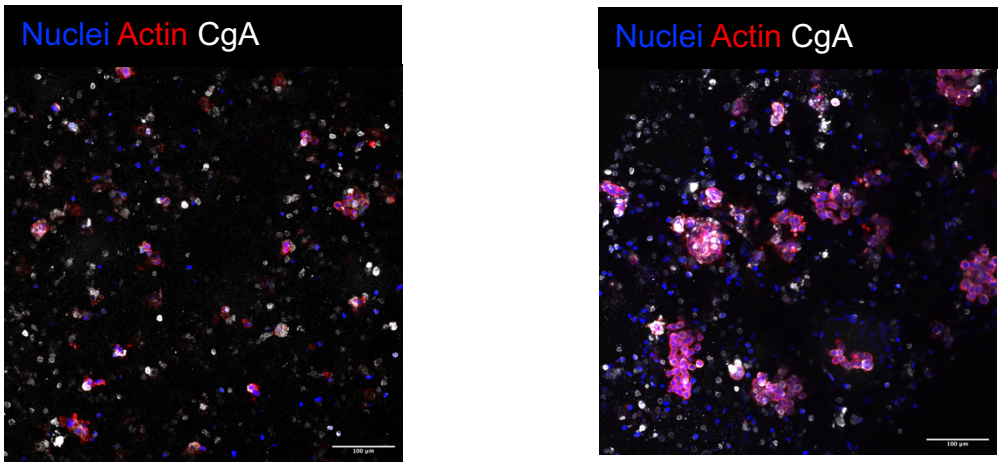

These results confirmed that GelXA LAMININK 411 supports the growth of diverse PanNEN cell types while maintaining their phenotype-dependent morphologies.

Tumour microenvironment

Human Pancreatic Stellate Cells (hPSCs) constructs

To include a tissue specific stromal compartment Human pancreatic stellate cells (hPSCs) were embedded in GelXA LAMININK 411 (10×10^6 cells/mL) and cultured for 21 days. The cells exhibited uniform viability (**Figure 31A**), and immunofluorescence for actin showed elongated, spindle-shaped morphology characteristic of activated fibroblasts (**Figure 31B**). These findings indicate that GelXA LAMININK 411 supports hPSC structural integrity and functional phenotype, validating their use as stromal components in future multicellular models

Figure 31. human Pancreatic Stellate Cells (hPSCs) viability and behaviour in GelXA LAMININK 411. *Live/dead assay thought the culture period is depicted in panel (A). Cellular morphology was evaluated through immunofluorescence stainings (B) for hoescht (blue) and phalloidin (red).*

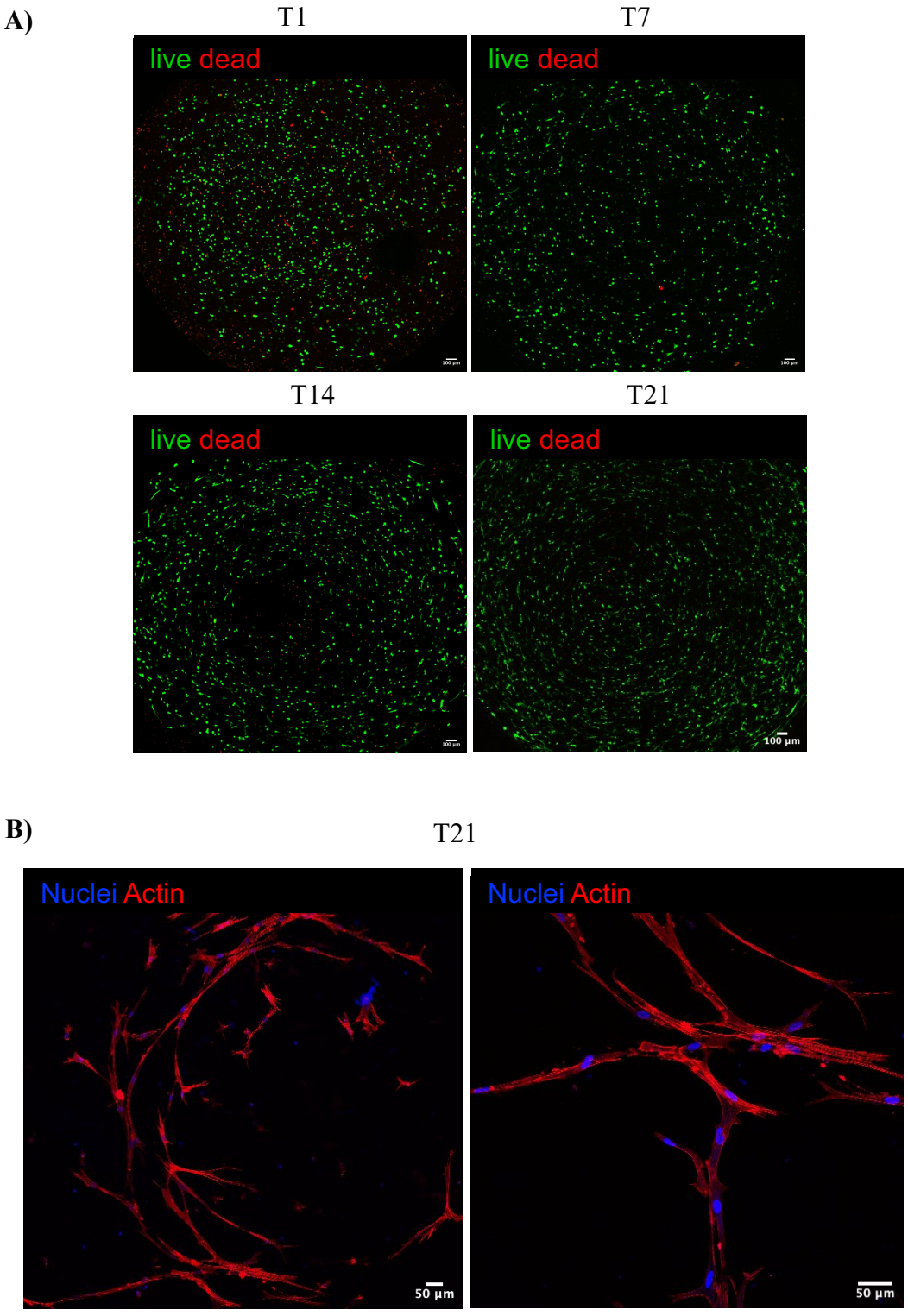

Human Umbilical Vein Endothelial Cells (HUVEC) constructs

HUVEC compatibility with GelXA LAMININK 411 was also evaluated. Bioprinted constructs were generated at a density of 10×10^6 cells/mL and maintained in culture for 14 days. Cell viability critically decreased throughout the culture period, and by day 14 only few cells were still detectable within the constructs (**Figure 32)**, none of which exhibited the characteristic elongated, activated endothelial morphology.

Figure 32. HUVEC cells demonstrated poor compatibility with GelXA LAMININK 411. *Live/dead staining of HUVEC constructs are reported through the culture period (day 1-7-14).*

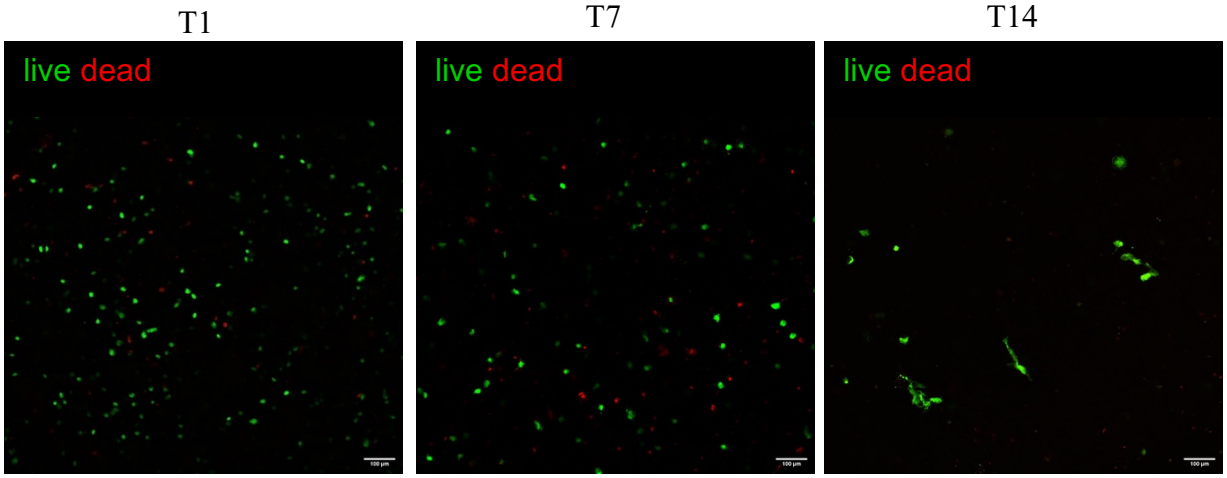

Given the limited compatibility of GelXA LAMININK 411 with endothelial cells, additional biomaterials were evaluated to enable the development of models capable of integrating both endothelial and tumour components.

4.1.2. PureCol

PureCol, a collagen type I–based hydrogel, was subsequently evaluated for its biocompatibility with endothelial and tumour cell populations.

HUVEC Droplets

Human umbilical vein endothelial cells (HUVECs) were embedded in PureCol and casted into droplets (50-100uL). 10×10^6 cells/mL concentration was selected as optimal cellular density. Droplets were cultured for 14 days to evaluate viability and morphogenesis. Cell survival was confirmed (**Figure 33A**), and immunofluorescence for CD31 revealed cellular activation and typical cobblestone morphology, suggesting initial endothelial network assembly (**Figure 33B**).

Figure 33. HUVEC viability and behaviour in PureCol hydrogel. *The panels show live/dead staining (**A**) and immunofluorescence stainigns (**B**) for hoescht (blue), phalloiding (red), and CD31 (green) at day 14 of droplets generation. White boxes indicate regions shown at higher magnification.*

A)

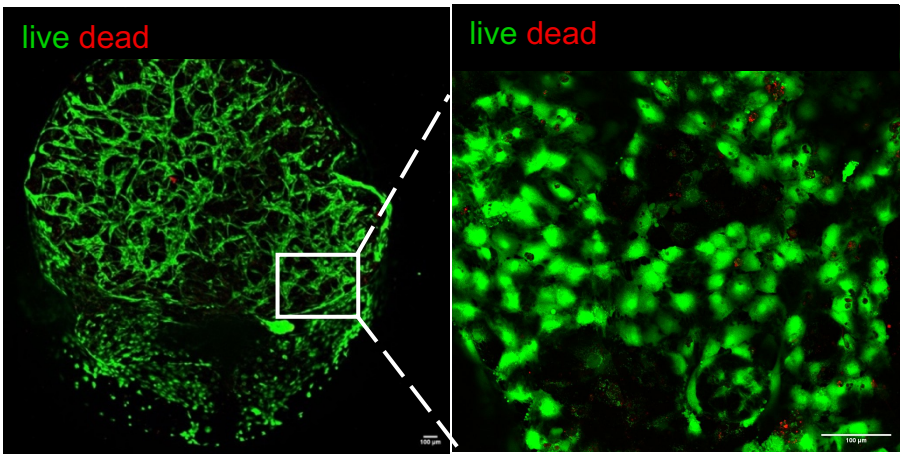

B)

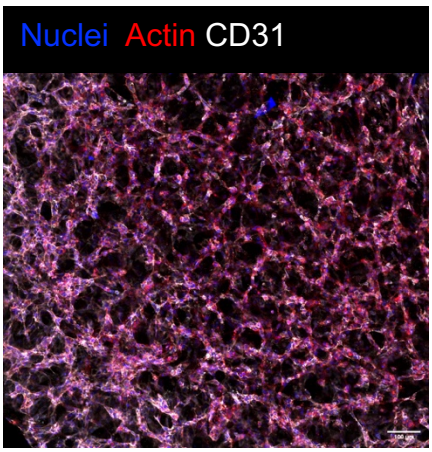

NT-18P and NT-18LM droplets

NT-18P and NT-18LM cells compatibility with PureCol awas also assessed. Droplets (10-100ul) were generated for each cell line and cultured for 21 days (**Figure 34 A**). Both cell lines retained high viability, and cellular aggregation was observed. Of note, morphological differences appeared between the two cell lines: NT-18P cells formed dense, spheroidal aggregates, while NT-18LM cells displayed a looser and irregular arrangement (**Figure 34 B).**

Figure 34. NT-18P and NT-18LM viability and behaviour in PureCol hydrogel. *Live/dead staining for NT-18P and NT-18LM are depicted in panels (**A**) and (**C**), respectively. Morphological assessment through hoechst (blue) and phalloidin (red) stainings are depicted in panels (**B**, NT-18P) and (**D**, NT-18LM).*

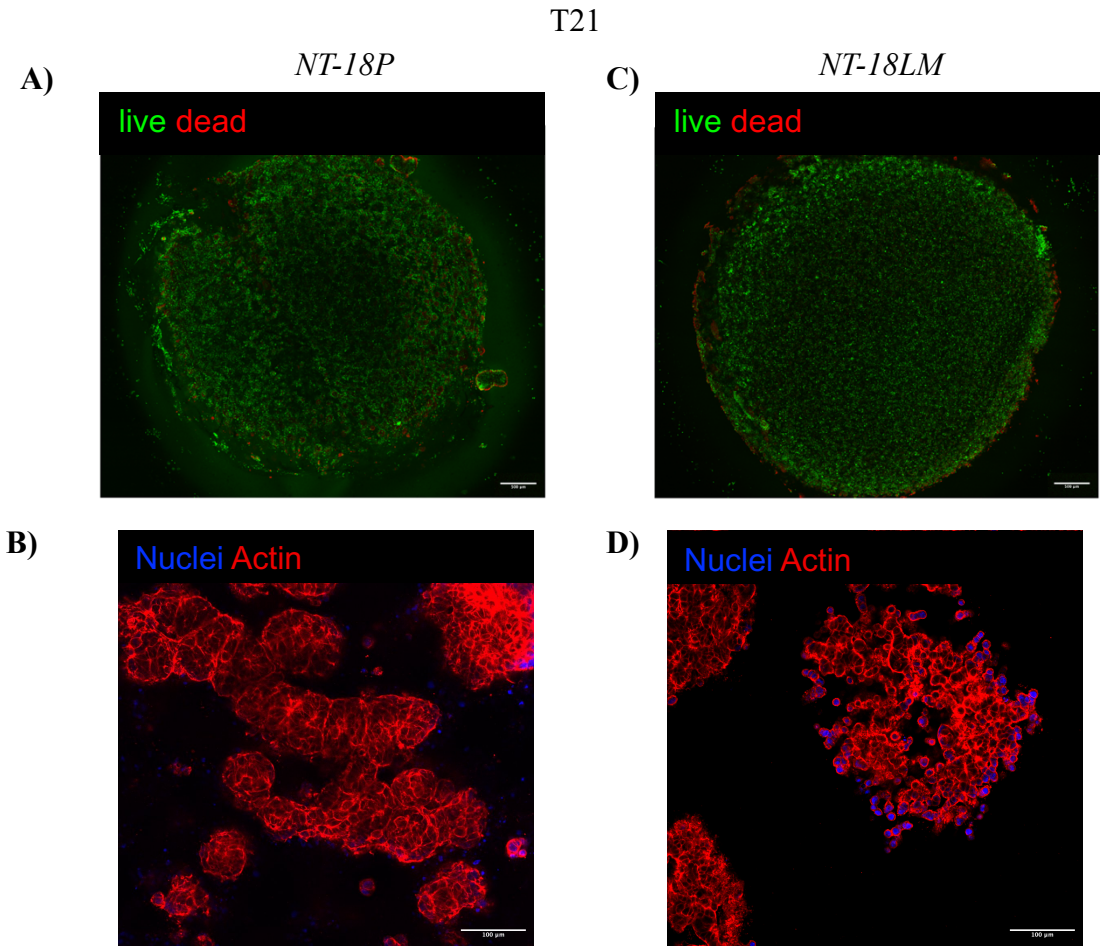

4.2. Complex multicellular models

Based on above-described assessments, the most prominent and biologically relevant cell populations and bioinks were selected for the generation of more complex constructs. Hetero-cellular models were then produced, mixing two cell lines together within the same hydrogel. The most appropriate biomaterial as well as the concentration of each cell type to promote balanced interactions and support co-viability were systematically tested. In parallel, the most appropriate culture medium composition required to sustain both viability and functional activation was evaluated and refined.

4.2.1 PureCol

Co-culture of NT-3 and HUVEC in PureCol

To enhance endothelial maintenance, NT-3 and HUVECs (1:1 ratio; 10×10^6 cells/mL) were co-cultured in PureCol for up to 21 days in EGM-2 : RPMI supplemented with EGF (20 ng/mL) and FGF (10 ng/mL) medium. Media 2:1 concentration was identified as the best ratio to support cellular requirements of both cell types. High cell viability and progressive cellular organization was obtained (**Figure 35A**). Homo- and hetero-typic interactions were observed. Immunofluorescence at day 14 revealed $CD31^+$ endothelial cords interspersed among $Synaptophysin^+$ tumour aggregates. By day 21, NT-3 cells formed large islet-like clusters anchored to a continuous cobblestone-like endothelial layer surrounding the scaffold, suggesting reciprocal stabilization between tumour and endothelial compartments (**Figure 35B**). Although PureCol supported cell viability and inter-cellular interactions, the matrix exhibited progressive shrinkage over time, resulting in structural deformation of the construct. Consequently, PureCol was deemed unsuitable for incorporation into complex or multi-bioink models.

Figure 35. NT-3 interactions with HUVECs in PureCol droplets*. Live/dead staining (**A**) were performed throught the culture period (14 days)**.** Immunofluorescence staining (**B**) for hoechst (blue), phalloidin (red), CD31 (red), and synaptophysin (white) revealed time-dependent homo- and heterotypic cellular interactions. Panels (i) show immunofluorescence at T7, whereas panels (ii) and (iii) depict cultures at T14, with panel (iii) providing a higher-magnification view of endothelial–tumour interactions.White boxes indicate regions shown at higher magnification.*

A)

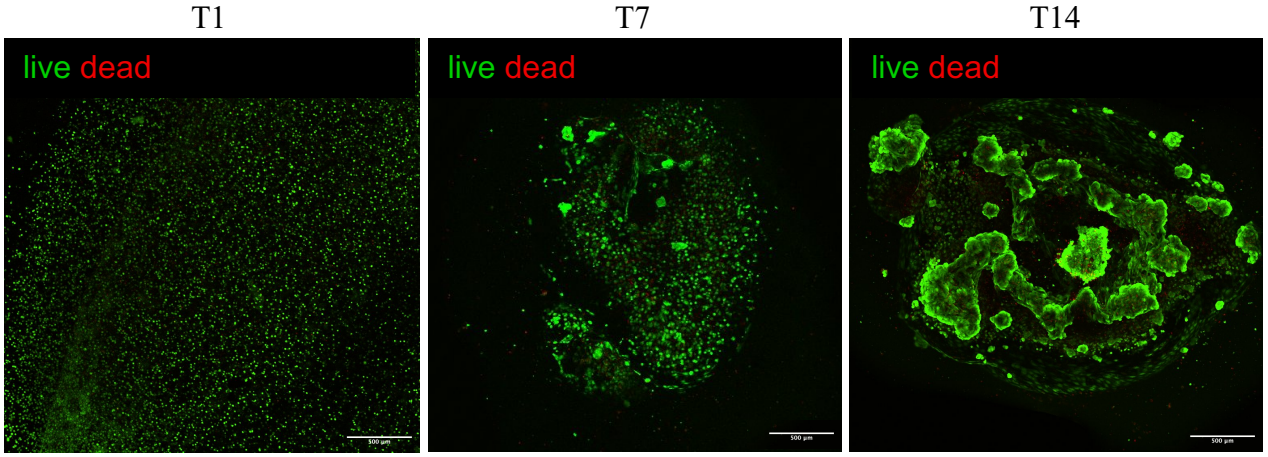

B)

i)

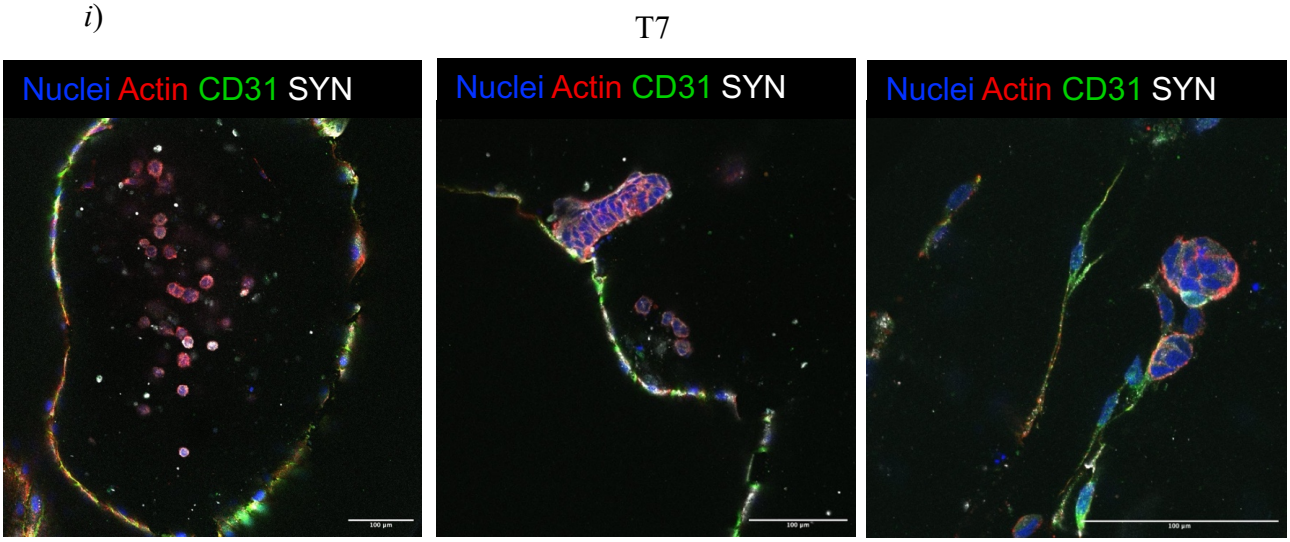

T14

ii)

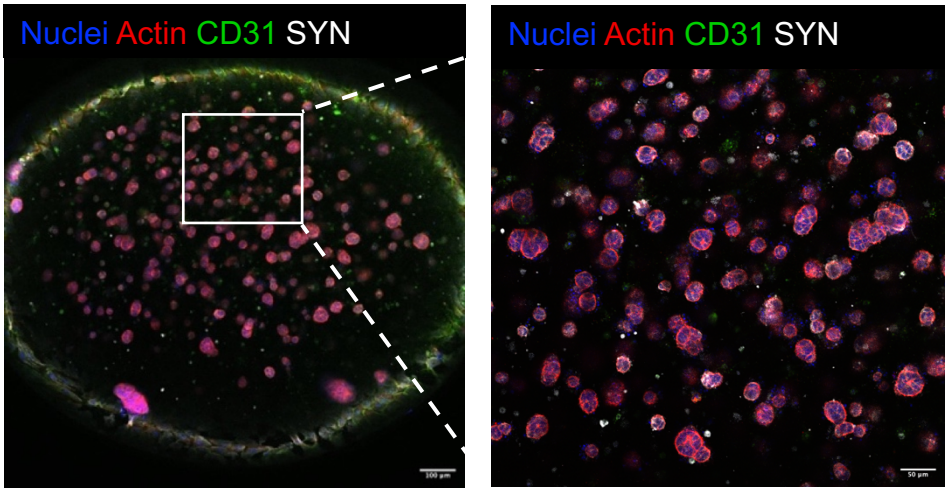

iii)

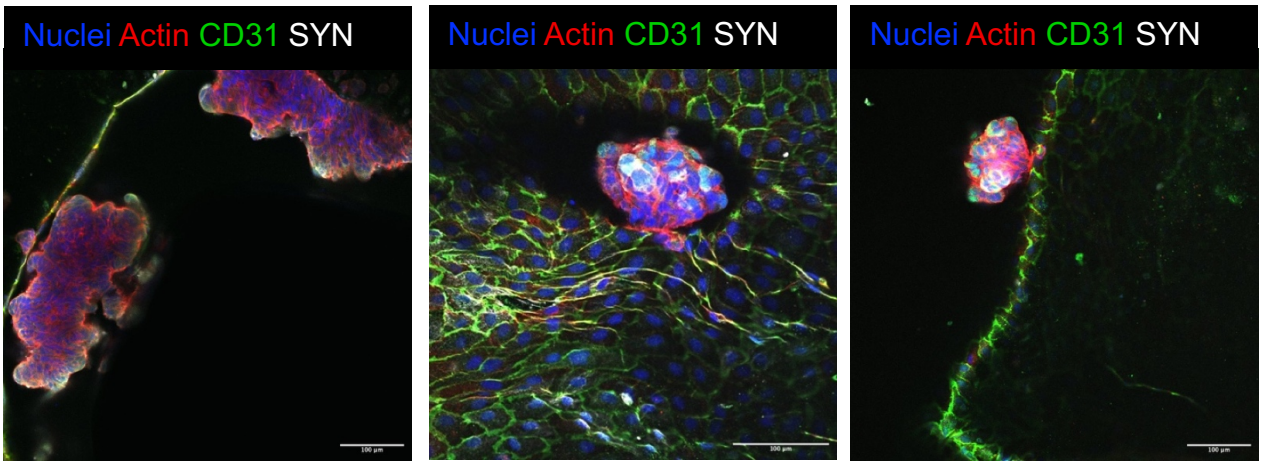

4.2.2. GelMA Fibrin

Further optimization was achieved using GelMA Fibrin, a hybrid bioink with enhanced mechanical performance and stability.

Co-Culture of NT-3 cells and HUVEC in GelMA Fibrin

Droplets containing HUVEC and NT-3 cells (1:1 ratio) were casted as 50–100 µL GelMA-Fibrin droplets for 14 days. A 2:1 ratio of EGM-2 to RPMI supplemented with EGF (20 ng/mL) and FGF (10 ng/mL) was identified as the most appropriate medium formulation. Live/dead staining demonstrated sustained viability throughout the culture period (**Figure 36A**). Immunofluorescence for CD31 and SYN confirmed close spatial association of tumour and endothelial cells (**Figure 36B**). Tumour cells self-aggregation

into clusters (SYN+) and interaction with endothelial (CD-31+) component was observed. These findings validated GelMA–Fibrin as a proper matrix for supporting dual-cell-type constructs.

Figure 36. NT-3 interactions with HUVEC in GelMA–Fibrin droplets. *Live/dead staining (**A**) and immunofluorescence (**B**) for hoescht (blue), phalloiding (red), CD31(green), and Synaptophysin (white) were performed through the culture period. White boxes indicate regions shown at higher magnification.*

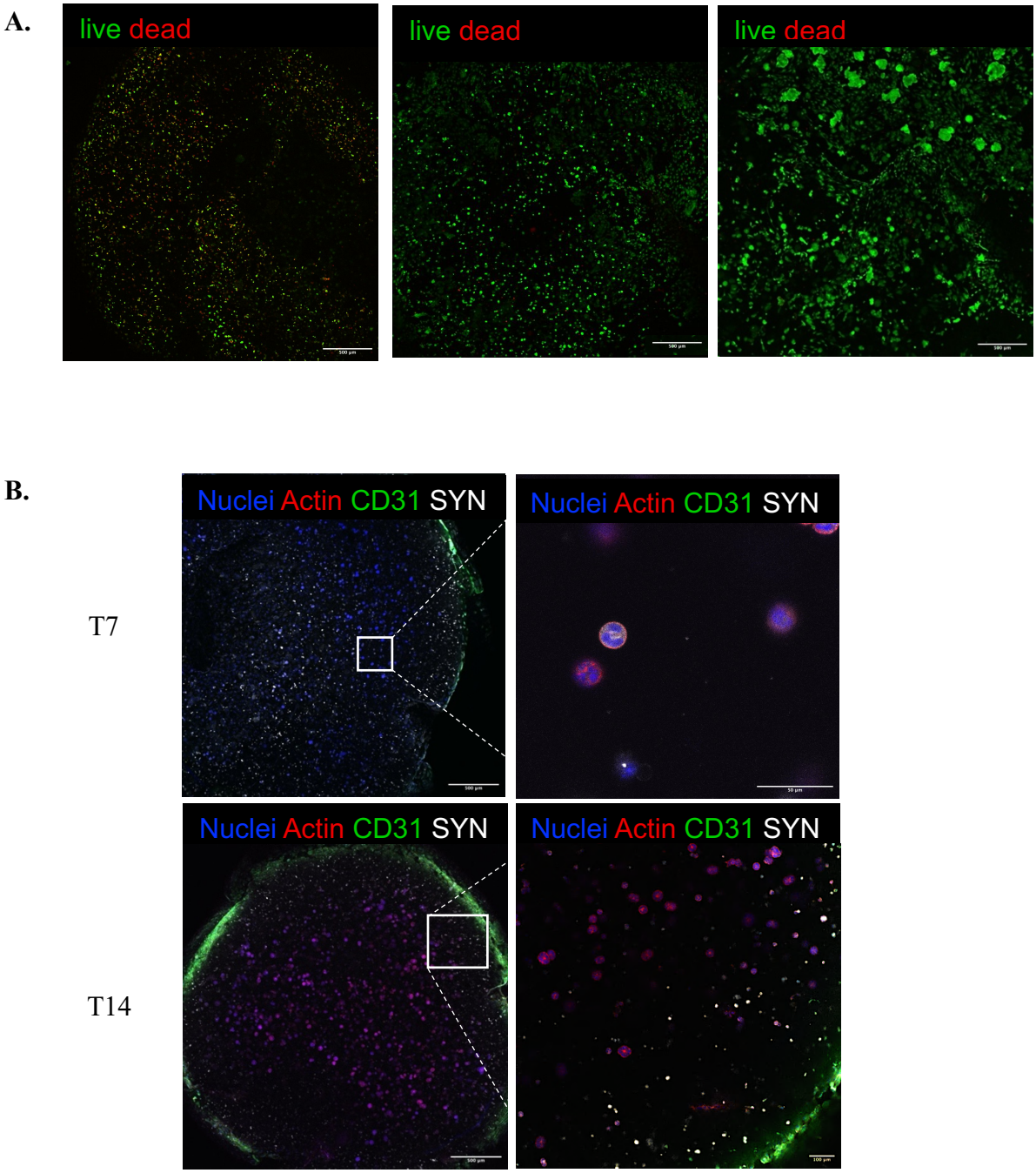

Co-cultures of NT-18P and NT-18LM with HUVEC in GelMA Fibrin

NT-18P (**Figure 37A**) and NT-18LM (**Figure 37B**) PanNET cells were co-cultured with HUVECs (1:1 ratio; 10 × 10^6 cells/mL) in GelMA Fibrin. 50-100 µL droplets were generated and maintained in culture for up to 21 days in EGM-2 : RPMI medium supplemented with growth factors (2:1). High cell viability and structural coherence was reported across all time points. Immunofluorescence for actin, CD31, and SYN revealed coexistence of tumour and endothelial cells with organized multicellular aggregates and peripheral endothelial networks. Both PanNET cell lines maintained their morphological identity, with cobblestone-like structures becoming evident in both models from day 14 after droplet generation.

Figure 36. NT-18P and NT-18LM cells interactions with HUVECs in GelMA Fibrin droplets. *Co-culture of NT-18P and NT-18LM with HUVEC are depicted in panels (**A**) and (**B**), respectively. Live/dead staining (i) confirmed high overall viability of the constructs. Immunofluorescence (ii) for hoechst (blue), phalloidin (red), CD31(green), and synaptophysin (SYN, white) showed homo- and hetero-cellular interactions between tumour and endothelial cells. White boxes indicate regions shown at higher magnification.*

A.

i) T7 T14 T21

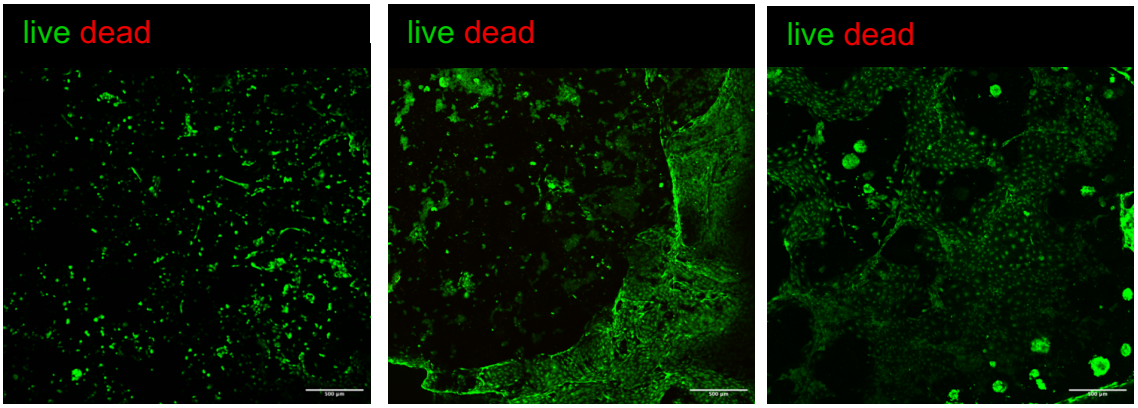

ii) T21

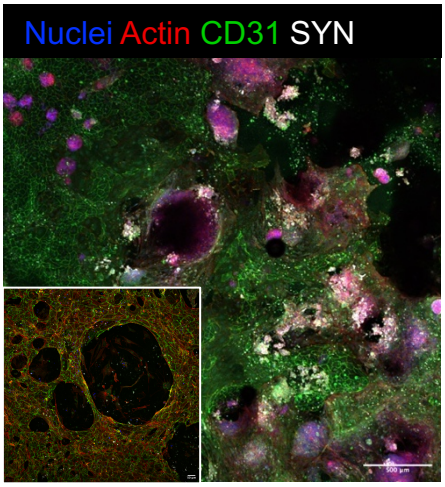

B.

i) T7 T14 T21

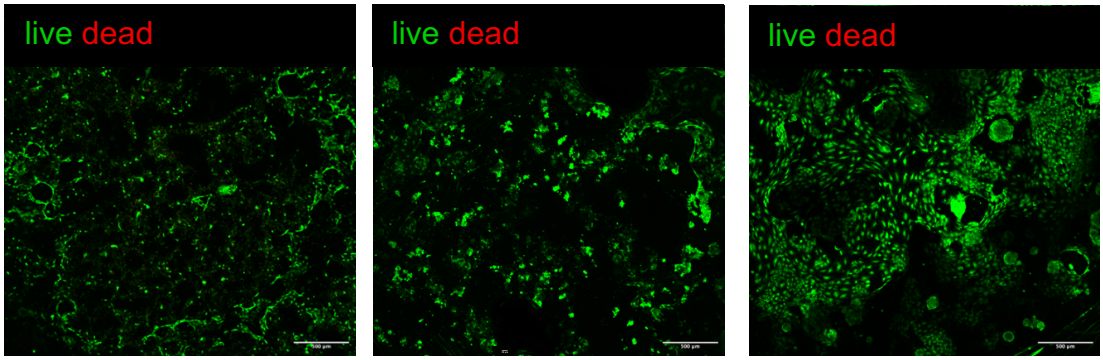

ii) T21

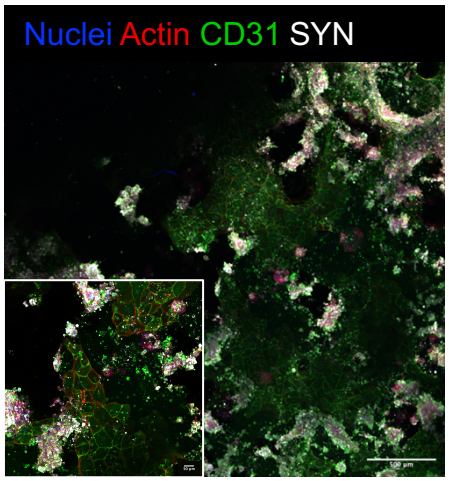

Co-culture of HUVEC and hMSC in GelMA Fibrin

To engineer a functional vascular compartment, HUVECs (10×10^6 cells/mL) and hMSCs (5×10^6 cells/mL) were co-cultured in GelMA Fibrin for 21 days in EGM-2 : RPMI supplemented with EGF (20 ng/mL) and FGF (10 ng/mL) (2:1) medium. Immunofluorescence for nuclei, actin, CD31, and vWF demonstrated aligned endothelial cords and lumen formation at day 7 (**Figure 37A-B**). HUVECs exhibited strong CD31 and vWF expression, confirming endothelial maturation and polarization supported by hMSC-derived structural stabilization and differentiation.

Figure 37. HUVECs and hMSCs interactions in GelMA Fibrin droplets. *Immunofluorescence for hoescht (blue), phalloidin (red), CD31(green), and von Willebrand factor (white) performed through the culture period (day 7-14-21). Evidence of lumen formation are depicted in panels (A). A1, upper focal plane; A2, middle plane of the vascular structure; white arrow indicates lumen. vWF, von Willebrand factor.*

T7

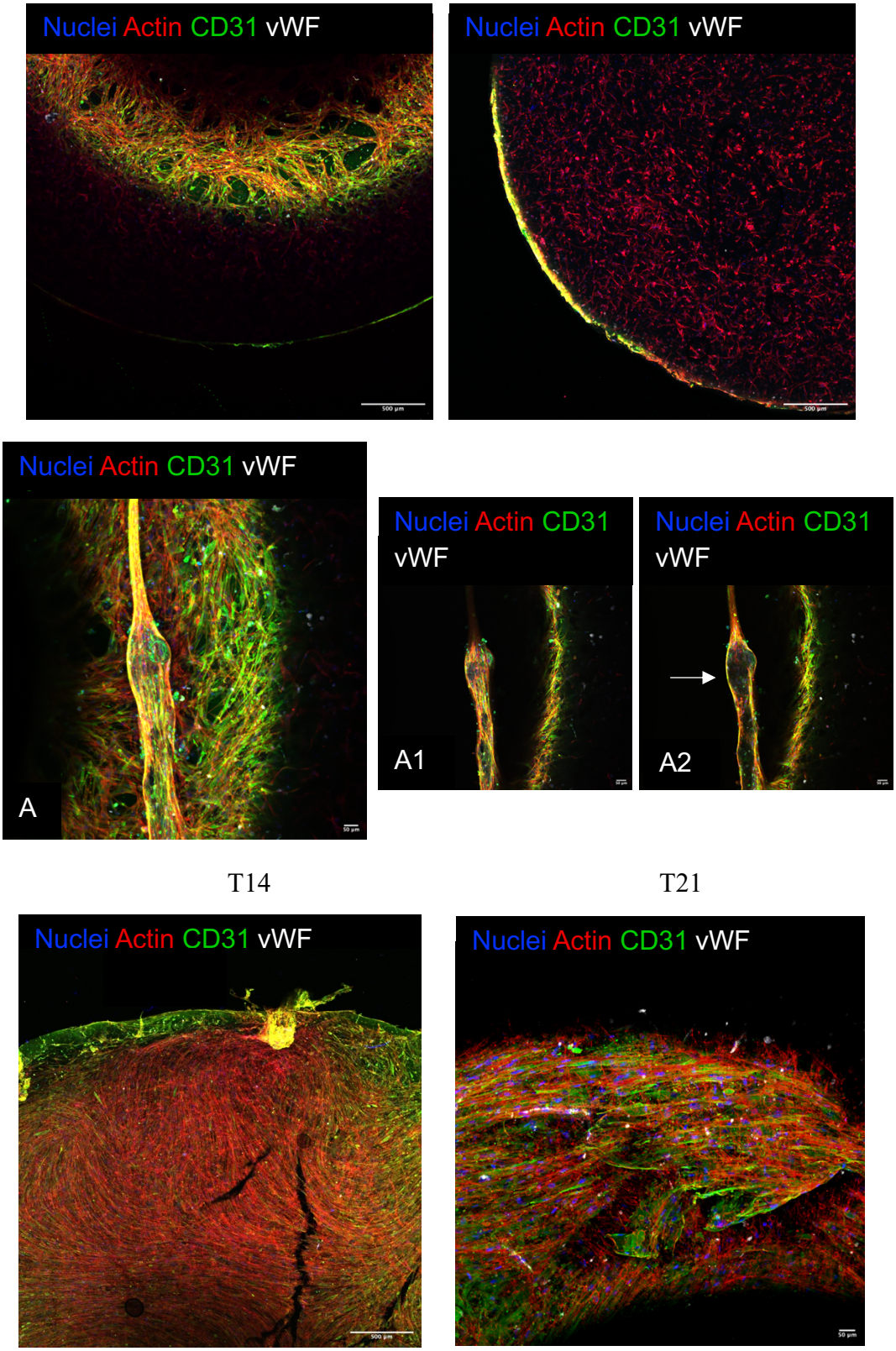

4.3. Generation of perfusable, vessel-like PanNET Constructs

Tri-culture constructs incorporating PanNET cells (NT-3, NT-18P, or NT-18LM), HUVECs, and hMSCs were generated using GelMA Fibrin and GelXA LAMININK 411 bioinks.

The scaffolds were generated using a hybrid two-step technique recently established in our laboratory (*Pinos et al.*, submitted) and it was adapted and optimized in this study to the neuroendocrine context. This method combines 3D bioprinting of the tumour outer compartment, which allows precise control over cell distribution within the surrounding microenvironment, and casting of pre-mixed HUVEC and hMSCs cells in GelMA Fibrin to generate a well-defined central lumen. First we bioprinted in GelXA LAMININK 411 PanNET cell lines (NT-3, NT-18P, NT-18LM, $10x10^6$ cells/ml) in the tumour outer compartment, generating a $7x7x6mm^3$ scaffold, with a 5.5mm in diameter central channel (**Figure 38A**). Subsequently we filled the central hollow cavity with endothelial and mesenchymal cells. Specifically, HUVEC ($10x10^6$ cells/ml) and hMSC ($5x10^6$ cells/ml) mixed with GelMA Fibrin were casted within the central channel of the bioprinted scaffold (**Figure 38B**). Immediately, a 3D printed tool (diameter 2.5mm) (**Figure 38C**) was inserted inside the casted material to create a space for the vascular lumen, then gently removed after crosslinking. The final result was an inner endothelialized lumen surrounded by a an outer PanNET compartment (**Figure 38D**).

Figure 38. Steps to obtain the vessel-like scaffold. *A) GelXA LAMININK 411is mixed with PanNET cell lines and bioprinted.* ***B)*** *GelMA Fibrin mixed with HUVECs and hMSCs is casted inside the hole.* ***C)*** *Rapidly the pin is allocated in the middle of the gel to allow the formation of the central hole.* ***D)*** *The scaffold is crosslinked and the pin gently removed. HUVEC, human umbilical vein endothelial cells; hMSCs, human mesenchymal stem cells.*

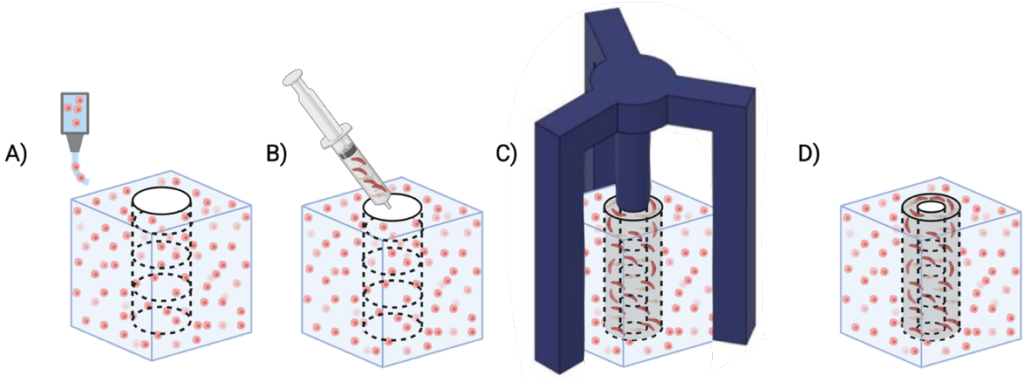

Constructs were first matured under static conditions for 14 days and then transferred into a custom-designed milli-fluidic bioreactor (Vessel-Box, Italian Patent Application n. 102023000024429, R. Pinos, **Figure 39**), which enables selective perfusion of the vascular lumen at 100 mL/min (**Figure 40**). Optimization of the medium ratio was performed and a 2:1 mixture of EGM2:RPMI supplemented with previously described growth factors was identified as the most appropriate formulation to support all cell types present in the construct.

Figure 39. Schematic representation of the VesselBox device and its components. *Rendering of the exploded view of the VesselBox device* ***(A)****, illustrating threads on lid (I) and adapters (III) which ensure tight sealing of the device, together with the optical window (II) on the lid that enables direct monitoring of the scaffold over-time. The customed scaffolds are hosted within the base (IV), into which the adapters partially insert to maintain controlled and selective perfusion.* ***(B)*** *Assembled VesselBox bioreactor demonstrating the final configuration used for dynamic culture.*

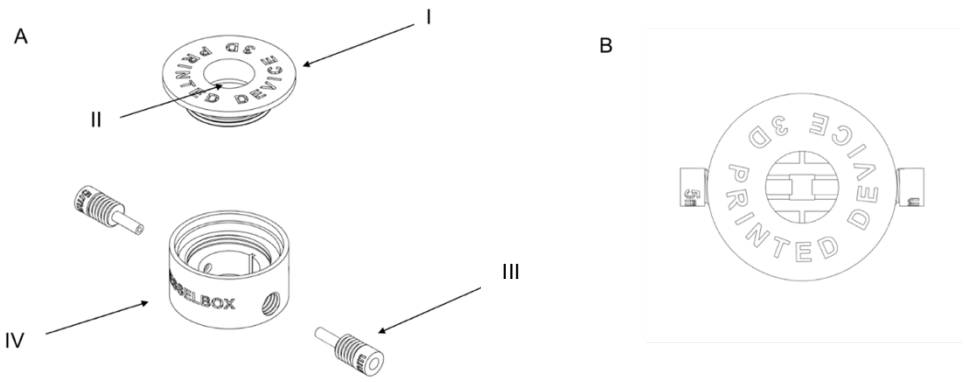

Figure 40. Workflow illustrating culture conditions following scaffold generation. *HUVEC, human umbilical vein endothelial cells, hMSC, human mesenchymal stem cells*

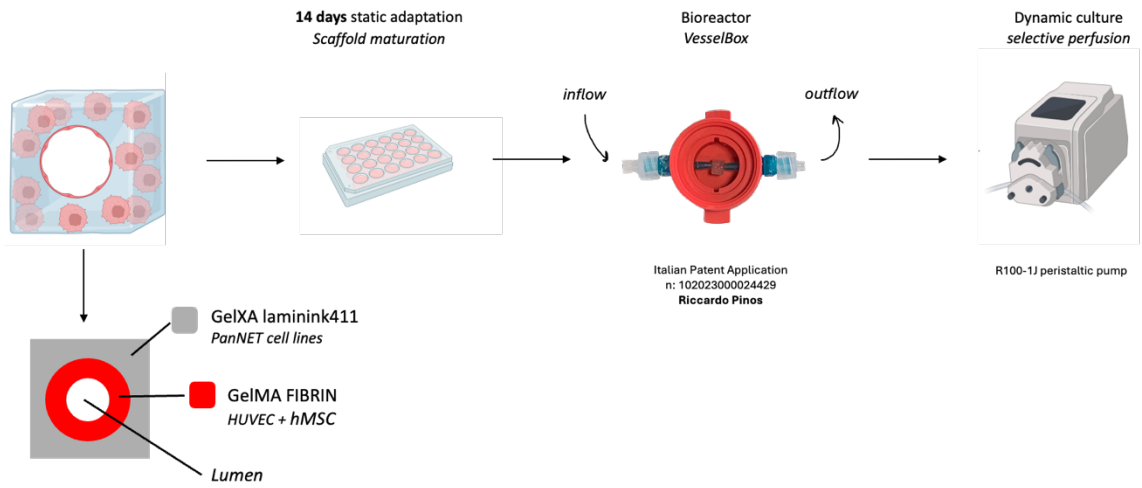

Following 14 days of static maturation, all vessel-like constructs (NT-3, NT-18P and NT-18LM based) exhibited high viability and clear compartmentalization between tumour and endothelial regions. Under dynamic flow, endothelial activation and alignment along the luminal surface were markedly enhanced, and overall structural integrity was preserved. Distinct phenotypic behaviours emerged depending on the PanNET cell line employed.

NT-3 based vessel-like construct

After 14 days of static culture, the constructs demonstrated high viability (**Figure 41A**), pronounced endothelial alignment, maintenance of a patent central lumen, and clear tumour–vascular interactions (**Figure 41B**), including early endothelial sprouting directed toward the tumour compartment. The constructs were then maintained for an additional 7 days under either static (**Figure 41C**) or dynamic (**Figure 41D**) culture conditions. Under static conditions, a reduction in endothelial activation, reflected by diminished CD31 expression, was observed. This was accompanied by a more flattened endothelial morphology and a sharper demarcation between the endothelial and tumour compartments, with only sparse endothelial elongation at the periphery.

In contrast, dynamic perfusion markedly enhanced endothelial–tumour interplay. Immunofluorescence for CD31 revealed increased endothelial activation and improved structural organization, characterised by pronounced finger-like projections extending toward the tumour compartment, resulting in more frequent tumour–endothelial contacts. Despite these heterotypic interactions, only small and infrequent tumour cell clusters were observed. Tumour cell infiltration into the endothelial compartment remained minimal in both culture conditions.

Figure 41. NT-3-based vessel-like scaffold. *A) Live/dead and (**B**) immunofluorescence stianing after 14 days of static culture (14s). Comparison of PanNET constructs cultured under 7 days of static (7s) (**C**) and dynamic (7d) (**D**) conditions after a 14-day static adaptation period. Schematic representations beneath each image indicate the corresponding location within the construct: the light-blue region denotes the tumour compartment, the red region represents the endothelial compartment, and the white circle marks the inner lumen. The black rectangle indicates the specific area shown in the corresponding image. Immunofluorescence for hoechst (blue), phalloidin (red), CD31 (green), and CgA (white) are depicted. Lumen indicated by "*" in the images.*

A) 14s

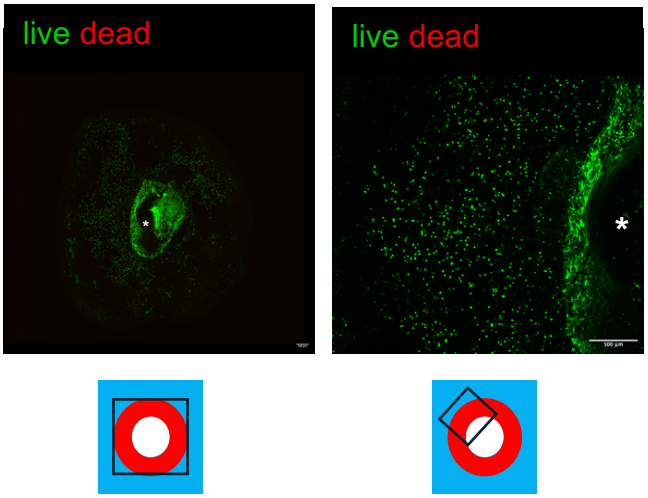

B) 14s

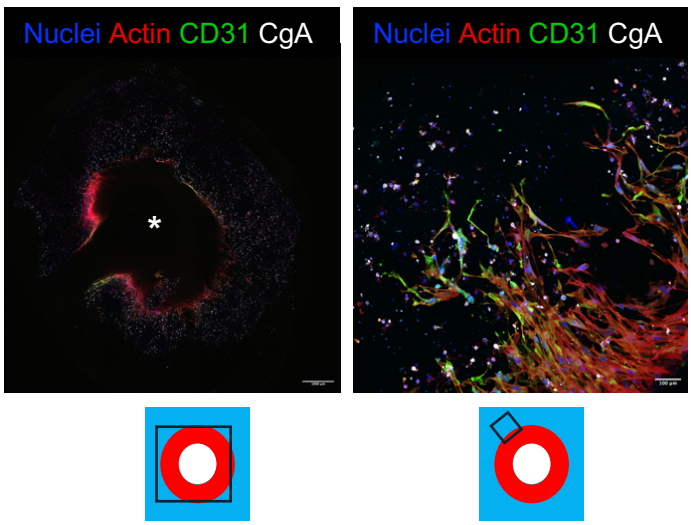

C) 14s + 7s

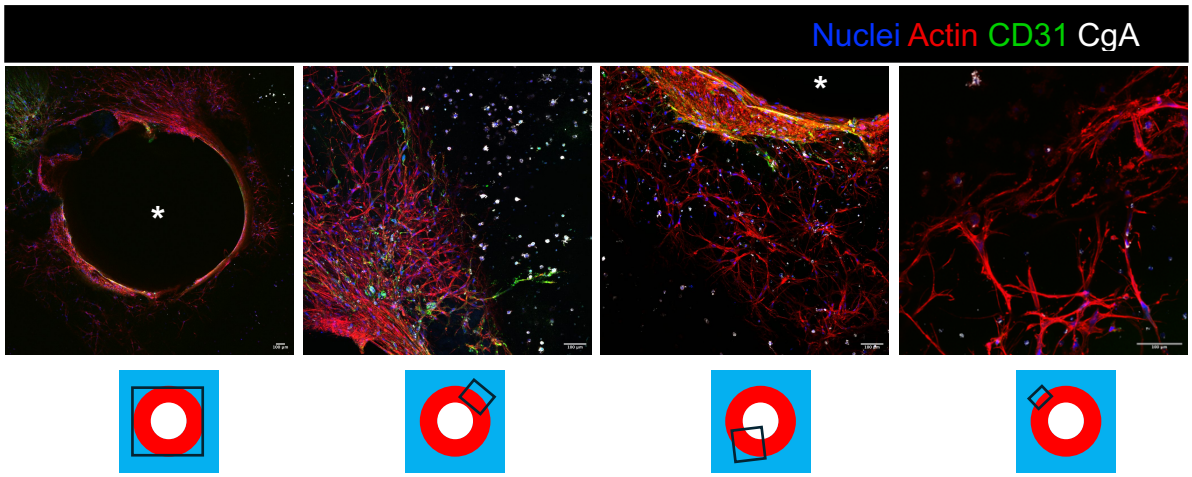

D) 14s + 7d

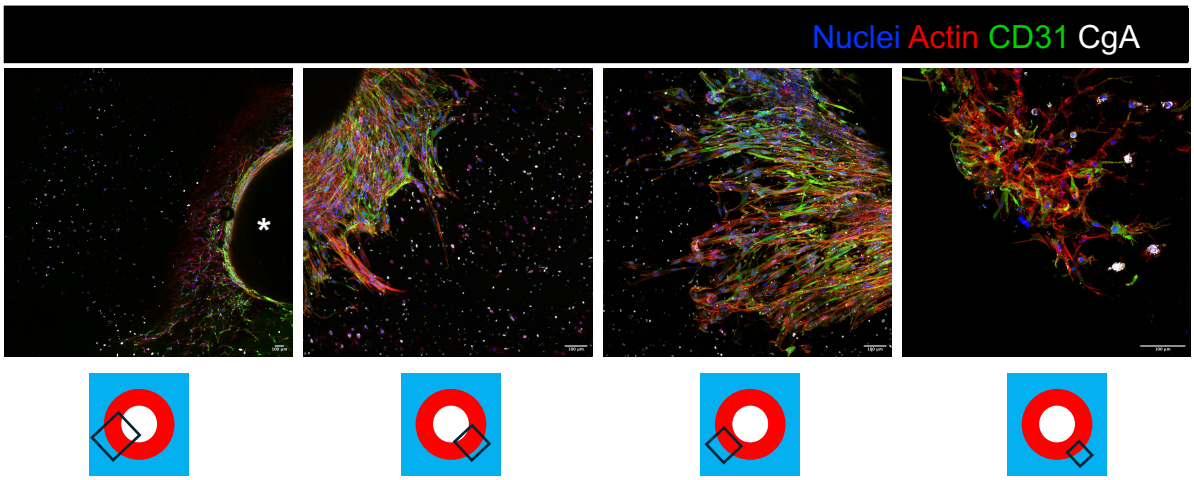

NT-18P based vessel-like construct

After 14 days of static culture, the constructs demonstrated high overall viability (**Figure 42A**). Constructs maintained under either static or dynamic conditions preserved the general morphology of both compartments; however, endothelial activation, reflected by increased CD31 expression, was more pronounced in the perfused constructs (**Figure 42B**), consistent with previous observations in NT-3 based models. In NT-18P constructs subjected to dynamic perfusion, only limited endothelial protrusions toward the tumour compartment were observed, and the boundary between endothelial and tumour regions

remained relatively flat and sharply demarcated (**Figure 42C-2**). In contrast, marked tumour cell and tumour aggregate invasion toward the perfused lumen was evident (**Figure 42C-1**), accompanied by pronounced endothelial–tumour interactions within the endothelial compartment (**Figure 42C-3**).

Figure 42. NT-18P-based vessel-like constructs. *Live/dead staining after 14 days of static culture (14s, **A**). Comparison of constructs after 7 days of static (14s + 7s) versus dynamic (14s +7d) culture following static adaptation is represented in panel (**B**). Immunofluoresce stainings for hoescht (blue), phalloidin (red), CD31 (green), and CgA (white) are reported. Schematic representations beneath each image indicate the corresponding location within the construct: the yellow region denotes the tumour compartment, the red region represents the endothelial compartment, and the white circle marks the inner lumen. The black rectangle indicates the specific area shown in the corresponding image. Panels (**C**) illustrates immunofluorescence stainings for hoescht (blue), phalloidin (red), CD31(green), and CgA (white) in the dynamic condition (14s + 7d). Borders between tumour-endothelial compartment are depicted in panels (ii). Tumour-endothelial interaction is reported in panel (iii). White arrows, tumour cells aggregate within the endothelial compartment. Yellow arrows, endothelial extroflection toward the tumour region. Lumen indicated by "*" in the images. White boxes indicate regions shown at higher magnification.*

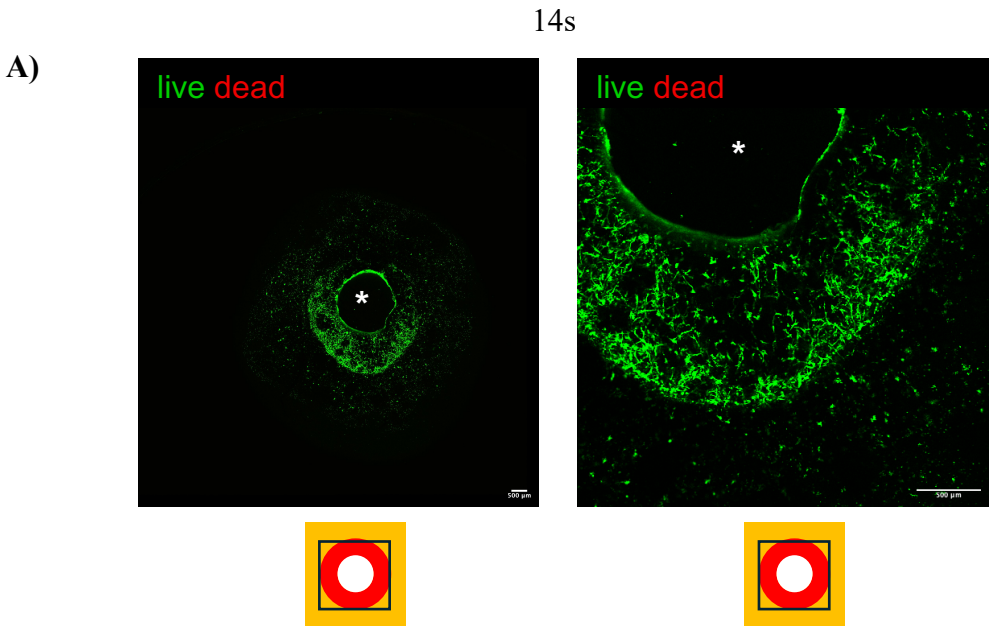

B)

14s + 7s

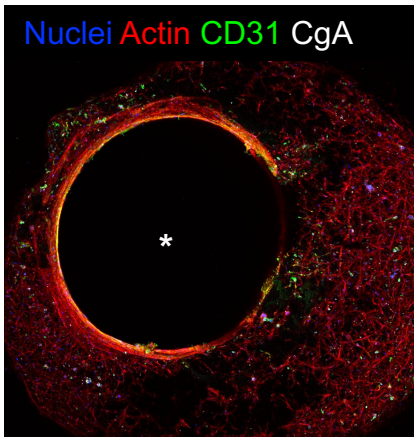

14s + 7d

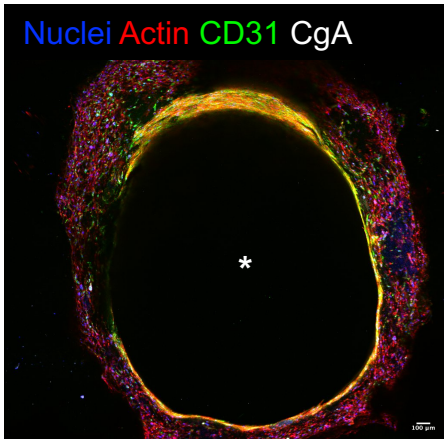

C)

14s + 7d

i)

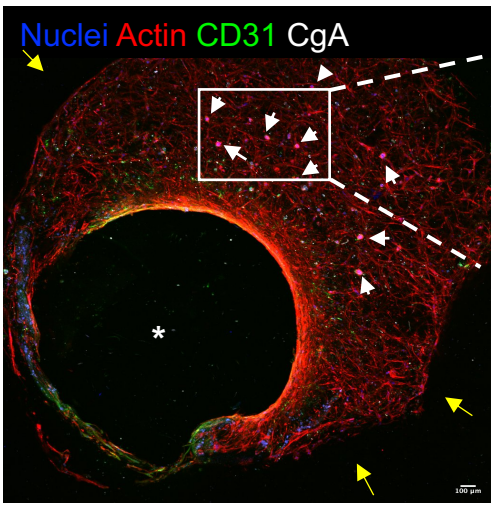

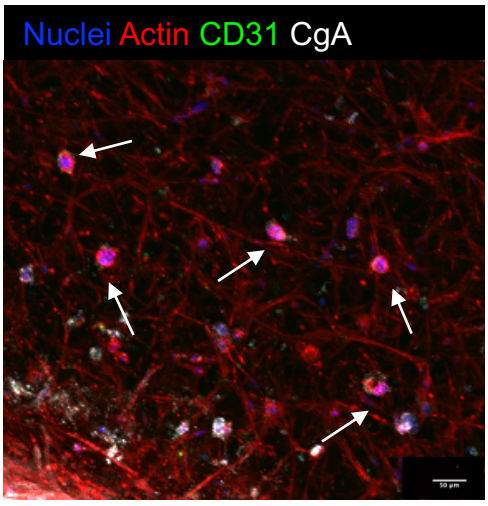

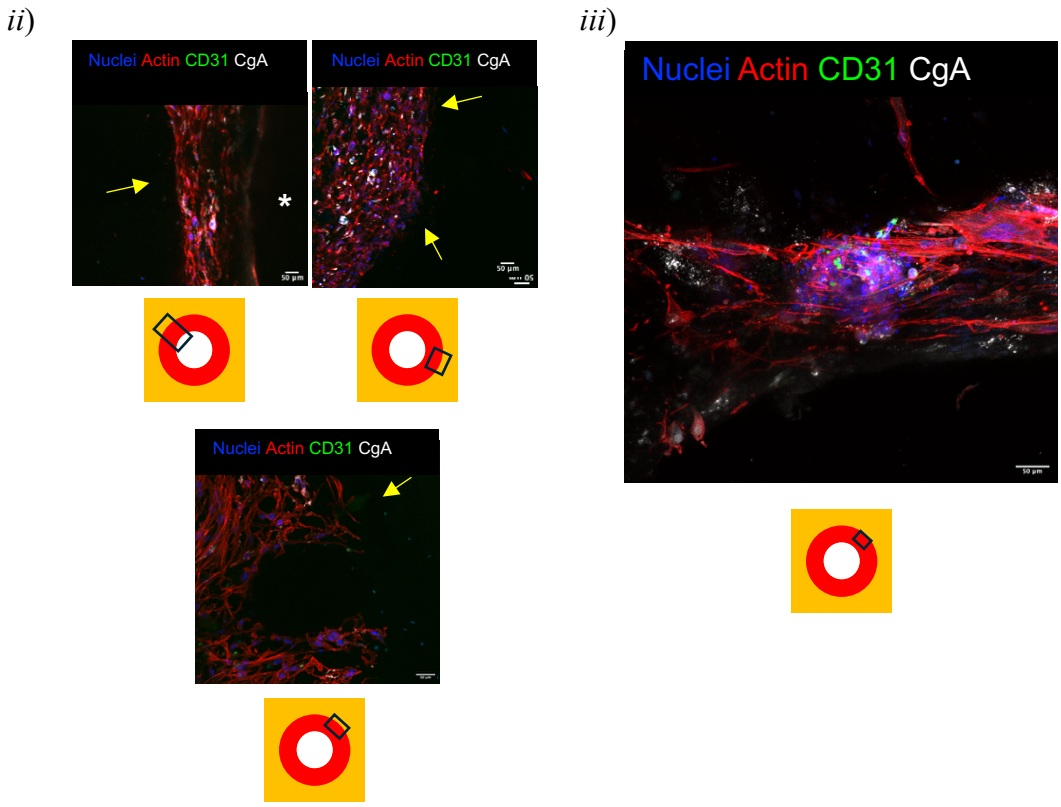

NT-18LM- based vessel-like construct

The constructs demonstrated high viability after 14 days of static adaptation (**Figure 43A**). Upon transfer to dynamic culture for an additional 7 days, the scaffolds exhibited marked endothelial activation, evidenced by pronounced CD31 expression, together with enhanced intercellular interactions. Notably, a bidirectional tumour–endothelial interplay emerged, characterised by endothelial projections extending into the tumour compartment (**Figure 43B-1**) and tumour infiltration toward the endothelial layer. The latter was limited in extent and consisted of small mono- to few-cell clusters localised to the outer endothelial surface, with no evidence of deeper invasion (**Figure 43B-2**).

Figure 43. NT-18LM-based vessel-like construct. *Live/dead staining (**A**) depicts cell viability after 14 days of static culture (14s). Panels (**B**) show immunofluorescence staining after the subsequent 7 days under dynamic conditions (14s + 7d), including hoechst (blue), phalloidin (red), CD31 (green), and CgA (white). Panel (ii) presents a higher-magnification view of the endothelial–tumour interface. Lumen is indicated by "*" in the images. Schematic representations beneath/side at each image indicate the correspondIng location within the construct: the green region denotes the tumour compartment, the red region represents the endothelial compartment, and the white circle marks the inner lumen. The black rectangle indicates the specific area shown in the corresponding image. White boxes indicate regions shown at higher magnification. CgA, Chromogranin A.*

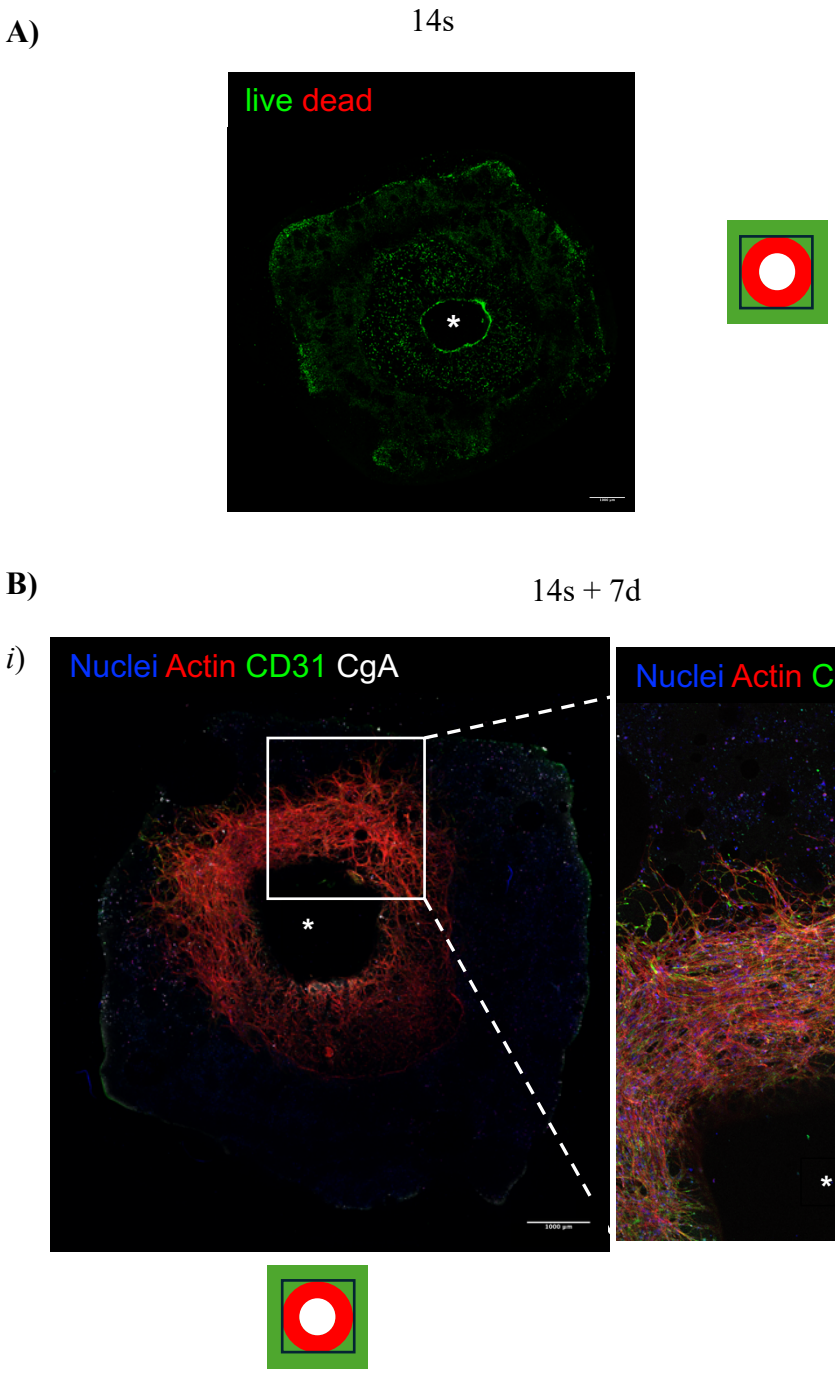

ii)

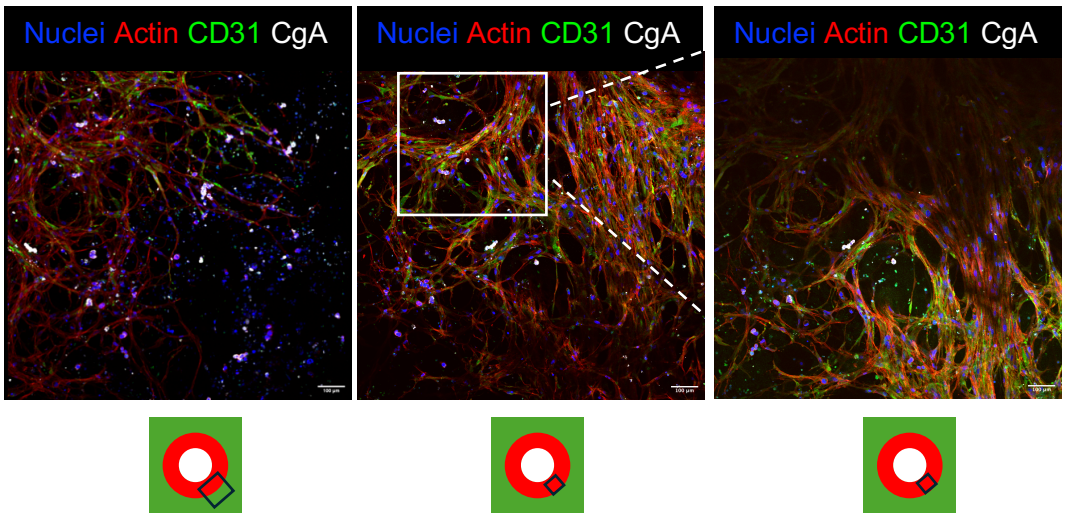

A semiquantitative heat-map analysis was generated to compare endothelial–tumour interactions across the three construct settings (NT-3, NT-18P, and NT-18LM) (**Figure 44**). Endothelial projections and the degree of tumour infiltration were evaluated for each PanNET model. Both features were scored on a 0–5 scale based on immunofluorescence patterns. Because automated quantitative assessment of tumour infiltration within the endothelial compartment was hindered by technical limitations related to the granular nature of the tumour immunostaining, all IF images were independently reviewed by two experts in the field (D.B. and R.P.), who assigned scores for each parameter evaluated. NT-3 constructs exhibited maximal endothelial protrusion and minimal tumour invasion whereas NT-18P constructs showed the opposite profile, with limited endothelial projections and greater tumour infiltration. NT-18LM constructs demonstrated an intermediate phenotype.

Figure 44. Heat Map of PanNET Vessel-like models phenotypes. *Heat-map scoring of endothelial projections and tumour infiltration (scale 0–5) was performed on immunofluorescence images. 0=absence of the feature, 5=maximal expression of the feature.*

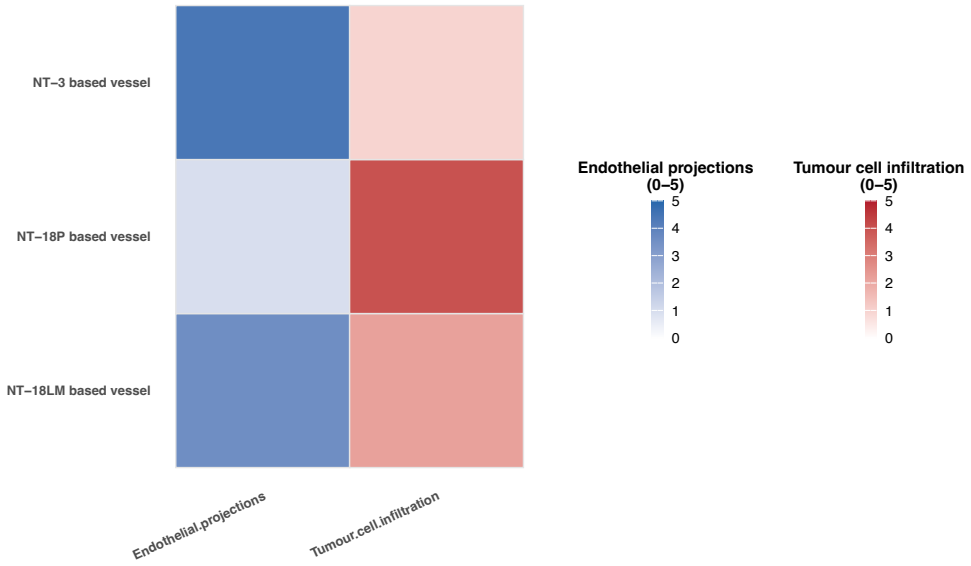

2D migration potential of PanNET cell lines

A 2D migration assay was performed for the NT-3, NT-18P, and NT-18LM cell lines to assess their intrinsic characteristics in a simple 2D setting. NT-18P exhibited the highest migratory potential among the tested lines, fully traversing the gap by 120 hours. At the same time point, the other two cell lines demonstrated markedly reduced migration, with NT-3 showing almost no movement and NT-18LM displaying an intermediate phenotype (**Figure 45**), validating the cellular behaviours identified in the 3D setting.

Figure 45. Different migration potential between NT-3 (A), NT-18P (B) and NT-18LM (C). *Representative images at T0 (after insert removal, 500-µm cell-free gap) and after 120 hours (5× magnification).*

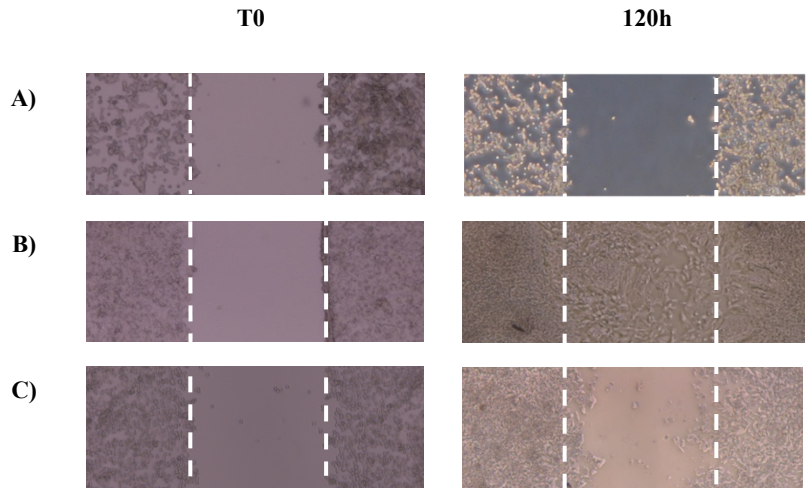

Discussion

At present, only a limited number of preclinical models exist for NF-PanNETs (Ear *et al*, 2024; Cros *et al*, 2025b). Existing systems provide only a partial representation of tumour biology and lack meaningful incorporation of the microenvironmental elements, critical players of PanNET behaviour (Cives *et al*, 2019). This gap substantially limits our ability to investigate disease pathophysiology and continues to hinder progress toward a mechanistic understanding of PanNET progression. Within this context, we introduce a novel experimental platform designed to more faithfully recapitulate tumour-microenvironment crosstalk, by integrating, within a defined 3D architecture, tumor, vascular and stromal components that collectively shape PanNET biology.

Extrusion-based bioprinting technique was employed to generate a spectrum of 3D constructs, ranging from simple monocellular systems to complex compartimentalized multicellular architectures. In particular, hydrogel-based 3D cultures were established for all PanNEN cell lines, in parallel with stromal and endothelial components. Viability and morphological behaviour were assessed for each cell line, and the most suitable bioink was selected accordingly. In line with their intrinsic properties, PanNEN cell lines displayed distinct morphologies and aggregation capacity (Benten *et al*, 2018; Viol *et al*, 2022; Detjen *et al*, 2021): BON-1 cells formed large islet-like clusters consistent with

their aggressive behaviour; NT-3 cells showed limited aggregation reflecting their intrinsically slow growth characteristics; and NT-18P and NT-18LM exhibited intermediate phenotypes, with NT-18P demonstrating greater migratory capacity and more defined islet-like structures compared with its corresponding metastatic derivative, NT-18LM. A heterogeneous, mixed co-culture model was first developed in which endothelial and biologically relevant PanNET cell lines (NT-3, NT-18P and NT-18LM) were co-embedded within a single hydrogel matrix, without predefined segregation. Spatial relationships in these constructs emerged through self-organisation, governed by intrinsic cellular cues, paracrine gradients, and matrix-dependent biophysical constrains, as reported in literature (Correa de Sampaio *et al*, 2012; Szot *et al*, 2013). A key advantage of this approach lies in its independence from printing parameters. Indeed, mixed co-cultures can be generated either as bioprinted constructs or as droplets through a casting-based techniques, enabling the use of biologically favourable but non-printable matrices, including fibrin- and collagen-rich hydrogels (GelMA Fibrin, PureCol), well-established to sustain endothelial maturation, activation, and sprouting (Rioja *et al*, 2016; Bayless *et al*, 2009).

Within these self-organising constructs, PanNET cell lines adopted phenotypes reflective of their biological identities clustering into “islet-like structures” (April-Monn *et al*, 2021), while endothelial cells spontaneously aligned into cord-like networks, forming primitive luminal structures. Both homotypic and heterotypic interactions were evident, highlighting the reciprocal crosstalk between tumour and endothelial compartments. This mutual adaptation positions the mixed co-culture system as a valid mechanistic platform with which to interrogate key axes of PanNET biology, including angiogenic signalling, hypoxia-induced programs, metabolic reprogramming, and (epi)genetic/transcriptional plasticity that drives disease progression (Capdevila *et al*, 2017; Cros *et al*, 2025b). These systems also provide a physiologically relevant milieu in which to evaluate therapeutic responses under complex multicellular conditions that could incorporate vascular and stromal influences.

Building on the biological insights gained from mixed systems, we next implemented compartmentalised constructs engineered for spatial precision and tissue-level architecture. Using a hybrid printing–casting strategy, required due to hydrogel rheology

and cellular compatibility constraints (Hull *et al*, 2022), we successfully designed and generated dynamic vessel-like channels surrounded by PanNET compartment.

Although both PureCol and GelMA Fibrin supported endothelial viability and activation, GelMA Fibrin was selected for the endothelial compartment due to its superior mechanical stability. Due to its progressive shrinkage over culture, PureCol would ultimately lead to its detachment from the surrounding tumour compartment ultimately compromising construct integrity over time. GelXA LAMININK 411 was chosen as PanNET-hydrogel, as it consistently promoted tumour cell viability and aggregation, and its rheological properties were compatible with extrusion bioprinting, thereby allowing the fabrication of the outer structural tumour framework of the vessel-like model.

These complex constructs reproduced hallmark vascular behaviours, including endothelial alignment in the direction of flow, lumen preservation, active sprouting, and shear-stress–induced polarisation and remodelling as reported in previous studies (van Duinen *et al*, 2019; Osaki *et al*, 2015; Galie *et al*, 2014). Tumour cells displayed heterogeneous migration toward endothelial region, cell line specific intrinsic behaviours in a 3D setting. NT-3–based models exhibited prominent endothelial finger-like projections directed toward the tumour compartment, accompanied by minimal tumour infiltration into the inner lumen. In contrast, NT-18P–based constructs demonstrated marked tumour aggregation and extensive infiltration toward the endothelial compartment, with limited endothelial extensions. NT-18LM constructs again displayed an intermediate behaviour.

Collectively, these findings indicate that the bioprinted constructs faithfully recapitulate tumour-intrinsic migratory phenotypes while providing a versatile platform for probing the interplay between tumour aggressiveness, angiogenic signalling, and invasive potential, central determinants of PanNET progression and clinical outcome (Couvelard *et al*, 2005; Lauricella *et al*, 2022; Sesti *et al*, 2023). In this context, spatially resolved analyses integrated with scaffold dissociation for genomic, epigenetic, and transcriptomic profiling could elucidate the molecular pathways underpinning endothelial-tumour co-evolution and phenotypic plasticity.

Several limitations must be acknowledged. First, each biomaterial possesses intrinsic constraints related to bioprintability, rheological behaviour, crosslinking kinetics, and the capacity to support cellular maturation (Murphy & Atala, 2014; Jung *et al*, 2022a). These factors inevitably shape construct architecture and cellular behaviour. Nonetheless, advances in hydrogel chemistry, composite bioink formulation, and multi-material printing strategies are progressively mitigating these limitations and are expected to broaden the range of matrices compatible with structured 3D culture (Ribezzi *et al*, 2025). Moreover, the bioprinted models presented here relied on established PanNET cell lines, largely because current printing protocols require elevated cell densities per constructs, levels that cannot be obtained from dissociated primary PanNET tissue. Typically, bioprinting demands cell numbers on the order of 10^6 per construct, whereas primary PanNET samples generally yield only approximately 10^5 cells following dissociation. Although cell lines do not fully recapitulate the biological heterogeneity of primary PanNETs (Benten *et al*, 2018; Viol *et al*, 2022), they remain valuable for dissecting fundamental behaviours and mechanisms in controlled 3D microenvironments, including pathway interrogation through genetically modified derivatives (i.e., KO/KD/KI). Ongoing optimisation of biomaterials and printing parameters is likely to reduce cellular requirements, thereby enabling the incorporation of primary patient-derived material. Indeed, preliminary work from our laboratory demonstrating the successful embedding of primary organoids from other neoplasms (Daniele T., Pinos R. *et al.*, *in preparation*) provides a strong foundation for transitioning toward patient-specific constructs. By strategically integrating PDTs or primary stromal and endothelial cells into mixed or compartmentalised bioprinted architectures allow the development of advanced hybrid models that balance personalized application, physiological relevance and a controlled environment, thereby further enhancing the robustness and versatility of the system.

In conclusion, 3D bioprinting represents a promising methodological advance, addressing long-standing limitations of existing models by integrating tumour and microenvironmental components within a controlled 3D framework. This approach offers a novel comprehensive platform for functional and mechanistic interrogation of PanNET biology.

Conclusions

This project was conceived to address a critical unmet clinical need: the absence of reliable biological tools to guide treatment decisions in patients with PanNENs. With this aim in mind, several projects have been carried out. To contextualise this need, we first examined a surgical cohort to determine the clinical implications of this knowledge gap. We assessed the appropriateness of current treatment strategies in light of contemporary understanding of PanNEN biology and characterised the long-term morbidity associated with pancreatic resections in a population with long-term prognosis. This analysis underscored the limitations of existing clinical decision-making frameworks and highlighted the pressing need for biologically informed predictive models.

Building on this foundation, we then focused on one of the critical reasons underlying this unmet need: the scarcity of preclinical models that faithfully recapitulate both the tumour and its microenvironment, and that can be employed to investigate disease mechanisms and support personalised therapeutic testing. In this context, we first evaluated the utility of PDTs for predicting clinical response to standard therapies across G1-G3 PanNETs. PDTs demonstrated excellent concordance with patient outcomes for cytotoxic chemotherapy but showed limited predictive capacity for targeted therapies, an expected limitation given their lack of TME components, which are essential mediators of response to non–tumour-intrinsic agents. To overcome this constraint, we established and optimised a protocol for generating PCTSs from primary PanNET tissue. This platform preserves the native architecture and cellular heterogeneity of the tumour, including stromal, vascular, and immune elements, thereby enabling drug testing within a physiologically relevant microenvironment. Differences in drug response between PDTs and PCTSs further underscored the critical role of the TME in shaping treatment response.

In parallel, we employed 3D bioprinting approach to generated preclinical models able to recapitulate the major compartments of the PanNET niche. By embedding tumour and endothelial cells within defined hydrogel matrices, we generated controllable 3D environments suited for functional interrogation of tumour–microenvironment interactions. Notably, we successfully engineered vessel-like structures surrounded by tumour compartments and demonstrated that intrinsic tumour behaviours, such as

migration and invasive capacity, were retained within these complex constructs. These results support the relevance of the bioprinted models for studying disease progression, cellular interactions, and mechanisms of tumour behaviour.

Collectively, this work provides a multi-level experimental framework that spans tumour-intrinsic biology, microenvironmental interactions, and 3D tissue engineering. Althoguh further refinement and validation are needed, these complementary models offer promsing platforms for personalized drug testing and comprehensive mechanistic studies of PanNET biology, with the ultimate aim of supporting more individualised therapeutic stratification in this heterogeneous disease.

References

Allt G & Lawrenson JG (2001) Pericytes: Cell Biology and Pathology. *Cells Tissues Organs* 169: 1–11

Al-Toubah T, Cives M & Strosberg J (2020) Novel immunotherapy strategies for treatment of neuroendocrine neoplasms. *Transl Gastroenterol Hepatol* 5 doi:10.21037/tgh.2019.12.18 [PREPRINT]

Andreasi, Partelli, Capurso, Muffatti, Balzano, Crippa & Falconi (2019) Long-Term Pancreatic Functional Impairment after Surgery for Neuroendocrine Neoplasms. *J Clin Med* 8: 1611

Andreasi V, Ricci C, Partelli S, Guarneri G, Ingaldi C, Muffatti F, Crippa S, Casadei R & Falconi M (2022) Predictors of disease recurrence after curative surgery for nonfunctioning pancreatic neuroendocrine neoplasms (NF-PanNENs): a systematic review and meta-analysis. *J Endocrinol Invest* 45: 705–718 doi:10.1007/s40618-021-01705-2 [PREPRINT]

April-Monn SL, Kirchner P, Detjen K, Bräutigam K, Trippel MA, Grob T, Statzer C, Maire RS, Kollàr A, Chouchane A, *et al* (2024) Patient derived tumoroids of high grade neuroendocrine neoplasms for more personalized therapies. *NPJ Precis Oncol* 8

April-Monn SL, Wiedmer T, Skowronska M, Maire R, Schiavo Lena M, Trippel M, Di Domenico A, Muffatti F, Andreasi V, Capurso G, *et al* (2021) Three-Dimensional Primary Cell Culture: A Novel Preclinical Model for Pancreatic Neuroendocrine Tumors. *Neuroendocrinology* 111: 273–287

Baluk P, Hashizume H & McDonald DM (2005) Cellular abnormalities of blood vessels as targets in cancer. *Curr Opin Genet Dev* 15: 102–111

Bankhead P, Loughrey MB, Fernández JA, Dombrowski Y, McArt DG, Dunne PD, McQuaid S, Gray RT, Murray LJ, Coleman HG, *et al* (2017) QuPath: Open source software for digital pathology image analysis. *Sci Rep* 7: 16878

Barozzi D, Scagnoli F, Barbaglio F, Belloni D, Ribezzi D, Farè S, Berno V, Pinos R, Sampietro M, Pauri M, *et al* (2025) Dynamic stimulation promotes functional tissue-

like organization of a 3D human lymphoid microenvironment model in vitro. *Cell Reports Methods* 5: 101105

Barozzi D & Scielzo C (2023) Emerging Strategies in 3D Culture Models for Hematological Cancers. *Hemasphere* 7: e932

de Barros NR, Gomez A, Ermis M, Falcone N, Haghniaz R, Young P, Gao Y, Aquino A-F, Li S, Niu S, *et al* (2023) Gelatin methacryloyl and Laponite bioink for 3D bioprinted organotypic tumor modeling. *Biofabrication* 15: 045005

Bassi C, Marchegiani G, Dervenis C, Sarr M, Abu Hilal M, Adham M, Allen P, Andersson R, Asbun HJ, Besselink MG, *et al* (2017) The 2016 update of the International Study Group (ISGPS) definition and grading of postoperative pancreatic fistula: 11 Years After. *Surgery (United States)* 161: 584–591 doi:10.1016/j.surg.2016.11.014 [PREPRINT]

Battistella A, Partelli S, Andreasi V, Marinoni I, Palumbo D, Tacelli M, Lena MS, Muffatti F, Mushtaq J, Capurso G, *et al* (2022) Preoperative assessment of microvessel density in nonfunctioning pancreatic neuroendocrine tumors (NF-PanNETs). *Surgery (United States)* 172: 1236–1244

Battistella A, Prato F, Andreasi V, Rella R, Guccinelli E, Crippa S, Pecorelli N, Palumbo D, Falconi M & Partelli S (2026) Preoperative predictors of new-onset diabetes mellitus following distal pancreatectomy for nonfunctioning pancreatic neuroendocrine tumors. *Surgery* 190: 109866

Bayless KJ, Kwak H-I & Su S-C (2009) Investigating endothelial invasion and sprouting behavior in three-dimensional collagen matrices. *Nat Protoc* 4: 1888–1898

Beenken A & Mohammadi M (2009) The FGF family: biology, pathophysiology and therapy. *Nat Rev Drug Discov* 8: 235–253

Benten D, Behrang Y, Unrau L, Weissmann V, Wolters-Eisfeld G, Burdak-Rothkamm S, Stahl FR, Anlauf M, Grabowski P, Möbs M, *et al* (2018) Establishment of the first well-differentiated human pancreatic neuroendocrine tumor model. *Molecular Cancer Research* 16: 496–507

Bertani E, Fazio N, Radice D, Zardini C, Grana C, Bodei L, Funicelli L, Ferrari C, Spada F, Partelli S, *et al* (2016) Resection of the Primary Tumor Followed by Peptide Receptor Radionuclide Therapy as Upfront Strategy for the Treatment of G1–G2 Pancreatic Neuroendocrine Tumors with Unresectable Liver Metastases. *Ann Surg Oncol* 23: 981–989

Beyens M, Vandamme T, Peeters M, Van Camp G & Op de Beeck K (2019) Resistance to targeted treatment of gastroenteropancreatic neuroendocrine tumors. *Endocr Relat Cancer* 26: R109–R130

Bresciani G, Hofland LJ, Dogan F, Giamas G, Gagliano T & Zatelli MC (2019) Evaluation of Spheroid 3D Culture Methods to Study a Pancreatic Neuroendocrine Neoplasm Cell Line. *Front Endocrinol (Lausanne)* 10

Briest F & Grabowski P (2014) PI3K-AKT-mTOR-Signaling and beyond: the Complex Network in Gastroenteropancreatic Neuroendocrine Neoplasms. *Theranostics* 4: 336–365

Brighi N, Lamberti G, Andrini E, Mosconi C, Manuzzi L, Donati G, Lisotti A & Campana D (2023) Prospective Evaluation of MGMT-Promoter Methylation Status and Correlations with Outcomes to Temozolomide-Based Chemotherapy in Well-Differentiated Neuroendocrine Tumors. *Current Oncology* 30: 1381–1394

Burkhart RA, Gerber SM, Tholey RM, Lamb KM, Somasundaram A, McIntyre CA, Fradkin EC, Ashok AP, Felte RF, Mehta JM, *et al* (2015) Incidence and Severity of Pancreatogenic Diabetes After Pancreatic Resection. *Journal of Gastrointestinal Surgery* 19: 217–225

Caliari SR & Burdick JA (2016) A practical guide to hydrogels for cell culture. *Nat Methods* 13: 405–414

Capdevila J, Casanovas O, Salazar R, Castellano D, Segura A, Fuster P, Aller J, García-Carbonero R, Jimenez-Fonseca P, Grande E, *et al* (2017) Translational research in neuroendocrine tumors: Pitfalls and opportunities. *Oncogene* 36: 1899–1907 doi:10.1038/onc.2016.316 [PREPRINT]

Caplin ME, Pavel M, Ćwikła JB, Phan AT, Raderer M, Sedláčková E, Cadiot G, Wolin EM, Capdevila J, Wall L, *et al* (2014) Lanreotide in Metastatic Enteropancreatic Neuroendocrine Tumors. *New England Journal of Medicine* 371: 224–233

Capodanno Y, Altieri B, Elders R, Colao A, Faggiano A & Schrader J (2022) Canine insulinoma as a model for human malignant insulinoma research: Novel perspectives for translational clinical studies. *Transl Oncol* 15: 101269

Carrasco P, Zuazo-Gaztelu I & Casanovas O (2017) Sprouting strategies and dead ends in anti-angiogenic targeting of NETs. *J Mol Endocrinol* 59: R77–R91

Cavalcanti E, Ignazzi A, De Michele F & Caruso ML (2019) PDGFRα expression as a novel therapeutic marker in well-differentiated neuroendocrine tumors. *Cancer Biol Ther* 20: 423–430

Chan JA, Geyer S, Zemla T, Knopp M V., Behr S, Pulsipher S, Ou F-S, Dueck AC, Acoba J, Shergill A, *et al* (2025) Phase 3 Trial of Cabozantinib to Treat Advanced Neuroendocrine Tumors. *New England Journal of Medicine* 392: 653–665

Chen M, Shan H, Tao Q, Hu R, Sun Q, Zheng M, Chen Z, Lin Q, Yin M, Zhao S, *et al* (2024) Mimicking Tumor Metastasis Using a Transwell-Integrated Organoids-On-a-Chip Platform. *Small* 20

Chen MB, Whisler JA, Fröse J, Yu C, Shin Y & Kamm RD (2017) On-chip human microvasculature assay for visualization and quantification of tumor cell extravasation dynamics. *Nat Protoc* 12: 865–880

Chen Z, Shi N, Xing C, Zou Y, Zhang Y, Chen Z, Wu F, Jin H, Chen R & Dai M (2023) A novel clinical model for risk prediction and stratification of new-onset diabetes mellitus after distal pancreatectomy. *Hepatobiliary Surg Nutr* 12: 868–881

Cives M, Pelle E, Quaresmini D, Rizzo FM, Tucci M & Silvestris F (2019) The Tumor Microenvironment in Neuroendocrine Tumors: Biology and Therapeutic Implications. *Neuroendocrinology* 109: 83–99 doi:10.1159/000497355 [PREPRINT]

Cives M, Pelle E & Strosberg J (2020) Emerging treatment options for gastroenteropancreatic neuroendocrine tumors. *J Clin Med* 9 doi:10.3390/jcm9113655 [PREPRINT]

Coelho S, Costa C, Santos AP, Souteiro P, Oliveira J, Oliveira J, Azevedo I, Torres I & Bento MJ (2022) Pancreatic neuroendocrine neoplasms: survival trend analysis of a comprehensive center. *Endocrine Oncology* 2: 32–41

Collins AL, Kirkness K, Ramon-Gil E, Tzortzopoulou E, Geh D, Dishington J, Graham E, Muir R, Cameron R, Luli S, *et al* (2025) Precision-cut tumor slices for modeling hepatocellular carcinoma enable at-scale drug screening. *Hepatol Commun* 9

Correa de Sampaio P, Auslaender D, Krubasik D, Failla AV, Skepper JN, Murphy G & English WR (2012) A Heterogeneous In Vitro Three Dimensional Model of Tumour-Stroma Interactions Regulating Sprouting Angiogenesis. *PLoS One* 7: e30753

Couvelard A, Deschamps L, Rebours V, Sauvanet A, Gatter K, Pezzella F, Ruszniewski P & Bedossa P (2008) Overexpression of the oxygen sensors PHD-1, PHD-2, PHD-3, and FIH is associated with tumor aggressiveness in pancreatic endocrine tumors. *Clinical Cancer Research* 14: 6634–6639

Couvelard A, O'Toole D, Turley H, Leek R, Sauvanet A, Degott C, Ruszniewski P, Belghiti J, Harris A, Gatter K, *et al* (2005) Microvascular density and hypoxia-inducible factor pathway in pancreatic endocrine tumours: negative correlation of microvascular density and VEGF expression with tumour progression. *Br J Cancer* 92: 94–101

Cros J, Bucau M, Tihy M, Palazzo M, Bourgoin P, Chassac A, Albuquerque M, Sauvanet A, Dokmak S, Dioguardi Burgio M, *et al* (2025a) Predictive value of metabolic state on PanNET response to mTOR inhibitors. *Endocr Relat Cancer* 32

Cros J, Casanovas O, Castaño JP, Dayton T, Alvarez AG, Gibert B, Simbolo M, Vandamme T, Cives M & Marinoni I (2025b) White paper on best practices for translational research in neuroendocrine neoplasms. *J Neuroendocrinol* 37

Dai M, Xing C, Shi N, Wang S, Wu G, Liao Q, Zhang T, Chen G, Wu W, Guo J, *et al* (2020) Risk factors for new-onset diabetes mellitus after distal pancreatectomy. *BMJ Open Diabetes Res Care* 8

D'Amico F, Dormio S, Veronesi G, Guarracino F, Donadello K, Cinnella G, Rosati R, Pecorelli N, Baldini G, Pieri M, *et al* (2025) Home-based prehabilitation: a systematic review and meta-analysis of randomised trials. *Br J Anaesth* 134: 1018–1028

Dasari A, Shen C, Halperin D, Zhao B, Zhou S, Xu Y, Shih T & Yao JC (2017) Trends in the incidence, prevalence, and survival outcomes in patients with neuroendocrine tumors in the United States. *JAMA Oncol* 3: 1335–1342

Dasari A, Wallace K, Halperin DM, Maxwell J, Kunz P, Singh S, Chasen B & Yao JC (2025) Epidemiology of Neuroendocrine Neoplasms in the US. *JAMA Netw Open* 8: e2515798

Dayton TL, Alcala N, Moonen L, den Hartigh L, Geurts V, Mangiante L, Lap L, Dost AFM, Beumer J, Levy S, *et al* (2023) Druggable growth dependencies and tumor evolution analysis in patient-derived organoids of neuroendocrine neoplasms from multiple body sites. *Cancer Cell* 41: 2083-2099.e9

Detjen K, Hammerich L, Özdirik B, Demir M, Wiedenmann B, Tacke F, Jann H & Roderburg C (2021) Models of Gastroenteropancreatic Neuroendocrine Neoplasms: Current Status and Future Directions. *Neuroendocrinology* 111: 217–236

Detjen KM, Rieke S, Deters A, Schulz P, Rexin A, Vollmer S, Hauff P, Wiedenmann B, Pavel M & Scholz A (2010) Angiopoietin-2 promotes disease progression of neuroendocrine tumors. *Clinical Cancer Research* 16: 420–429

Dindo D, Demartines N & Clavien PA (2004) Classification of surgical complications: A new proposal with evaluation in a cohort of 6336 patients and results of a survey. *Ann Surg* 240: 205–213 doi:10.1097/01.sla.0000133083.54934.ae [PREPRINT]

Di Domenico A, Pipinikas CP, Maire RS, Bräutigam K, Simillion C, Dettmer MS, Vassella E, Thirlwell C, Perren A & Marinoni I (2020) Epigenetic landscape of

pancreatic neuroendocrine tumours reveals distinct cells of origin and means of tumour progression. *Commun Biol* 3

Dong D-H, Zhang X-F, Lopez-Aguiar AG, Poultsides G, Makris E, Rocha F, Kanji Z, Weber S, Fisher A, Fields R, *et al* (2020) Resection of pancreatic neuroendocrine tumors: defining patterns and time course of recurrence. *HPB* 22: 215–223

Doornebal EJ, Harris N, Riva A, Jagatia R, Pizanias M, Prachalias A, Menon K, Preziosi M, Zamalloa A, Miquel R, *et al* (2022) Human Immunocompetent Model of Neuroendocrine Liver Metastases Recapitulates Patient-Specific Tumour Microenvironment. *Front Endocrinol (Lausanne)* 13

van Duinen V, Zhu D, Ramakers C, van Zonneveld AJ, Vulto P & Hankemeier T (2019) Perfused 3D angiogenic sprouting in a high-throughput in vitro platform. *Angiogenesis* 22: 157–165

Dumortier J, Ratineau C, Roche C, Lombard-Bohas C, Chayvialle J-A & Scoazec J-Y (1999) Angiogenesis and endocrine tumors. *Bull Cancer*: 148–153

Dumortier J, Ratineau C, Scoazec J-Y, Pourreyron C, Anderson W, Jacquier M-F, Blanc M, Bernard C, Bellaton C, Remy L, *et al* (2000) Site-Specific Epithelial-Mesenchymal Interactions in Digestive Neuroendocrine Tumors. *Am J Pathol* 156: 671–683

Durymanov M (2025) Tumor Spheroids, Tumor Organoids, Tumor Explants, and Tumoroids: What Are the Differences between Them? *Biochemistry (Moscow)* 90: 200–213

Ear PH, Marinoni I, Dayton T, Guenter R, Quelle DE, Battistella A, Buishand FO, Chittaranjan S, Nancy Du Y-C, Marques I, *et al* (2024) NET Models Meeting 2024 white paper: the current state of neuroendocrine tumour research models and our future aspirations. *Endocrine Oncology* 4

Eisenhauer EA, Therasse P, Bogaerts J, Schwartz LH, Sargent D, Ford R, Dancey J, Arbuck S, Gwyther S, Mooney M, *et al* (2009) New response evaluation criteria in solid tumours: Revised RECIST guideline (version 1.1). *Eur J Cancer* 45: 228–247

von Elm E, Altman DG, Egger M, Pocock SJ, Gøtzsche PC & Vandenbroucke JP (2014) The strengthening the reporting of observational studies in epidemiology (STROBE) statement: Guidelines for reporting observational studies. *International Journal of Surgery* 12: 1495–1499

Falconi M, Eriksson B, Kaltsas G, Bartsch DK, Capdevila J, Caplin M, Kos-Kudla B, Kwekkeboom D, Rindi G, KlÖppel G, *et al* (2016) ENETS consensus guidelines update for the management of patients with functional pancreatic neuroendocrine tumors and non-functional pancreatic neuroendocrine tumors. In *Neuroendocrinology* pp 153–171. S. Karger AG

Falconi M, Mantovani W, Crippa S, Mascetta G, Salvia R & Pederzoli P (2008) Pancreatic insufficiency after different resections for benign tumours. *Br J Surg* 95: 85–91

Fang JM & Shi J (2019) A clinicopathologic and molecular update of pancreatic neuroendocrine neoplasms with a focus on the New World Health Organization classification. *Arch Pathol Lab Med* 143: 1317–1326

Fazio N, Kulke M, Rosbrook B, Fernandez K & Raymond E (2021) Updated Efficacy and Safety Outcomes for Patients with Well-Differentiated Pancreatic Neuroendocrine Tumors Treated with Sunitinib. *Target Oncol* 16: 27–35

Figueroa-Vega N, Díaz Á, Adrados M, Álvarez-Escolá C, Paniagua A, Aragonés J, Martín-Pérez E, Leskela S, Moreno-Otero R, González-Amaro R, *et al* (2010) The association of the angiopoietin/Tie-2 system with the development of metastasis and leukocyte migration in neuroendocrine tumors. *Endocr Relat Cancer* 17: 897–908

Frilling A, Li J, Malamutmann E, Schmid K-W, Bockisch A & Broelsch CE (2009) Treatment of liver metastases from neuroendocrine tumours in relation to the extent of hepatic disease. *British Journal of Surgery* 96: 175–184

Fujino M, Aishima S, Shindo K, Oda Y, Morimatsu K, Tsutsumi K, Otsuka T, Tanaka M & Oda Y (2016) Expression of glucose transporter-1 is correlated with hypoxia-inducible factor 1α and malignant potential in pancreatic neuroendocrine tumors. *Oncol Lett* 12: 3337–3343

Galie PA, Nguyen D-HT, Choi CK, Cohen DM, Janmey PA & Chen CS (2014) Fluid shear stress threshold regulates angiogenic sprouting. *Proceedings of the National Academy of Sciences* 111: 7968–7973

Gallo M, Ruggeri RM, Muscogiuri G, Pizza G, Faggiano A & Colao A (2018) Diabetes and pancreatic neuroendocrine tumours: Which interplays, if any? *Cancer Treat Rev* 67: 1–9

Garcia-Carbonero R, Sorbye H, Baudin E, Raymond E, Wiedenmann B, Niederle B, Sedlackova E, Toumpanakis C, Anlauf M, Cwikla JB, *et al* (2016) ENETS consensus guidelines for high-grade gastroenteropancreatic neuroendocrine tumors and neuroendocrine carcinomas. In *Neuroendocrinology* pp 186–194. S. Karger AG

Gaudenzi G, Carra S, Dicitore A, Cantone MC, Persani L & Vitale G (2020) Fishing for neuroendocrine tumors. *Endocr Relat Cancer* 27: R163–R176 doi:10.1530/ERC-19-0437 [PREPRINT]

Gaujoux S, Partelli S, Maire F, D'Onofrio M, Larroque B, Tamburrino D, Sauvanet A, Falconi M & Ruszniewski P (2013) Observational Study of Natural History of Small Sporadic Nonfunctioning Pancreatic Neuroendocrine Tumors. *J Clin Endocrinol Metab* 98: 4784–4789

Genç CG, Jilesen AP, Partelli S, Falconi M, Muffatti F, van Kemenade FJ, van Eeden S, Verheij J, van Dieren S, van Eijck CHJ, *et al* (2018) A New Scoring System to Predict Recurrent Disease in Grade 1 and 2 Nonfunctional Pancreatic Neuroendocrine Tumors. *Ann Surg* 267: 1148–1154

Guilmette JM & Nosé V (2019) Neoplasms of the Neuroendocrine Pancreas: An Update in the Classification, Definition, and Molecular Genetic Advances. *Adv Anat Pathol*: 13–30

Gulde S, Foscarini A, April-Monn SL, Genio E, Marangelo A, Satam S, Helbling D, Falconi M, Toledo RA, Schrader J, *et al* (2022) Combined Targeting of Pathogenetic Mechanisms in Pancreatic Neuroendocrine Tumors Elicits Synergistic Antitumor Effects. *Cancers (Basel)* 14: 5481

Guruswamy Damodaran R & Vermette P (2018) Decellularized pancreas as a native extracellular matrix scaffold for pancreatic islet seeding and culture. *J Tissue Eng Regen Med* 12: 1230–1237

Hafner M, Niepel M, Chung M & Sorger PK (2016) Growth rate inhibition metrics correct for confounders in measuring sensitivity to cancer drugs. *Nat Methods* 13: 521–527

Halfdanarson TR, Rubin J, Farnell MB, Grant CS & Petersen GM (2008) Pancreatic endocrine neoplasms: Epidemiology and prognosis of pancreatic endocrine tumors. *Endocr Relat Cancer* 15: 409–427

Halloran CM, Cox TF, Chauhan S, Raraty MGT, Sutton R, Neoptolemos JP & Ghaneh P (2011) Partial Pancreatic Resection for Pancreatic Malignancy Is Associated with Sustained Pancreatic Exocrine Failure and Reduced Quality of Life: A Prospective Study. *Pancreatology* 11: 535–545

Hanahan D (1985) Heritable formation of pancreatic beta-cell tumours in transgenic mice expressing recombinant insulin/simian virus 40 oncogenes. *Nature* 315: 115–122

Harris AL (2002) Hypoxia — a key regulatory factor in tumour growth. *Nat Rev Cancer* 2: 38–47

Herring B, Jang S, Whitt J, Goliwas K, Aburjania Z, Dudeja V, Ren B, Berry J, Bibb J, Frost A, *et al* (2021) Ex Vivo Modeling of Human Neuroendocrine Tumors in Tissue Surrogates. *Front Endocrinol (Lausanne)* 12

van Hilst J, de Rooij T, Bosscha K, Brinkman DJ, van Dieren S, Dijkgraaf MG, Gerhards MF, de Hingh IH, Karsten TM, Lips DJ, *et al* (2019) Laparoscopic versus open pancreatoduodenectomy for pancreatic or periampullary tumours (LEOPARD-2): a multicentre, patient-blinded, randomised controlled phase 2/3 trial. *Lancet Gastroenterol Hepatol* 4: 199–207

Huang D, Ding Y, Li Y, Luo W-M, Zhang Z-F, Snider J, VandenBeldt K, Qian C-N & Teh BT (2010) Sunitinib Acts Primarily on Tumor Endothelium rather than Tumor Cells to Inhibit the Growth of Renal Cell Carcinoma. *Cancer Res* 70: 1053–1062

Hull SM, Brunel LG & Heilshorn SC (2022) 3D Bioprinting of Cell-Laden Hydrogels for Improved Biological Functionality. *Advanced Materials* 34

Imamura S, Niwano F, Babaya N, Hiromine Y, Matsumoto I, Kamei K, Yoshida Y, Taketomo Y, Yoshida S, Takeyama Y, *et al* (2024) High Incidence of Diabetes Mellitus After Distal Pancreatectomy and Its Predictors: A Long-term Follow-up Study. *Journal of Clinical Endocrinology and Metabolism* 109: 619–630

Ireson CR, Alavijeh MS, Palmer AM, Fowler ER & Jones HJ (2019) The role of mouse tumour models in the discovery and development of anticancer drugs. *Br J Cancer* 121: 101–108

Izumo W, Higuchi R, Furukawa T, Shiihara M, Uemura S, Yazawa T, Yamamoto M & Honda G (2024) The importance of microvascular invasion in patients with non-functioning pancreatic neuroendocrine neoplasm. *Langenbecks Arch Surg* 410: 8

Izumo W, Higuchi R, Yazawa T, Uemura S, Shiihara M & Yamamoto M (2020) Evaluation of allowable pancreatic resection rate depending on preoperative risk factors for new-onset diabetes mellitus after distal pancreatectomy. *Pancreatology* 20: 1526–1533

Jensen C & Teng Y (2020) Is It Time to Start Transitioning From 2D to 3D Cell Culture? *Front Mol Biosci* 7

Ji S, Cao L, Gao J, Du Y, Ye Z, Lou X, Liu F, Zhang Y, Xu J, Shi X, *et al* (2025) Proteogenomic characterization of non-functional pancreatic neuroendocrine tumors unravels clinically relevant subgroups. *Cancer Cell* 43: 776-796.e14

Jung M, Ghamrawi S, Du EY, Gooding JJ & Kavallaris M (2022a) Advances in 3D Bioprinting for Cancer Biology and Precision Medicine: From Matrix Design to Application. *Adv Healthc Mater* 11

Jung M, Ghamrawi S, Du EY, Gooding JJ & Kavallaris M (2022b) Advances in 3D Bioprinting for Cancer Biology and Precision Medicine: From Matrix Design to Application. *Adv Healthc Mater* 11

Kaemmer CA, Umesalma S, Maharjan CK, Moose DL, Narla G, Mott SL, Zamba GKD, Breheny P, Darbro BW, Bellizzi AM, *et al* (2021) Development and comparison of

novel bioluminescent mouse models of pancreatic neuroendocrine neoplasm metastasis. *Sci Rep* 11

Kaku M, Nishiyama T, Yagawa K & Abe M (1980) Establishment of a carcinoembryonic antigen-producing cell line from human pancreatic carcinoma. *Gan* 71: 596–601

Katz SC, Donkor C, Glasgow K, Pillarisetty VG, Gönen M, Espat NJ, Klimstra DS, D'Angelica MI, Allen PJ, Jarnagin W, *et al* (2010) T cell infiltrate and outcome following resection of intermediate-grade primary neuroendocrine tumours and liver metastases. *HPB* 12: 674–683

Khanna L, Prasad SR, Sunnapwar A, Kondapaneni S, Dasyam A, Tammisetti VS, Salman U, Nazarullah A & Katabathina VS (2020) Pancreatic neuroendocrine neo-plasms: 2020 update on pathologic and imaging findings and classification. *Radiographics* 40: 1240–1262

Kim DW, Kim HJ, Kim KW, Byun JH, Song KB, Kim JH & Hong SM (2015) Neuroendocrine neoplasms of the pancreas at dynamic enhanced CT: comparison between grade 3 neuroendocrine carcinoma and grade 1/2 neuroendocrine tumour. *Eur Radiol* 25: 1375–1383

Kim JY, Lee SH, An S, Kim SJ, Sung YN, Song KB, Hwang DW, Kim SC & Hong SM (2018) Carbonic anhydrase 9 expression in well-differentiated pancreatic neuroendocrine neoplasms might be associated with aggressive behavior and poor survival. *Virchows Archiv* 472: 739–748

Klimstra DS, Modlin IR, Coppola D, Lloyd R V & Suster S (2010) The Pathologic Classification of Neuroendocrine Tumors A Review of Nomenclature, Grading, and Staging Systems

Kos-Kudła B, Castaño JP, Denecke T, Grande E, Kjaer A, Koumarianou A, de Mestier L, Partelli S, Perren A, Stättner S, *et al* (2023) European Neuroendocrine Tumour Society (ENETS) 2023 guidance paper for nonfunctioning pancreatic neuroendocrine tumours. *J Neuroendocrinol* 35

Kos-Kudła B, Castaño JP, Denecke T, Grande E, Kjaer A, Koumarianou A, de Mestier L, Partelli S, Perren A, Stättner S, *et al* (2023) European Neuroendocrine Tumour

Society (<scp>ENETS</scp>) 2023 guidance paper for nonfunctioning pancreatic neuroendocrine tumours. *J Neuroendocrinol* 35

Kunz PL, Graham NT, Catalano PJ, Nimeiri HS, Fisher GA, Longacre TA, Suarez CJ, Martin BA, Yao JC, Kulke MH, *et al* (2023) Randomized Study of Temozolomide or Temozolomide and Capecitabine in Patients With Advanced Pancreatic Neuroendocrine Tumors (ECOG-ACRIN E2211). *Journal of Clinical Oncology* 41: 1359–1369

Lakis V, Lawlor RT, Newell F, Patch A-M, Mafficini A, Sadanandam A, Koufariotis LT, Johnston RL, Leonard C, Wood S, *et al* (2021) DNA methylation patterns identify subgroups of pancreatic neuroendocrine tumors with clinical association. *Commun Biol* 4: 155

Lauricella E, Mandriani B, Cavallo F, Pezzicoli G, Chaoul N, Porta C & Cives M (2022) Angiogenesis in NENs, with a focus on gastroenteropancreatic NENs: from biology to current and future therapeutic implications. *Front Oncol* 12 doi:10.3389/fonc.2022.957068 [PREPRINT]

Lee E, O'Keefe S, Leong A, Park H-R, Varadarajan J, Chowdhury S, Hiner S, Kim S, Shiva A, Friedman RA, *et al* (2023) Angiopoietin-2 blockade suppresses growth of liver metastases from pancreatic neuroendocrine tumors by promoting T cell recruitment. *Journal of Clinical Investigation* 133

Li Y, Fan Z, Zhang F, Yang J, Shi M, Liu S, Meng Y & Zhan H (2022) Neoadjuvant therapy in pancreatic neuroendocrine neoplasms: A systematic review and meta-analysis. *Front Oncol* 12 doi:10.3389/fonc.2022.981575 [PREPRINT]

Liu L & Gerson SL (2006) Targeted Modulation of MGMT: Clinical Implications. *Clinical Cancer Research* 12: 328–331

Lloyd R, Osamura R, Klopper G & Rosai J (2017) WHO Classification of Tumours of Endocrine Organs, 4th ed. IARC, Lyon.

Lou X, Shi Y, Zhao F, Xu X, Wang Y, Qin Y, Zhang W, Ye Z, Wang F, Ding T, *et al* (2025) Pancreatic Neuroendocrine Tumors Secrete Apolipoprotein E to Induce Tip

Endothelial Cells That Remodel the Tumor–Stroma Ratio and Promote Cancer Progression. *Cancer Res* 85: 2805–2819

De Luca R, Gianotti L, Pedrazzoli P, Brunetti O, Rizzo A, Sandini M, Paiella S, Pecorelli N, Pugliese L, Pietrabissa A, *et al* (2023) Immunonutrition and prehabilitation in pancreatic cancer surgery: A new concept in the era of ERAS® and neoadjuvant treatment. *European Journal of Surgical Oncology* 49: 542–549

Macheda ML, Rogers S & Best JD (2005) Molecular and cellular regulation of glucose transporter (GLUT) proteins in cancer. *J Cell Physiol* 202: 654–662

Madeira I, Terris B, Voss M, Denys A, Sauvanet A, Flejou J-F, Vilgrain V, Belghiti J, Bernades P & Ruszniewski P (1998) Prognostic factors in patients with endocrine tumours of the duodenopancreatic area. *Gut* 43: 422–427

Maharjan C, Ear P, Tran C, Howe J, Chandrasekharan C & Quelle D (2021) Pancreatic Neuroendocrine Tumors: Molecular Mechanisms and Therapeutic Targets. *Cancers (Basel)* 13: 5117

Mandriani B, Pellè E, Mannavola F, Palazzo A, Marsano RM, Ingravallo G, Cazzato G, Ramello MC, Porta C, Strosberg J, *et al* (2022) Development of anti-somatostatin receptors CAR T cells for treatment of neuroendocrine tumors. *J Immunother Cancer* 10

Marinoni I, Kurrer AS, Vassella E, Dettmer M, Rudolph T, Banz V, Hunger F, Pasquinelli S, Speel EJ & Perren A (2014) Loss of DAXX and ATRX are associated with chromosome instability and reduced survival of patients with pancreatic neuroendocrine tumors. *Gastroenterology* 146

Marion–Audibert A, Barel C, Gouysse G, Dumortier J, Pilleul F, Pourreyron C, Hervieu V, Poncet G, Lombard–Bohas C, Chayvialle J, *et al* (2003) Low Microvessel Density Is an Unfavorable Histoprognostic Factor in Pancreatic Endocrine Tumors. *Gastroenterology* 125: 1094–1104

Mcdonald PC, Winum J-Y, Supuran CT & Dedhar S (2012) Recent Developments in Targeting Carbonic Anhydrase IX for Cancer Therapeutics

Medici B, Caffari E, Maculan Y, Benatti S, Piacentini F, Dominici M & Gelsomino F (2025) Everolimus in the Treatment of Neuroendocrine Tumors: Lights and Shadows. *Biomedicines* 13: 455

De Mestier L, Védie AL, Faron M, Cros J, Rebours V, Hentic O, Do Cao C, Bardet P, Lévy P, Sauvanet A, *et al* (2020) The Postoperative Occurrence or Worsening of Diabetes Mellitus May Increase the Risk of Recurrence in Resected Pancreatic Neuroendocrine Tumors. *Neuroendocrinology* 110: 967–976

Morgan RE, Pommier SJ & Pommier RF (2018) Expanded criteria for debulking of liver metastasis also apply to pancreatic neuroendocrine tumors. *Surgery* 163: 218–225

Mosalem OM, Starr JS, Bassam SM, Hobday T, Alberts S, Eiring R, McGarrah P & Halfdanarson TR (2025) Temozolomide induced hypermutation in pancreatic neuroendocrine tumors: a case series. *Endocrine Abstracts*

Moser E, Ura A, Vogel L, Steiger K, Mogler C, Evert M, Märkl B, Scheidhauer K, Martignoni M, Friess H, *et al* (2024) ARX, PDX1, ISL1, and CDX2 Expression Distinguishes 5 Subgroups of Pancreatic Neuroendocrine Tumors With Correlations to Histology, Hormone Expression, and Outcome. *Modern Pathology* 37

Mossmann D, Park S & Hall MN (2018) mTOR signalling and cellular metabolism are mutual determinants in cancer. *Nat Rev Cancer* 18: 744–757

Motz GT & Coukos G (2011) The parallel lives of angiogenesis and immunosuppression: cancer and other tales. *Nat Rev Immunol* 11: 702–711

Motz GT & Coukos G (2013) Deciphering and Reversing Tumor Immune Suppression. *Immunity* 39: 61–73

Murphy S V & Atala A (2014) 3D bioprinting of tissues and organs. *Nat Biotechnol* 32: 773–785

Neufeld L, Yeini E, Pozzi S & Satchi-Fainaro R (2022) 3D bioprinted cancer models: from basic biology to drug development. *Nat Rev Cancer* 22: 679–692

Nyga A, Cheema U & Loizidou M (2011) 3D tumour models: novel in vitro approaches to cancer studies. *J Cell Commun Signal* 5: 239–248

Öberg K (1994) Biology, diagnosis, and treatment of neuroendocrine tumors of the gastrointestinal tract. *Curr Opin Oncol* 6: 441–51

Osaki T, Kakegawa T, Kageyama T, Enomoto J, Nittami T & Fukuda J (2015) Acceleration of Vascular Sprouting from Fabricated Perfusable Vascular-Like Structures. *PLoS One* 10: e0123735

De Palma M, Biziato D & Petrova T V. (2017) Microenvironmental regulation of tumour angiogenesis. *Nat Rev Cancer* 17: 457–474 doi:10.1038/nrc.2017.51 [PREPRINT]

De Palma M, Venneri MA, Galli R, Sergi LS, Politi LS, Sampaolesi M & Naldini L (2005) Tie2 identifies a hematopoietic lineage of proangiogenic monocytes required for tumor vessel formation and a mesenchymal population of pericyte progenitors. *Cancer Cell* 8: 211–226

Panzuto F, Andrini E, Lamberti G, Pusceddu S, Rinzivillo M, Gelsomino F, Raimondi A, Bongiovanni A, Davì MV, Cives M, *et al* (2024) Sequencing Treatments in Patients with Advanced Well-Differentiated Pancreatic Neuroendocrine Tumor (pNET): Results from a Large Multicenter Italian Cohort. *J Clin Med* 13

Partelli S, Bartsch DK, Capdevila J, Chen J, Knigge U, Niederle B, Nieveen van Dijkum EJM, Pape U-F, Pascher A, Ramage J, *et al* (2017) ENETS Consensus Guidelines for the Standards of Care in Neuroendocrine Tumours: Surgery for Small Intestinal and Pancreatic Neuroendocrine Tumours. *Neuroendocrinology* 105: 255–265

Partelli S, Battistella A, Andreasi V, Muffatti F, Tamburrino D, Pecorelli N, Crippa S, Balzano G & Falconi M (2024a) Critical appraisal of the adequacy of surgical indications for non-functioning pancreatic neuroendocrine tumours. *BJS Open* 8

Partelli S, Bertani E, Bartolomei M, Perali C, Muffatti F, Grana CM, Schiavo Lena M, Doglioni C, Crippa S, Fazio N, *et al* (2018a) Peptide receptor radionuclide therapy as neoadjuvant therapy for resectable or potentially resectable pancreatic neuroendocrine neoplasms. *Surgery (United States)* 163: 761–767

Partelli S, Cirocchi R, Crippa S, Cardinali L, Fendrich V, Bartsch DK & Falconi M (2016) Systematic review of active surveillance *versus* surgical management of

asymptomatic small non-functioning pancreatic neuroendocrine neoplasms. *British Journal of Surgery* 104: 34–41

Partelli S, Guarneri G, Rancoita PM, De Martino I, Provinciali L, De Mestier L, Dokmak S, Hallet J, Sauvanet A & Falconi M (2025) Defining Biological Borderline Resectable Non-Functioning Pancreatic Neuroendocrine Tumors (NF-PanNETs). *Ann Surg*

Partelli S, Javed AA, Andreasi V, He J, Muffatti F, Weiss MJ, Sessa F, la Rosa S, Doglioni C, Zamboni G, *et al* (2018b) The number of positive nodes accurately predicts recurrence after pancreaticoduodenectomy for nonfunctioning neuroendocrine neoplasms. *European Journal of Surgical Oncology* 44: 778–783

Partelli S, Landoni L, Bartolomei M, Zerbi A, Grana CM, Boggi U, Butturini G, Casadei R, Salvia R & Falconi M (2024b) Neoadjuvant 177Lu-DOTATATE for non-functioning pancreatic neuroendocrine tumours (NEOLUPANET): multicentre phase II study. *British Journal of Surgery* 111

Patel N, Barbieri A & Gibson J (2019) Neuroendocrine Tumors of the Gastrointestinal Tract and Pancreas. *Surg Pathol Clin* 12: 1021–1044

Pavel M, Öberg K, Falconi M, Krenning EP, Sundin A, Perren A & Berruti A (2020) Gastroenteropancreatic neuroendocrine neoplasms: ESMO Clinical Practice Guidelines for diagnosis, treatment and follow-up. *Annals of Oncology* 31: 844–860

Pecorelli N, Carrara G, De Cobelli F, Cristel G, Damascelli A, Balzano G, Beretta L & Braga M (2016) Effect of sarcopenia and visceral obesity on mortality and pancreatic fistula following pancreatic cancer surgery. *British Journal of Surgery* 103: 434–442

Pecorelli N, Palumbo D, Guarneri G, Gritti C, Prato F, Schiavo Lena M, Vallorani A, Partelli S, Crippa S, Doglioni C, *et al* (2023) Preoperative CT image analysis to improve risk stratification for clinically relevant pancreatic fistula after distal pancreatectomy. *British Journal of Surgery* 110: 891–895

Peloso A, Citro A, Zoro T, Cobianchi L, Kahler-Quesada A, Bianchi CM, Andres A, Berishvili E, Piemonti L, Berney T, *et al* (2018) Regenerative Medicine and

Diabetes: Targeting the Extracellular Matrix Beyond the Stem Cell Approach and Encapsulation Technology. *Front Endocrinol (Lausanne)* 9

Phillips JB & Westerfield M (2014) Zebrafish models in translational research: tipping the scales toward advancements in human health. *Dis Model Mech* 7: 739–743

Phillips ME (2015) Pancreatic exocrine insufficiency following pancreatic resection. *Pancreatology* 15: 449–455

Pulvirenti A, Javed AA, Michelakos T, Sekigami Y, Zheng J, Kalvin MSPH HL, McIntyre CA, Nebbia M, Chou MS JF, Gonen M, *et al* (2023) Recurring Pancreatic Neuroendocrine Tumor: timing and pattern of recurrence, and current treatment.

Pyonteck SM, Gadea BB, Wang H-W, Gocheva V, Hunter KE, Tang LH & Joyce JA (2012) Deficiency of the macrophage growth factor CSF-1 disrupts pancreatic neuroendocrine tumor development. *Oncogene* 31: 1459–1467

Quintard C, Tubbs E, Jonsson G, Jiao J, Wang J, Werschler N, Laporte C, Pitaval A, Bah T-S, Pomeranz G, *et al* (2024) A microfluidic platform integrating functional vascularized organoids-on-chip. *Nat Commun* 15: 1452

Raymond E, Dahan L, Raoul J-L, Bang Y-J, Borbath I, Lombard-Bohas C, Valle J, Metrakos P, Smith D, Vinik A, *et al* (2011a) Sunitinib Malate for the Treatment of Pancreatic Neuroendocrine Tumors. *n engl j med* 364: 501–514

Raymond E, Dahan L, Raoul J-L, Bang Y-J, Borbath I, Lombard-Bohas C, Valle J, Metrakos P, Smith D, Vinik A, *et al* (2011b) Sunitinib Malate for the Treatment of Pancreatic Neuroendocrine Tumors. *New England Journal of Medicine* 364: 501–513

Raymond E, Kulke MH, Qin S, Yu X, Schenker M, Cubillo A, Lou W, Tomasek J, Thiis-Evensen E, Xu J-M, *et al* (2018) Efficacy and Safety of Sunitinib in Patients with Well-Differentiated Pancreatic Neuroendocrine Tumours. *Neuroendocrinology* 107: 237–245

de Reuver PR, Mehta S, Gill P, Andrici J, D'Urso L, Clarkson A, Mittal A, Hugh TJ, Samra JS & Gill AJ (2016) Immunoregulatory Forkhead Box Protein p3-Positive

Lymphocytes Are Associated with Overall Survival in Patients with Pancreatic Neuroendocrine Tumors. *J Am Coll Surg* 222: 281–287

Ribezzi D, Català P, Pignatelli C, Citro A & Levato R (2025) Bioprinting and synthetic biology approaches to engineer functional endocrine pancreatic constructs. *Trends Biotechnol* doi:10.1016/j.tibtech.2025.03.005 [PREPRINT]

Ribezzi D, Gueye M, Florczak S, Dusi F, de Vos D, Manente F, Hierholzer A, Fussenegger M, Caiazzo M, Blunk T, *et al* (2023) Shaping Synthetic Multicellular and Complex Multimaterial Tissues via Embedded Extrusion-Volumetric Printing of Microgels. *Advanced Materials* 35

Ricci C, Partelli S, Landoni L, Rinzivillo M, Ingaldi C, Andreasi V, Savegnago G, Muffatti F, Fontana M, Tamburrino D, *et al* (2022) Survival after active surveillance *versus* upfront surgery for incidental small pancreatic neuroendocrine tumours. *British Journal of Surgery*

Rindi G, D'Adda T, Froio E, Fellegara G & Bordi C (2007) Prognostic factors in gastrointestinal endocrine tumors. *Endocr Pathol* 18: 145–149

Rindi G, Klöppel G, Alhman H, Caplin M, Couvelard A, De Herder WW, Erikssson B, Falchetti A, Falconi M, Komminoth P, *et al* (2006) TNM staging of foregut (neuro)endocrine tumors: A consensus proposal including a grading system. *Virchows Archiv* 449: 395–401

Rindi G, Mete O, Uccella S, Basturk O, La Rosa S, Brosens LAA, Ezzat S, de Herder WW, Klimstra DS, Papotti M, *et al* (2022) Overview of the 2022 WHO Classification of Neuroendocrine Neoplasms. *Endocr Pathol* 33: 115–154 doi:10.1007/s12022-022-09708-2 [PREPRINT]

Rinke A, Auernhammer CJ, Bodei L, Kidd M, Krug S, Lawlor R, Marinoni I, Perren A, Scarpa A, Sorbye H, *et al* (2021) Treatment of advanced gastroenteropancreatic neuroendocrine neoplasia, are we on the way to personalised medicine? *Gut* 70: 1768–1781

Rinke A & Krug S (2016) Neuroendocrine tumours – Medical therapy: Biological. *Best Pract Res Clin Endocrinol Metab* 30: 79–91

Rinke A, Wittenberg M, Schade-Brittinger C, Aminossadati B, Ronicke E, Gress TM, Müller H-H & Arnold R (2017) Placebo-Controlled, Double-Blind, Prospective, Randomized Study on the Effect of Octreotide LAR in the Control of Tumor Growth in Patients with Metastatic Neuroendocrine Midgut Tumors (PROMID): Results of Long-Term Survival. *Neuroendocrinology* 104: 26–32

Rioja AY, Tiruvannamalai Annamalai R, Paris S, Putnam AJ & Stegemann JP (2016) Endothelial sprouting and network formation in collagen- and fibrin-based modular microbeads. *Acta Biomater* 29: 33–41

Rosellini E & Cascone MG (2025) Scaffolds Mimicking the Tumor Microenvironment for In Vitro Malignancy Models. *Biomimetics* 10: 695

Rosenberg AM, Friedmann P, Del Rivero J, Libutti SK & Laird AM (2016) Resection versus expectant management of small incidentally discovered nonfunctional pancreatic neuroendocrine tumors. In *Surgery (United States)* pp 302–310. Mosby Inc.

Sampedro-Núñez M, Bouthelier A, Serrano-Somavilla A, Martínez-Hernández R, Adrados M, Martín-Pérez E, Muñoz de Nova JL, Cameselle-Teijeiro JM, Blanco-Carrera C, Cabezas-Agricola JM, *et al* (2020) LAT-1 and GLUT-1 Carrier Expression and Its Prognostic Value in Gastroenteropancreatic Neuroendocrine Tumors. *Cancers (Basel)* 12: 2968

Saxena S, Hayashi Y, Wu L, Awaji M, Atri P, Varney ML, Purohit A, Rachagani S, Batra SK & Singh RK (2018) Pathological and functional significance of Semaphorin-5A in pancreatic cancer progression and metastasis. *Oncotarget* 9: 5931–5943

Saydé T, El Hamoui O, Alies B, Gaudin K, Lespes G & Battu S (2021) Biomaterials for Three-Dimensional Cell Culture: From Applications in Oncology to Nanotechnology. *Nanomaterials* 11: 481

Sbrana FV, Pinos R, Barbaglio F, Ribezzi D, Scagnoli F, Scarfò L, Redwan IN, Martinez H, Farè S, Ghia P, *et al* (2021) 3D Bioprinting Allows the Establishment of Long-Term 3D Culture Model for Chronic Lymphocytic Leukemia Cells. *Front Immunol* 12

Scarpa A, Chang DK, Nones K, Corbo V, Patch AM, Bailey P, Lawlor RT, Johns AL, Miller DK, Mafficini A, *et al* (2017) Whole-genome landscape of pancreatic neuroendocrine tumours. *Nature* 543: 65–71

Schindelin J, Arganda-Carreras I, Frise E, Kaynig V, Longair M, Pietzsch T, Preibisch S, Rueden C, Saalfeld S, Schmid B, *et al* (2012) Fiji: an open-source platform for biological-image analysis. *Nat Methods* 9: 676–682

Scoazec J-Y (2013) Angiogenesis in neuroendocrine tumors: Therapeutic applications. *Neuroendocrinology* 97: 45–56

Scott AT & Howe JR (2019) Evaluation and Management of Neuroendocrine Tumors of the Pancreas. *Surgical Clinics of North America* 99: 793–814 doi:10.1016/j.suc.2019.04.014 [PREPRINT]

Semenza GL (2003) Targeting HIF-1 for cancer therapy. *Nat Rev Cancer* 3: 721–732

Semenza GL & Glazer PM (2000) Hypoxia, Clonal Selection, and the Role of HIF-1 in Tumor Progression. *Crit Rev Biochem Mol Biol* 35: 71–103

Sesti F, Puliani G, Feola T, Campolo F, Sciarra F, Hasenmajer V, Lenzi A, Faggiano A, Isidori AM, Venneri MA, *et al* (2023) Characterization of circulating immune cells and correlation with Tie2/Angiopoietins level in well differentiated neuroendocrine gastroenteropancreatic tumors: a cross-sectional analysis. *Endocrine* 80: 221–230

Sharma R, Restan Perez M, da Silva VA, Thomsen J, Bhardwaj L, Andrade TAM, Alhussan A & Willerth SM (2023) 3D bioprinting complex models of cancer. *Biomater Sci* 11: 3414–3430

Shen J, Cao J, He J, Yu H & Chen M (2023) Clinical utility of resected pancreatic volume ratio calculation for predicting postoperative new-onset diabetes mellitus after distal pancreatectomy-a propensity-matched analysis. *Heliyon* 9

Shin HJ, Rho SB, Jung DC, Han IO, Oh ES & Kim JY (2011) Carbonic anhydrase IX (CA9) modulates tumor associated cell migration and invasion. *J Cell Sci* 124: 1077–1087

Shirakawa S, Matsumoto I, Toyama H, Shinzeki M, Ajiki T, Fukumoto T & Ku Y (2012) Pancreatic Volumetric Assessment as a Predictor of New-Onset Diabetes Following Distal Pancreatectomy. *Journal of Gastrointestinal Surgery* 16: 2212–2219

Shukla AK, Yoon S, Oh S-O, Lee D, Ahn M & Kim BS (2024) Advancement in Cancer Vasculogenesis Modeling through 3D Bioprinting Technology. *Biomimetics* 9: 306

Singh S, Dey C, Kennecke H, Kocha W, Maroun J, Metrakos P, Mukhtar T, Pasieka J, Rayson D, Rowsell C, *et al* (2015) Consensus Recommendations for the Diagnosis and Management of Pancreatic Neuroendocrine Tumors: Guidelines from a Canadian National Expert Group. *Ann Surg Oncol* 22: 2685–2699

Singh S, Halperin D, Myrehaug S, Herrmann K, Pavel M, Kunz PL, Chasen B, Tafuto S, Lastoria S, Capdevila J, *et al* (2024) [177Lu]Lu-DOTA-TATE plus long-acting octreotide versus high-dose long-acting octreotide for the treatment of newly diagnosed, advanced grade 2–3, well-differentiated, gastroenteropancreatic neuroendocrine tumours (NETTER-2): an open-label, randomised, phase 3 study. *The Lancet* 403: 2807–2817

Singhi AD & Klimstra DS (2018) Well-differentiated pancreatic neuroendocrine tumours (PanNETs) and poorly differentiated pancreatic neuroendocrine carcinomas (PanNECs): concepts, issues and a practical diagnostic approach to high-grade (G3) cases. *Histopathology* 72: 168–177 doi:10.1111/his.13408 [PREPRINT]

Slezak LA & Andersen DK (2001) Pancreatic resection: Effects on glucose metabolism. *World J Surg* 25: 452–460

Soucek L, Lawlor ER, Soto D, Shchors K, Swigart LB & Evan GI (2007) Mast cells are required for angiogenesis and macroscopic expansion of Myc-induced pancreatic islet tumors. *Nat Med* 13: 1211–1218

Souche R, Hobeika C, Hain E & Gaujoux S (2020) Surgical management of neuroendocrine tumours of the Pancreas. *J Clin Med* 9: 1–18 doi:10.3390/jcm9092993 [PREPRINT]

Spolverato G, Bagante F, Aldrighetti L, Poultsides G, Bauer TW, Field RC, Marques HP, Weiss M, Maithel SK & Pawlik TM (2017) Neuroendocrine Liver Metastasis:

Prognostic Implications of Primary Tumor Site on Patients Undergoing Curative Intent Liver Surgery. *Journal of Gastrointestinal Surgery* 21: 2039–2047

Srirajaskanthan R, Dancey G, Hackshaw A, Luong T, Caplin ME & Meyer T (2009) Circulating angiopoietin-2 is elevated in patients with neuroendocrine tumours and correlates with disease burden and prognosis. *Endocr Relat Cancer* 16: 967–976

Standards of Medical Care in Diabetes—2022 Abridged for Primary Care Providers (2022) *Clinical Diabetes* 40: 10–38

Straub J, Bräutigam K, Di Domenico A, Galván J A, Maire R, Skowronska M, Dettmer M S, Marinoni I & Perren A Change of Lactate Transporter (MCT4) Expression in Pancreatic Microadenomas and Stages of Pancreatic Neuroendocrine. *17th Annual ENETS Conference 2020 (2020)* [PREPRINT]

Strosberg J (2018) Gastroenteropancreatic neuroendocrine tumors. In *The American Cancer Society's Oncology in Practice: Clinical Management* pp 552–570. wiley

Strosberg J, El-Haddad G, Wolin E, Hendifar A, Yao J, Chasen B, Mittra E, Kunz PL, Kulke MH, Jacene H, *et al* (2017) Phase 3 Trial of ^{177} Lu-Dotatate for Midgut Neuroendocrine Tumors. *New England Journal of Medicine* 376: 125–135

Švastová E, Žilka N, Zat'ovičová M, Gibadulinová A, Čiampor F, Pastorek J & Pastoreková S (2003) Carbonic anhydrase IX reduces E-cadherin-mediated adhesion of MDCK cells via interaction with β-catenin. *Exp Cell Res* 290: 332–345

Szot CS, Buchanan CF, Freeman JW & Rylander MN (2013) *In Vitro* Angiogenesis Induced by Tumor-Endothelial Cell Co-Culture in Bilayered, Collagen I Hydrogel Bioengineered Tumors. *Tissue Eng Part C Methods* 19: 864–874

Takahashi Y, Akishima-Fukasawa Y, Kobayashi N, Sano T, Kosuge T, Nimura Y, Kanai Y & Hiraoka N (2007) Prognostic value of tumor architecture, tumor-associated vascular characteristics, and expression of angiogenic molecules in pancreatic endocrine tumors. *Clinical Cancer Research* 13: 187–196

Tariq M, Jajja MR, Maxwell DW, Galindo RJ, Sweeney JF & Sarmiento JM (2020) Diabetes development after distal pancreatectomy: results of a 10 year series. *HPB* 22: 1034–1041

Terris B, Scoazec JY, Rubbia L, Bregeaud L, Pepper MS, Ruszniewski P, Belghiti J, Flejou J & Degott C. (1998) Expression of vascular endothelial growth factor in digestive neuroendocrine tumours. *Histopathology* 32: 133–138

Thiis-Evensen E & Boyar Cetinkaya R (2023) Incidence and prevalence of neuroendocrine neoplasms in Norway 1993–2021. *J Neuroendocrinol* 35

Titan AL, Norton JA, Fisher AT, Foster DS, Harris EJ, Worhunsky DJ, Worth PJ, Dua MM, Visser BC, Poultsides GA, *et al* (2020) Evaluation of Outcomes Following Surgery for Locally Advanced Pancreatic Neuroendocrine Tumors. *JAMA Netw Open* 3: e2024318

Townsend JCM, Beauchamp RD, Evers BM & Mattox KL (2016) Sabiston Textbook of Surgery, The Biological Basis of Modern Surgical Practice 20° edition. Elsevier

Turner HE, Harris AL, Melmed S & Wass JAH (2003) Angiogenesis in Endocrine Tumors. *Endocr Rev* 24: 600–632

Ullah MS, Davies AJ & Halestrap AP (2006) The plasma membrane lactate transporter MCT4, but not MCT1, is up-regulated by hypoxia through a HIF-1α-dependent mechanism. *Journal of Biological Chemistry* 281: 9030–9037

Vandamme T, Peeters M, Dogan F, Pauwels P, Van Assche E, Beyens M, Mortier G, Vandeweyer G, de Herder W, Van Camp G, *et al* (2015) Whole-exome characterization of pancreatic neuroendocrine tumor cell lines BON-1 and QGP-1. *J Mol Endocrinol* 54: 137–147

Vinik AI & Raymond E (2013) Pancreatic neuroendocrine tumors: Approach to treatment with focus on sunitinib. *Therap Adv Gastroenterol* 6: 396–411

Viol F, Sipos B, Fahl M, Clauditz TS, Amin T, Kriegs M, Nieser M, Izbicki JR, Huber S, Lohse AW, *et al* (2022) Novel preclinical gastroenteropancreatic neuroendocrine neoplasia models demonstrate the feasibility of mutation-based targeted therapy. *Cellular Oncology* 45: 1401–1419

Vitale G, Cozzolino A, Malandrino P, Minotta R, Puliani G, Saronni D, Faggiano A & Colao A (2021) Role of FGF System in Neuroendocrine Neoplasms: Potential Therapeutic Applications. *Front Endocrinol (Lausanne)* 12

Vitale G, Gaudenzi G, Dicitore A, Cotelli F, Ferone D & Persani L (2014) Zebrafish as an innovative model for neuroendocrine us. *Endocr Relat Cancer* 21 doi:10.1530/ERC-13-0388 [PREPRINT]

Walter T, van Brakel B, Vercherat C, Hervieu V, Forestier J, Chayvialle J-A, Molin Y, Lombard-Bohas C, Joly M-O & Scoazec J-Y (2015) O6-Methylguanine-DNA methyltransferase status in neuroendocrine tumours: prognostic relevance and association with response to alkylating agents. *Br J Cancer* 112: 523–531

Wei IH, Harmon CM, Arcerito M, Cheng DF, Minter RM & Simeone DM (2014) Tumor-Associated Macrophages Are a Useful Biomarker to Predict Recurrence After Surgical Resection of Nonfunctional Pancreatic Neuroendocrine Tumors. *Ann Surg* 260: 1088–1094

Wood-Trageser MA, Nichols CT, Hutchings DA, Bell D, Wald AI, Smith K, Hong SM, Luchini C, Brosens LAA, Verschuur AVD, *et al* (2025) Recurrent BEND2 Fusion Genes Identified by Whole Transcriptome Sequencing of Nonfunctional Pancreatic Neuroendocrine Tumors Correlate With Poor Patient Prognosis. *Modern Pathology* 38

Wullschleger S, Loewith R & Hall MN (2006) TOR Signaling in Growth and Metabolism. *Cell* 124: 471–484

Yao JC, Fazio N, Singh S, Buzzoni R, Carnaghi C, Wolin E, Tomasek J, Raderer M, Lahner H, Voi M, *et al* (2016) Everolimus for the treatment of advanced, non-functional neuroendocrine tumours of the lung or gastrointestinal tract (RADIANT-4): a randomised, placebo-controlled, phase 3 study. *The Lancet* 387: 968–977

You T, Tang H, Xu X, Ying H, Sun Z, Cheng Y & Bai C (2022) Patients with non-functional metastatic <scp>G2</scp> pancreatic neuroendocrine tumor benefit from palliative surgery: A 20-year single-center retrospective analysis. *J Neuroendocrinol* 34

You W-K, Sennino B, Williamson CW, Falcón B, Hashizume H, Yao L-C, Aftab DT & McDonald DM (2011) VEGF and c-Met Blockade Amplify Angiogenesis Inhibition in Pancreatic Islet Cancer. *Cancer Res* 71: 4758–4768

Yu J, Sun R, Han X & Liu Z (2020) New-Onset Diabetes Mellitus after Distal Pancreatectomy: A Systematic Review and Meta-Analysis. *Journal of Laparoendoscopic and Advanced Surgical Techniques* 30: 1215–1222

Zanini S, Renzi S, Giovinazzo F & Bermano G (2020) mTOR Pathway in Gastroenteropancreatic Neuroendocrine Tumor (GEP-NETs). *Front Endocrinol (Lausanne)* 11

Zhang T, Ren Y, Yang P, Wang J & Zhou H (2022) Cancer-associated fibroblasts in pancreatic ductal adenocarcinoma. *Cell Death Dis* 13: 897

Zhao Z, Chen X, Dowbaj AM, Sljukic A, Bratlie K, Lin L, Fong ELS, Balachander GM, Chen Z, Soragni A, *et al* (2022) Organoids. *Nature Reviews Methods Primers* 2: 94

Zuazo-Gaztelu I, Pàez-Ribes M, Carrasco P, Martín L, Soler A, Martínez-Lozano M, Pons R, Llena J, Palomero L, Graupera M, *et al* (2019) Antitumor Effects of Anti-Semaphorin 4D Antibody Unravel a Novel Proinvasive Mechanism of Vascular-Targeting Agents. *Cancer Res* 79: 5328–5341

van der Zwan WA, Bodei L, Mueller-Brand J, de Herder WW, Kvols LK & Kwekkeboom DJ (2015) GEP–NETs UPDATE: Radionuclide therapy in neuroendocrine tumors. *Eur J Endocrinol* 172: R1–R8